WALL SLIP OF POLYDISPERSE LINEAR POLYMERS: EFFECTS OF MOLECULAR WEIGHT CHARACTERISTICS, AND SURFACE CONDITIONS

by

Marzieh Ebrahimi

B.Sc., Amirkabir University of Technology, Tehran, Iran, 2011

M.Sc., Amirkabir University of Technology, Tehran, Iran, 2013

A THESIS SUBMITTED IN PARTIAL FULFILLMENT OF

THE REQUIREMENTS FOR THE DEGREE OF

DOCTOR OF PHILOSOPHY

in

THE FACULTY OF GRADUATE AND POSTDOCTORAL STUDIES

(Chemical and Biological Engineering)

THE UNIVERSITY OF BRITISH COLUMBIA

(Vancouver)

September 2017

Abstract

The classical no-slip boundary condition of fluid mechanics is not always a valid assumption for the flow of complex fluids including polymer melts. Since the slip velocity of polymer melts complicates analysis of rheological data and it is needed for simulation of polymer processes and process optimization, a comprehensive predictive slip velocity model should be developed. In this thesis, the slip behavior of monodisperse and polydisperse linear polymers including high-density polyethylenes (HDPEs), polybutadienes (PBDs), and polystyrenes (PSs) is studied to fully understand the effect of molecular weight (MW) and molecular weight distribution (MWD). Concepts from double reptation mixing rule are used to develop an expression for slip velocity of polydisperse polymers based on their MW and MWD. Very good agreement between experimental data and predictions of proposed model is observed, validating the applicability of the model.

Surface enrichment of short chains next to solid boundaries due to entropic effects complicates slip analysis specially in the case of bimodal polymers. To address surface segregation, the slip behavior of several HDPEs with broad range of molecular weight including bimodals is studied. Moreover, the developed slip model coupled with a model of surface molecular weight fractionation is used to predict the slip velocity of the studied polymers. It is observed that surface fractionation has a minor effect on slip of narrow to moderate MWD polymers (particularly unimodal), but its role is significant for broad bimodal polymers.

Moreover, the dynamic slip behavior of a polymer melt was investigated by performing dynamic shear experiments using the stress/strain controlled rotational rheometer equipped with parallel partitioned plate geometry. The multimode integral Kaye-Bernstein-Kearsley-Zapas (KBKZ) constitutive model is applied and it is found that a dynamic slip model with a slip relaxation time is needed to adequately predict the experimental data at large shear deformations.

Finally, the effects of surface topology and energy on slip velocity of high-density HDPEs was studied using treated and untreated smooth and patterned slit dies. It was found that the slip velocity is decreased by roughness and is increased by silanization. These effects have been incorporated into the slip velocity model.

Lay Summary

Although there is considerably a large body of experimental data on polymer slip, few studies quantify the slip velocity in a systematic manner to address effects of polymer and surface characteristics [Hatzikiriakos (2012, 2015)]. In this thesis, the slip behavior of monodisperse and polydisperse linear polymers on substrates with different surface roughness and energy is studied to fully understand the effects of molecular weight (MW) and molecular weight distribution (MWD) of polymers and surface conditions. The double reptation mixing rule was used to develop a general expression to calculate the dependence of the slip velocity on polymer MW and MWD. Moreover, the effects of surface energy and topology (roughness) were incorporated in the model to take into account surface conditions and develop a fully predictive slip model.

Preface

This thesis entitled "Wall slip of polydisperse linear polymers: effects of molecular weight characteristics and surface conditions" presents the research the author performed during her PhD study under the supervision of Professor Savvas G. Hatzikiriakos. Slip velocity of different groups of polymers especially high-density polyethylenes has been extensively studied attempting to fully understand wall slip.

The following journal papers and conference presentations have been published or submitted for publication from the research work presented in this dissertation:

Journal Papers

1. **M. Ebrahimi**, M. Ansari, and S. G. Hatzikiriakos, "Wall slip of polydisperse linear polymers using double reputation", Journal of Rheology, 2015, 59(3), 885-901. (This paper is based on the data presented in Chapter 3 of this thesis.)
2. **M. Ebrahimi**, M. Ansari, Y. W. Inn, and S. G. Hatzikiriakos, "Surface fractionation effects on slip of polydisperse polymer melts", Physics of Fluids, 2016, 28(9), 093101. (This publication is based on the data discussed in Chapter 4 of this thesis.)
3. **M. Ebrahimi**, V. K. Konaganti, S. Moradi, A. K. Doufas, and S. G. Hatzikiriakos, 2016. "Slip of polymer melts over micro/nano-patterned metallic surfaces", Soft Matter, 2016,12(48), 9759-9768. (This paper is based on the data presented in Chapter 5 of this thesis.)
4. **M. Ebrahimi**, V. K. Konaganti, and S. G. Hatzikiriakos, 2017. "Slip of polymer melts over micro/nano-patterned metallic surfaces", in preparation for publication. (This paper is based on the data presented in Chapter 6 of this thesis.)
5. E. Chatzigiannakis, **M. Ebrahimi**, and S. G. Hatzikiriakos, "On the Molecular Weight Dependence of Slip Velocity of Polymer Melts", Journal of Rheology, 2017, *61*(4), 731-739 (Part of this paper is presented in Chapter 3 of this thesis.)

Conference Presentations

1. **M. Ebrahimi**, M. Ansari, and S. G. Hatzikiriakos, "Slip of HDPEs in capillary flow: broad MWD effects", 10th Annual Conference of the European Society of Rheology, April 14-17, 2015, Nantes, France.
2. **M. Ebrahimi**, M. Ansari, and S. G. Hatzikiriakos, "Wall Slip of HDPEs: MW, MWD and Surface Conditions Effects", 87th Annual Meeting of the Society of Rheology, October 11-15, 2015, Baltimore, MA, USA.
3. **M. Ebrahimi**, M. Ansari, and S. G. Hatzikiriakos, "Surface Fractionation Effects on Slip of Polydisperse Polymer Melts", 17th International Congress on Rheology, Kyoto, Japan August 8-13, 2016, Kyoto, Japan.
4. **M. Ebrahimi**, V. K. Konaganti, S. Moradi, A. K. Doufas, and S. G. Hatzikiriakos, "Surface roughness and energy on slip of polymer melts", Proceedings of the Technical Conference & Exhibition ANTEC 2017, May 8-10, 2017, Anaheim, CA, USA.

The fifth journal paper is written mostly by Emmanuil Chatzigiannakis. All other manuscripts were written mostly by the author of this thesis and revised by the supervisor (Prof. S.G. Hatzikiriakos) and the other co-authors.

Table of Contents

List of Tables

List of Figures

List of Symbols

V_S	slip velocity
b	slip or extrapolation length
$\dot{\gamma}_w$	wall shear rate
η	viscosity
σ_w	wall shear stress
$\dot{\gamma}$	true shear rate
$\dot{\gamma}_n$	nominal shear rate
V	velocity of the moving plate
h	distance between parallel disks
σ_c	critical shear stress
r	radial position from the center
$\dot{\gamma}_{nr}$	nominal shear rate at r
Ω	angular velocity
T	torque
R	radius of the disk or capillary die
σ_R	shear stress at R
$\dot{\gamma}_{nR}$	nominal shear rate at R
$\dot{\gamma}_R$	true shear rate at R
D	diameter of the capillary die
L	length of the die
σ_{rz}	shear stress in r and z axis
$\dot{\gamma}_A$	apparent shear rate
Q	volumetric flow rate
$\dot{\gamma}_{A,S}$	apparent shear rate corrected for the effect of slip
H	slit die height
W	slit die width
K	power law constant
n	local slope of the flow curve / power law exponent

M_n	number average molecular weight
M_w	weight average molecular weight
M_z	z-average molecular weight
M	molecular weight
M_i	ith chain molecular weight
n_i	number of chains of molecular weight M_i
ν	adsorbed polymer density per unit area
W_{adh}	work of adhesion
γ_{LV}	interfacial tension between the molten polymer and its vapor
θ	contact angle
E	activation energy
T	absolute temperature
k	Boltzman constant
c_1	emprical constant
c_2	emprical constant
c_3	emprical constant
ξ_0	empirical constant
σ_n	normal stress at the wall
λs	slip relaxation time
A'	slip coefficient
m	slip power law exponent
σ_{12} or $\sigma_{\theta z}$	shear stress in θ and z axis
θ'	rotation angle
p	pressure
Δp	applied pressure or pressure drop
$2\omega_0$	beam spot size
λ'	laser wavelength
F	focal length of the lens
D'	beam waist
Φ	laser energy

V'	laser scanning speed
a_T	temperature dependence of slip velocity
a_p	pressure dependence of slip velocity
β	slip molecular weight dependency exponent
A	slip coefficient independent of molecular weight
M_e	molecular weight between entanglements
ρ	density
G_N^0	plateau modulus
$w(M)$	molecular weight distribution
σ_{std}	log normal distribution standard deviation
$\overline{M}_m$	log normal distribution median value
A^*	log normal distribution constant
η_o	zero-shear viscosity
N	chain length
$\tau(N)$	reptation time of chains of length N
$w(N)$	volume fraction of chains of length N
η_i	viscosity of the melt in the interfacial layer
α	interfacial layer thickness
N_e	number of monomers between entanglements
τ_{AR}	characteristic relaxation time due to arm retraction
τ_1	microscopic jump time
μ	numerical coefficient
τ_{CR}	characteristic relaxation time due to the constraint release mechanism
θ_N^{ex}	the surface excess volume fraction
φ_N^b	bulk volume fraction
N_w	weight average chain lengths
A_C	universal prefactor

$w_s(M)$	molecular weight distribution next to the surface
$w_b(M)$	bulk molecular weight distribution
$\nu_{ex}(M)$	excess weight fraction
φ_{LM}	weight fraction of the low-MW resin
$w(LM)$	log normal distribution of low-MW component
$w(HM)$	log normal distribution of high-MW component
ω	angular frequency
G'	storage modulus
G''	loss modulus
η^*	complex viscosity
η_0	zero shear viscosity
$\lvert\dot{\gamma}\rvert$	local shear rate or magnitude of strain rate tensor
II	second invariant of strain rate tensor
a	empirically determined constant
n'	empirically determined constant
λ	empirically determined constant
G^*	complex modulus
v	velocity vector
$\boldsymbol{\tau}$	extra stress tensor (excluding pressure)
D	rate of deformation tensor
$\nabla\mathbf{v}$	velocity gradient tensor
σ_w	wall shear stress
k'	friction coefficient
ε_s	attraction between substrate and liquid
$W_{adh,e}$	work of adhesion of a coated surface
φ	free surface fraction
A_s	slip coefficient of a rough surface
A_e	slip coefficient of a coated surface

g_i	relaxation modulus
λ_i	relaxation time
$h(\gamma)$	damping function
$\mathbf{C_t}$	Cauchy-Green tensor
$\mathbf{C_t^{-1}}$	Finger strain tensor
I_C	first invariant of $\boldsymbol{C_t}$
I_C^{-1}	first invariant of $\boldsymbol{C_t^{-1}}$
N	number of relaxation modes
N_1	first normal stress difference
N_2	second normal stress difference
α_p	shear parameter of PSM damping function
β_p	extensional parameter of PSM damping function

List of Abbreviations

AR	Arm Retraction
CA	Contact Angle
CAH	Contact Angle Hysteresis
CR	Constraint Release
FEM	Finite Element Method
GPC	Gel Permeation Chromatography
HDPE	High-Density Polyethylene
K-BKZ	Kaye-Bernstein-Kearsley-Zapas
LLDPE	Linear Low-Density Polyethylene
LVE	Linear Viscoelastic Envelope
m-HDPE	metallocene High-Density Polyethylene
MW	Molecular Weight
MWD	Molecular Weight Distribution
PBD	Polybutadiene
PDMS	Polydimethylsiloxane
PE	Polyethylene
PI	Polydispersity index
PIP	Polyisoprene
PLA	Polylactide
PP	Parallel Plate
PPP	Parallel Partitioned Plate
PS	Polystyrene
SAOS	Small Amplitude Oscillatory Shear
SEC	Size Exclusion Chromatography
SS	Stainless Steel
TTS	Time-Temperature Superposition
ZN-HDPE	Ziegler-Natta High-Density Polyethylene

Acknowledgements

First and foremost, I would like to thank my supervisor Prof. Savvas G. Hatzikiriakos for his sincere support, advice and encouragement throughout my PhD research. Without his guidance, this work would never have been done. I would also like to acknowledge my supervisory committee members Professor Mark Martinez, Dr. Roberto DiRaddo, and Mr. Haile Atsbha for their time and helpful comments.

Sincere gratitude to my wonderful friends and colleagues, Vinod, Mahmoud, Salma, Vasilii, Dimitris, Tanja, Emmanouil, and Sona for their heartwarming friendships and for their great support along my journey over the past four years.

I gratefully acknowledge the financial assistance from the University of British Columbia and Natural Sciences and Engineering Research Council of Canada (NSERC), for giving me the opportunity to pursue my passion in science through their generous support, funding, and fellowship.

The most profound and loving thanks go to my family; my twin sister, Samaneh who was always there for me through my ups and downs, and my wonderful sister and brothers, Nafiseh, Ebi and Amir for their endless love, encouragement and caring. My deepest gratitude goes to my parents, Sorayya and Firouz whom supported me and loved me each and every day.

To my lovely parents, Sorayya and Firouz.

Chapter 1: Introduction

The classical no-slip boundary condition of fluid mechanics states that the velocity of a fluid in contact with a solid substrate is equal to the velocity of the substrate. This was in agreement with early experimental results for simple fluids such as water and therefore slip has received little attention for Newtonian fluids [Goldstein, 1938]. However, violations to no-slip have been reported even for simple Newtonian liquids in the case of nonwetting or very smooth substrates, or when the dimensions of flow channels become comparable to molecular size [Schnell (1956); Reiter *et al*. (1994); Zhu and Granick (2002)]. Slip is more commonly observed for polymeric fluids [Galt and Maxwell (1964); Ramamurthy (1986); Hatzikiriakos and Dealy (1991); Mhetar and Archer (1998a); Archer (2005); Hatzikiriakos (2012)]. According to the slip theory developed by Brochard-Wyart and deGennes (1992), polymer melts, of interest to the present PhD thesis, slip no matter how small the applied forces are. Therefore, it is important to study polymer melt slip to develop slip velocity expressions which can be used in the simulation of polymer processes for process optimization.

Navier (1823) first proposed an interfacial rheological law for the case of a passive polymer/wall interface (no interaction between the polymer and solid surface) as follows;

$$V_S = b\left[\frac{dV}{dy}\right]_{y=0} = b\dot{\gamma}_w = \left[\frac{b}{\eta}\right]\sigma_w \tag{1.1}$$

Where V_S is the slip velocity, b is the slip or extrapolation length (see FIGURE 1.1), $\dot{\gamma}_w$ is the wall shear rate (slope of the velocity profile at the wall), η is the melt viscosity at $\dot{\gamma}_w$ and σ_w is the wall shear stress. Brochard-Wyart and deGennes (1992) extended this theory for an adsorbing interface where some polymer chains are grafted to the surface. Therefore, comprehensive understanding of polymer adsorption and interactions between polymer chains near the interface are important in studying polymer slip.

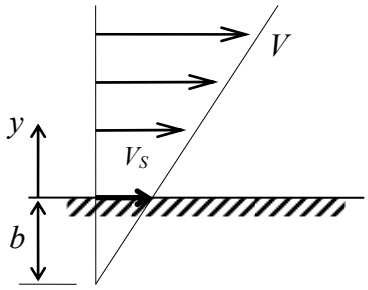

FIGURE 1.1: Navier's view of wall slip in shear flow of molten polymers.

The slip mechanism in the case of polymer melts occurs within the first monolayer of macromolecules adsorbed at the wall [Brochard-Wyart and deGennes (1994)]. Polymer chains are attached to the wall at several sites along their backbone. The adsorbed chains are further entangled with chains in the bulk again at several sites depending on the entanglement density. There are two main mechanisms of slip: desorption of molecules from the surface (adhesive slip) and disentanglement of molecules from a monolayer adsorbed on the interface (cohesive slip) [Brochard-Wyart *et al.* (1994,1996)]. In the first case, slip occurs directly between the bulk polymer chains and the surface and is governed by the bare friction between the polymer chains and the surface. This type of slip has been termed true/adhesive slip. In the latter, slip occurs between the bulk polymer chains and the adsorbed ones at the surface. Therefore, it arises from failure at a polymer-polymer interface and is termed cohesive slip. This type of slip is controlled by the friction developed between adsorbed and the bulk chains. Based on these mechanisms, two main slip regimes can be observed, i.e.,(i) the weak slip regime (chain desorption/detachment from the surface and partial disentanglement) and (ii) the strong slip which is for the case of sudden complete disentanglement of polymer chains in the bulk from the monolayer adsorbed on the interface. The weak slip regime has been observed at relatively small values of the wall shear stress where there are small deviations from the no-slip boundary condition. Linear polymers show a transition from a weak to a strong slip at a critical wall shear stress value [Ramamurthy (1986); Kalika and Denn (1987); Hatzikiriakos and Dealy (1992a), Sabzevari (2015)]. The velocity profile in the strong slip regime approaches nearly plug flow [Münstedt *et al*. (2000)].

Polymer melt slip is dependent on the physicochemical characteristics of both polymer and surface and it is affected by several factors including wall shear stress, wall normal stress (pressure), temperature, surface energy and roughness, polymer molecular weight (MW), molecular weight distribution (MWD), and molecular architecture [Hatzikiriakos (2012,2015)]. Moreover, in pressure driven flows migration/fractionation effects will also continuously change the local wall molecular weight distribution thus altering slip [Rorrer and Dorgan (2014)]. These factors will be investigated in the present thesis. Specifically, a fully predictive slip velocity model will be developed for linear polymers that is capable of capturing all these effects quantitatively.

1.1 Literature review

In this section the important parameters affecting polymer slip are discussed. In addition, several experimental and theoretical studies used to understand the slip flow of polymer melts near interfaces are also explained. Furthermore, the experimental techniques for quantifying slip, the mechanisms of slip, the critical factors in polymer slip and slip velocity models are reviewed.

1.1.1 Experimental methods for determining slip

1.1.1.1 Indirect methods (gap dependence)

Gap dependent measurements of stresses or flow rates in simple flow geometries are of the most common methods for quantifying slip, known as the Mooney method [Mooney (1931)].

1.1.1.1.1 Gap dependent measurements in planar Couette shear flow

Couette flow is the flow of a fluid between two parallel plates, one of which is moving relative to the other (FIGURE 1.2).

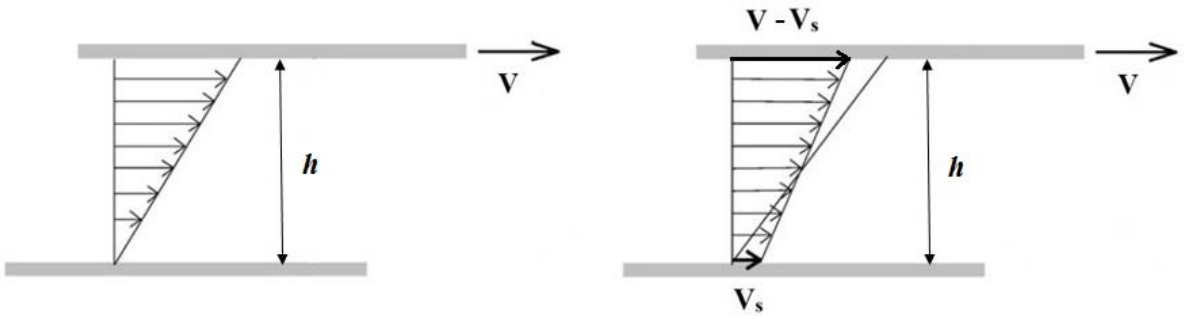

FIGURE 1.2: Planar Couette shear flow under no slip (left) and slip conditions (right).

In the case of no-slip, the true shear rate experienced by the fluid, $\dot{\gamma}$, is equal to the nominal shear rate, $\dot{\gamma}_n$ defined by V/h where V is the velocity of the moving plate and h is the spacing between the plates. For the case of slip, it is assumed that the slip velocity is a function of wall shear stress and is the same on both plates, leading to the following equation between nominal and true shear rates;

$$\dot{\gamma}_n = \dot{\gamma} + \frac{2V_S}{h} \tag{1.2}$$

Based on this equation, the gap dependency of the flow curve indicates the presence of wall slip. The shear rate required at a constant shear stress in a fluid under planar Couette shear flow depends inversely on the gap spacing. Therefore, a plot of $\dot{\gamma}_n$ versus $1/h$ at fixed values of shear stress results in straight lines with slope of $2V_S$ and intercept of $\dot{\gamma}$ [Mooney (1931)]. Hatzikiriakos and Dealy (1991) used this method to determine the slip violations of a commercial high-density polyethylene (HDPE). They utilized a sliding plate rheometer with a shear stress transducer, and performed steady shear experiments at three different gap spacings. Their results showed that slip occurs above a critical shear stress, σ_c of 0.09 MPa and slip velocity is a strong function of shear stress. Similarly, Dao and Archer (2002) studied the slip velocity of a series of narrow molecular weight distribution polybutadiene melts using planar Couette flow measurements. Their measurements imply that the slip velocity increases linearly with shear stress up to a certain value of stress.

1.1.1.1.2 Gap dependent measurements in torsional shear flow

Gap dependent measurements can also be used to determine slip velocity of polymer melts subjected to torsional shear flow, which is the case in rotational rheometers equipped with parallel plate geometry. The nominal shear rate in a parallel plate geometry is a function of radial position from the center, r as $\dot{\gamma}_{nr} = r\Omega/h$ where Ω is the angular velocity of the upper plate and h is the gap size between the plates (FIGURE 1.3). The torque required to rotate the upper plate, T, needs to be differentiated and converted to meaningful rheological data such as shear stress at the edge of the disk, σ_R [Yoshima and Prud'homme (1988)];

$$\sigma_R = \frac{T}{2\pi R^3}\left[3 + \frac{d\ln T}{d\ln \dot{\gamma}_{nR}}\right] \tag{1.3}$$

Where R is the radius of the disks and $\dot{\gamma}_{nR}$ is the nominal shear rate at the edge of the disk. The gap dependence of the flow curve implies the occurrence of slip. By assuming that slip is a function of wall shear stress (similar slip on both plates), the following equation can be derived;

$$\dot{\gamma}_{nR} = \dot{\gamma}_R + \frac{2V_S}{h} \tag{1.4}$$

Where $\dot{\gamma}_{nR}$ and $\dot{\gamma}_R$ are nominal and true shear rates at the edge of the disk, respectively.

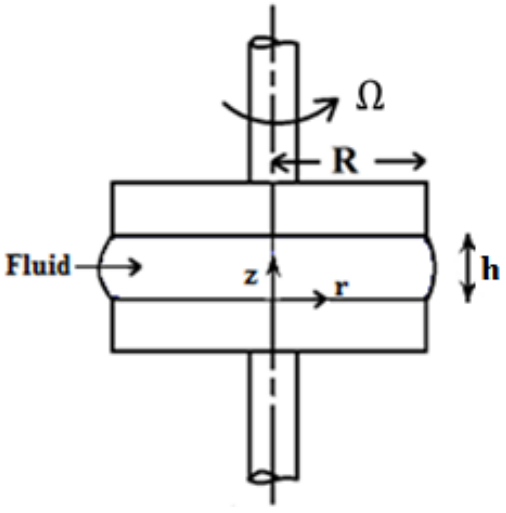

FIGURE 1.3: Schematic representation of parallel plate rheometer.

This method has been used by several researchers to measure slip velocity. Yoshima and Prud'homme (1988) used this parallel disk method to determine slip in an emulsion of paraffin oil in water. Hanson and Mackay (1995) characterized the slip behavior of monodisperse polystyrene (PS) melts. They found that PS melts slip no matter how small the applied forces are. Therefore, the critical shear stress for the onset of slip, σ_c, cannot be uniquely defined. However, σ_c is simply a convenient parameter, which can be defined from macroscopic rheological experiments, where the flow curves start exhibiting apparent gap dependence. Hey *et al.* (2000) compared slip of a commercial linear low-density polyethylene (LLDPE) using torsional shear and pressure driven flows. They concluded that, although there is no sign of slip effects at low stress levels with the capillary rheometer, the torsional rheometer shows slip at all shear stresses. This can be attributed to the sensitivity of experimental measurements in tortional rheometry.

1.1.1.1.3 Diameter dependent measurements in pressure driven shear flows

Poiseuille flow measurements in capillary and slit dies with different diameters and gap heights, can also be used to study slip violations. Consider the pressure driven, laminar flow of an incompressible non-Newtonian flow in a capillary of diameter $D=2R$ and length L along z-axis. Under wall slip, and assuming that V_S to be only a function of wall shear stress, the volumetric flow rate, Q at an arbitrary shear stress, σ_{rz} can be written as [Mooney, 1931];

$$Q = \pi R^2 V_S + \frac{\pi R^3}{\sigma_w^3} \int_0^{\sigma_w} \dot{\gamma} \sigma_{rz}^2 d\sigma_{rz} \tag{1.5}$$

Where σ_w is the wall shear stress. The second term in this equation is the volumetric flow rate in the absence of slip. For such flow, the shear rate is termed the apparent shear rate defined as $\dot{\gamma}_A = 4Q/\pi R^3$. Introducing $\dot{\gamma}_A$ into Equation 1.5 yields [Mooney, 1931];

$$\dot{\gamma}_A = \dot{\gamma}_{A,S} + \frac{4V_S}{R} = \dot{\gamma}_{A,S} + \frac{8V_S}{D} \tag{1.6}$$

Where $\dot{\gamma}_{A,S}$ is the apparent shear rate corrected for the effect of slip and *D* and *R* show the diameter and radius of the capillary die, respectively. Therefore, in the presence of slip the flow curves obtained using dies with the same *L/D* ratio and different diameter diverge, and a plot of $\dot{\gamma}_A$ versus *1/D* at constant wall shear stress (known as Mooney plot), yields a straight line with slope of $8V_S$ and intercept of $\dot{\gamma}_{A,S}$. Similarly, for a slit die with height of *H* and width of *W*, the apparent shear rate is equal to $\dot{\gamma}_A = 6Q/WH^2$. The following equation under slip applies (derived with a similar fashion as Equation 1.5);

$$\dot{\gamma}_A = \dot{\gamma}_{A,S} + \frac{6V_S}{H} \tag{1.7}$$

It is important to note that end effects are neglected in developing this equation. The aspect ratio of the slit die (*W/H*) should be large (typically more than 10) to obtain accurate results from this analysis (negligible end effects). For a power-law fluid ($\sigma = K\dot{\gamma}^n$) the following expressions can be derived for capillary and slit flows;

$$\dot{\gamma}_A = \frac{4n}{3n+1}\left(\frac{\sigma_w}{K}\right)^{1/n} + \frac{8V_S}{D} \tag{1.8}$$

$$\dot{\gamma}_A = \frac{3n}{2n+1}\left(\frac{\sigma_w}{K}\right)^{1/n} + \frac{6V_S}{H} \tag{1.9}$$

Where *K* and *n* are the power law constant and exponent, respectively.

In summary, the slip velocity of polymer melts can be studied by using capillary or slit rheometry. It can be done by plotting $\dot{\gamma}_A$ versus *1/D* for capillary or *1/H* for slit flow (Mooney plots), essentially using Equations 1.6 or 1.7 respectively. Moreover, if the no-slip flow curve is known, slip velocity can be calculated by deviation from the no-slip flow curve using Equations 1.8 or 1.9 [Kalika and Denn (1987), Ansari *et al.* (2013a)]. Several studies have used this technique to determine slip in pressure driven flows [Ramamurthy (1986), Hatzikiriakos and Dealy (1992a, 1992b, 1997), Wang and Drada (1996a, 1996b), Ansari *et al.* (2013b)].

1.1.1.2 Direct methods

In these methods, the slip is measured directly from observations of displacement of fluid particles at the interface. In most cases, flow tracers are used to detect fluid motion. These tracers are often larger than fluid elements and chemically different but compatible with the host fluid. These techniques include fluorescence recovery after photobleaching [Migler *et al.* (1993,1994), Leger *et al.* (1997, 1999), Durliat *et el.* (1997)] and particle image velocimetry [Galt and Maxwell (1964), den Otter *et al.* (1967), Mhetar and Archer (1998b)] and can be used to study slip at lower stresses and flow rates comparing to indirect methods. Studies using these methods have shown that polymer fluids slip at all stress levels verifying the theory of Brochard-Wyart and deGennes (1992).

1.1.2 Slip mechanisms

The origin of slip is an important fundamental question which has been the subject of interest in the literature for several decades. There are two main mechanisms of slip: (i) desorption/detachment of molecules from the surface referred to as true/adhesive slip and (ii) disentanglement of molecules from a monolayer adsorbed on the interface known as apparent/cohesive slip [Brochard-Wyart and deGennes (1992, 1994)]. These mechanisms are depicted in FIGURE 1.4. Polymer chains are adsorbed on the wall at several sites, and they are also entangled with chains in the bulk (FIGURE 1.4. (a)). Under flow, these chains can either desorb from the wall and slide along the surface (FIGURE 1.4. (b)) or disentangle from the bulk chains (FIGURE 1.4. (c)). If the drag force on the adsorbed chain is larger than the binding force between its adsorbed segments and the surface, shear induced detachment/desorption (adhesive failure) occurs. In this case, interfacial characteristics of polymer/wall interface plays an important role. Anastasiadis and Hatzikiriakos (1998) studied the slip of low-density and high-density polyethylenes on different surfaces including clean and fluoropolymer coated stainless steel. They found a linear correlation between the critical shear stress for the onset of slip and the work of adhesion of the polymer/wall interfaces in agreement with earlier studies [Hill *et al*. (1990); Hatzikiriakos *et al.* (1993)]. If adsorbed chains are strongly attached to the solid surface that the force required for disentanglement is less than that of detachment, the second mechanism (cohesive failure) occurs. In this mechanism, slip is governed by friction between the adsorbed

chains at wall and those at the bulk. Therefore, it is governed by the number of entanglements between the adsorbed and bulk chains as well as the surface density of adsorbed chains.

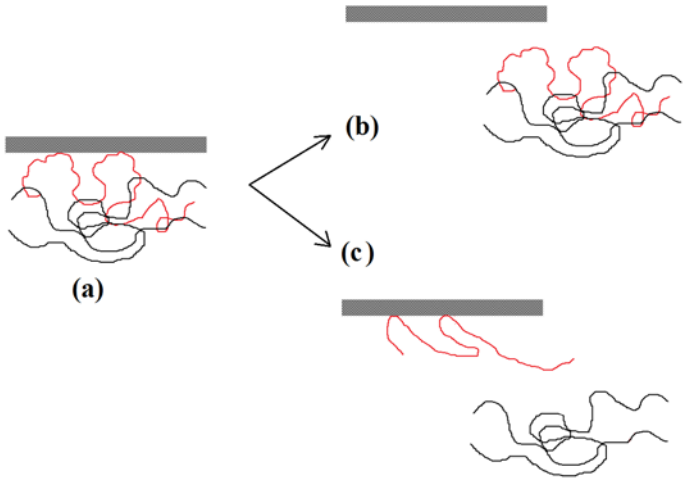

FIGURE 1.4: Schematic representation of (a) polymer molecules attached to a wall and (b) flow induced desorption and (c) disentanglement of polymer chains [(adapted from Black (2000)].

Based on these mechanisms, two main slip regimes can be observed, i.e., the weak slip regime (chain desorption or partial disentanglement) and the strong slip which is for the case of sudden and complete disentanglement of the polymer chains in the bulk from those adsorbed at the wall. The weak slip regime accounts for small deviations from the no-slip boundary condition, and it has been observed at relatively small values of the wall shear stress. In this regime, the slip velocity is a strong function of the molecular weight and its distribution [Wang and Drda (1996a, 1996b); Mhetar and Archer (1998b, 1998c); Awati *et al*. (2000); Hatzikiriakos and Dealy (1992a); Inn (2013); Ansari *et al*. (2013b)]. Linear polymers show a transition from a weak to a strong slip at a critical wall shear stress value typically leading to stick-slip transition [Ramamurthy (1986); Hatzikiriakos and Dealy (1992b); Migler *et al*. (1993, 1994); Kazatchkov *et al*. (1995), Rosenbaum *et al*. (1995); Wang and Drda (1996a, 1996b); Münstedt *et al*. (2000); Robert *et al*. (2004); Mitsoulis *et al*. (2005); Allal and Vergnes (2009); Kazatchkov and Hatzikiriakos (2010)]. It is explained that the stick-slip transition is due to periodic disentanglement/re-entanglement between surface adsorbed and bulk polymer chains [Brochard-Wyart and deGennes (1994); Mhetar and Archer (1998b)] before complete disentanglement occurs which results in strong slip. The velocity

profile in the strong slip regime approaches plug flow [Münstedt *et al*. (2000); Ansari *et al*. (2013b)]. The slip velocity in this regime is not expected to be a function of the molecular characteristics of the polymer as all entanglements are eliminated [Bergem (1976); Drda and Wang (1995); Allal and Vergnes (2007); Ansari *et al*. (2013b)]. Ansari *et al*. (2013b) have shown that the slip velocity of HDPEs for a large number of HDPEs of various MWs and MWDs at this regime, is only a function of shear stress that is a result of the friction developed between the slipping molecules over those adsorbed at the interface.

The transition from weak to strong slip has been observed in the capillary flow of solutions and melts of linear polyethylenes (PEs) [Ramamurthy (1986); Kalika and Denn (1987); Park *et al*. (2008)]. This transition has also been observed in simple shear for highly entangled polymeric solutions and melts [Archer *et al*. (1995); Mhetar and Archer (1998a); Dao and Archer (2002); Sanchez-Reyes and Archer (2003)]. This transition is mainly a characteristic of linear polymers typically with relatively narrow molecular weight distribution, including linear PEs such as high-density and linear low-density polyethylenes [Ramamurthy (1986); Drda and Wang (1995)], polyisoprenes (PIPs) [Vinogradov *et al*. (1972)], polybutadienes (PBDs) [Lim and Schowalter (1989); Park *et al*. (2008); Mhetar and Archer (1998b, 1998c)], fluoropolymers [Rosenbaum *et al*. (1995)], polydimethylsiloxanes (PDMSs) [El-Kissi and Piau (1990); Birinci and Kalyon (2006)], polypropylenes (PPs) [Kazatchkov *et al*. (1995); Mitsoulis *et al*. (2005)] and lately polylactides (PLAs) [Othman *et al*. (2012)] and polycaprolactones (PCLs) [Noroozi *et al*. (2012)]. As a result, the flow curve of such polymers is a discontinuous one, consisted of two branches, namely a low flow-rate branch (weak slip) and a high flow-rate branch (strong slip). On the other hand, linear polymers such as HDPEs of broad molecular weight distribution do not exhibit this transition [Myerholz (1967); Ansari *et al*. (2013b); Inn (2013)].

1.1.3 Factors influencing polymer wall slip

Polymer wall slip is influenced by many factors including temperature and pressure, polymer molecular weight and molecular weight distribution, molecular architecture, migration effects, surface roughness and surface energy.

1.1.3.1 Temperature and pressure

Hatzikiriakos and Dealy (1991, 1992a) studied the slip behavior of high-density polyethylenes in a sliding plate and a capillary rheometer at different temperatures and noted that slip velocity increases with temperature. It has been proven that effect of temperature on polymer wall slip is consistent with the time-temperature superposition [Hatzikiriakos and Dealy (1992a); Ansari *et al.* (2013b)].

Kalika and Denn (1987) found that the slip velocity was a function of the *L/D* ratio of a capillary, decreasing with increasing *L/D*. Hill *et al.* (1990) concluded from this that pressure affects the slip velocity, and by increasing pressure, slip velocity decreases. Hatzikiriakos and Dealy (1992a) further studied the slip of several high-density polyethylene blends at various pressures using a sliding plate rheometer and a capillary rheometer with capillaries of various *L/D* ratios and diameters and reported similar results.

By increasing temperature and decreasing pressure, the polymer free volume increases resulting in increase of slip velocity.

1.1.3.2 Molecular weight and molecular weight distribution

Most of commercially produced polymers are polydisperse with a broad molecular weight distribution. Therefore, the molecular weight of a polymer must be described by some average molecular weight calculated from the molecular weights of all the chains in the sample. The commonly used molecular weight averages that can be determined by gel permeation chromatography (GPC) and size exclusion chromatography (SEC), include number average, weight average, z-average, and z+1-average symbolized as M_n, M_w, M_z, and M_{z+1} respectively. The number average molecular weight is the first moment of the molecular weight distribution which is the statistical average molecular weight of all the polymer chains in the sample, and is defined by;

$$M_n = \frac{\sum n_i M_i}{\sum n_i} \tag{1.10}$$

where n_i is the number of chains of molecular weight M_i. The second moment of the molecular weight distribution is the weight average molecular weight defined as;

$$M_w = \frac{\sum n_i M_i^2}{\sum n_i M_i} \tag{1.11}$$

M_w considers the molecular weight of a chain in determining contributions to the average molecular weight. The more massive the chain, the more it contributes to M_w. The z-average and z+1-average molecular weights are the third and fourth moments of the molecular weight distribution defined as;

$$M_z = \frac{\sum n_i M_i^3}{\sum n_i M_i^2} \tag{1.12}$$

$$M_{z+1} = \frac{\sum n_i M_i^4}{\sum n_i M_i^3} \tag{1.13}$$

M_z and M_{z+1} are more sensitive to high molecular weight molecules compared to M_n and M_w. The polydispersity index, *PI*, defined as M_w/M_n is frequently used to represent the breadth of the distribution.

Very few studies have tried to address the dependence of slip velocity on molecular weight (MW) characteristics, such as weight average MW (M_w) and polydispersity index (*PI*). Mhetar and Archer (1998b, 1998c) and Park *et al.* (2008) for the case of nearly monodisperse polybutadienes, Awati *et al*. (2000) and Mackay and Henson (1998) for nearly monodisperse polystyrenes, and Othman *et al*. (2012) for narrow molecular weight distribution (MWD) polylactides of polydispersity less than 2, have shown that the slip velocity increases with decrease of MW. Similar findings were reported by Inn (2013) for bimodal HDPEs in capillary flow, concluding that low MW components contribute to slip more significantly compared to high MW ones. Considering the convective constraint release mechanism for bulk and tethered chains, Joshi *et al.* (2001) proposed scaling relationships, which are in agreement with these experimental observations. Hatzikiriakos and Dealy (1992a) studied the slip velocity of a series of polydisperse HDPEs (polydispersity index from 3.2 to 9.4) and scaled their slip velocity data with a critical shear stress for the onset of slip, σ_c and polydispersity to produce a slip master curve. Ansari *et al.* (2013b) studied the slip velocity of a series of commercial HDPEs with various MW and MWD,

and concluded that slip velocity increases with decrease of molecular weight and increase of polydispersity.

1.1.3.3 Molecular architecture

As mentioned above, linear polymers exhibit a transition from a weak to a strong slip resulting in discontinuity in their flow curve [Ramamurthy (1986); Hatzikiriakos and Dealy (1992b); Migler *et al*. (1993, 1994); Kazatchkov *et al*. (1995), Rosenbaum *et al*. (1995); Wang and Drda (1996a, 1996b); Münstedt *et al*. (2000); Robert *et al*. (2004); Mitsoulis *et al*. (2005); Allal and Vergnes (2009); Kazatchkov and Hatzikiriakos (2010)]. Sentmanat et al. (2004) observed a significant difference in flow curves of linear (linear-low and high density) and branched polyethylenes. They noted that by increasing shear rate, linear polymers undergo unstable oscillating or stick-slip flow regime, but their branched counterparts show no stick-slip transition and discontinuity in their flow curve. It is concluded that presence of long chain branching, at least in the case of polyethylene, suppresses transition from a weak to a strong slip regime [Sentmanat *et al.* (2004), Ansari *et al.* (2012a,2012b,2012c)]. Moreover, linear polymers with broad molecular weight distribution do not display such transition, instead they exhibit a continuous flow curve [Ansari *et al.* (2012a,2012c)].

1.1.3.4 Migration effects

Entropy driven migration of polymer molecules away or close to solid boundaries complicates the analysis of slip data in the case of broad molecular weight distribution polymers, where concentration gradients might occur to adopt a configuration with the lowest Gibbs free energy [Busse (1964); Schreiber and Storey (1965); Schreiber *et al*. (1966); Hariharan *et al.* (1990); Van der Gucht et al. (2002); Shelby and Caflisch (2004); Inn (2013); Rorrer and Drogan (2014)]. The presence of a solid surface reduces the conformational entropy of a polymer coil, and as a result, the entropy loss of a confined polymer chain is larger for long chains compared to the short ones [Helfand (1967); Theodorou (1988)]. Therefore, in a polydisperse system, it is rational to have a surface region enriched with shorter chains. Surface segregation is more profound in flow regimes with high shear rate gradient such as capillary flow [Schreiber and Storey (1965); Schreiber *et al*. (1966); Shelby and Caflisch (2004); Musil and Zatloukal (2011, 2012a, 2012b);

Inn (2013); Rorrer and Dorgan (2014)]. While flow-induced fractionation may be difficult to occur over the finite distance of a capillary die, flow-induced diffusion or molecular fractionation over a small distance from the solid wall might possibly occur [Inn (2013)].

Musil and Zatloukal (2012a) analyzed the die drool phenomenon during extrusion of linear HDPE melts and found that the die drool sample has narrower MWD containing lower molecular weight chains compared to the rest of the extrudate. They reported that the flow induced fractionation takes place only in a very thin layer near the die wall and its onset and intensity is in direct relation with the onset and intensity of the slip [Musil and Zatloukal (2011, 2012a, 2012b)]. Furthermore, Inn (2013) reported flow-induced molecular fractionation in capillary extrusion of bimodal HDPEs, which results in higher concentration of low MW component near the wall and high MW one in the mid-plane. Therefore, the flow-induced fractionation has been proposed as a possible physical mechanism of polymer wall slip [Musil and Zatloukal (2011, 2012a); Inn (2013)]. Rorrer and Dorgan (2014) performed molecular scale simulations of cross flow migration in polymer melts under various conditions; quiescent, shear and parabolic flows. Their results show a small depletion of longer chains near the wall for quiescent and shear flow, and profound migration effects in the parabolic flow case where significant gradients in shear rate are present.

1.1.3.5 Surface roughness

Surface roughness has a profound effect on slip by decreasing it and delaying the transition from weak slip to strong slip to higher flow rates [Wang and Drda (1997); Mhetar and Archer (1998c); Legrand *et al*. (1998); Sanchez-Reyes and Archer (2003)]. Wang and Drda (1997) studied the effect of surface topology of capillary die surfaces on the stick-slip transition in the flow of polyethylene melts, and found that surface roughness increases the critical stress for the onset of stick-slip instabilities. Mhetar and Archer (1998c) compared the slip velocity of a polybutadiene on smooth and rough silica surfaces, and observed that the slip velocities on the rough surface are lower than on a smooth one. Moreover, they reported that the critical shear stress for the onset of macroscopic slip is 2.1 times higher in the case of rough silica surface, due to the differences in molecular relaxation dynamics over smooth and rough surfaces. Typical roughness of length scales used in these studies, are of a few micrometers, which are much larger than the coil size of a typical polymer chain, which is of the order of a few nanometers. Therefore, many chains can be trapped

in the space between the asperities and thus the polymer/wall interface is replaced with a corresponding polymer/polymer interface. A penetrable polymer/polymer interface is more favorable for the adsorption of bulk chains than an impenetrable polymer/wall surface. Therefore, the adsorbed polymer density per unit area, ν, is higher for rough surfaces. Based on the Brochard-Wyart and de Gennes' theory (1992) the slip length, b is inversely proportional to ν (adsorbed polymer density per unit area), resulting in decrease of slip length for rough surfaces. However, the critical shear stress for macroscopic slip is proportional to ν, bringing the stick-slip transition to higher shear stresses for the case of rough surfaces as verified by experimental data.

1.1.3.6 Surface energy

The presence of low surface energy coatings suppresses polymer adsorption and slip becomes easier. There are many studies reported in the literature on the effect of fluoropolymer-based coatings on the slip behavior of polymer melts [Hill *et al.* (1990); Hatzikiriakos and Dealy (1993); Hatzikiriakos *et al.* (1993); Kissi *et al.* (1994); Kanoh *et al*. (1997); Wang and Drda (1997); Mhetar and Archer (1998c); Anastasiadis and Hatzikiriakos (1998); Barone and Wang (2000)]. It was observed that the magnitude of the slip velocity scales with the work of adhesion of these interfaces [Hill *et al.* (1990); Hatzikiriakos and Dealy (1993); Hatzikiriakos *et al.* (1993), Anastasiadis and Hatzikiriakos (1998)]. Wang and Drda (1997) reported that coating the capillary dies with fluoropolymer eliminates the stick-slip instability of polyethylene flow, and yields massive slip. They concluded that this observation can be attributed to change of slip mechanism from disentanglement to direct chain detachment in the presence of fluoropolymer coating. Mhetar and Archer (1998c) showed that the slip velocity of polybutadiene increases on fluorocarbon coated silica surface in comparison with bare silica, but it is still lower than the expected slip over ideal nonadsorbing surfaces.

The presence of fluoropolymer-based coatings reduces the surface energy and the adsorbed polymer density per unit area. It results in increase of slip velocity by a certain amount, which is a function of the work of adhesion, W_{adh} defined by Israelachvili (1985):

$$W_{adh} = \gamma_{LV}(1+\cos\theta) \tag{1.14}$$

where γ_{LV} is the interfacial tension between the molten polymer and its vapor (air) and θ is the contact angle of the polymer in the melt state over the solid interface.

1.1.4 Slip models

It is proven that the no-slip condition is violated in polymer melts. Therefore, for understanding the true rheological behavior of these materials, it is necessary to determine their slip behavior under both steady state and dynamic conditions.

1.1.4.1 Static slip models

Most of the slip velocity models which have been proposed in the literature, are static (no time-dependence) models. In these models, the slip velocity depends only on the instantaneous value of wall shear stress (Archer, 2005). These static models can only predict the steady-state slip behavior of polymer melts and are not valid under transient flows as slip relaxation effects might become important. Ramamurthy (1986) studied wall slip of a series of polyethylenes using capillary rheometry and proposed a simple empirical power-law model. Similarly, Kalika and Denn (1987) analyzed wall slip and extrudate distortion in a linear low-density polyethylenes through capillaries. They reported the following relation for a power law fluid experiencing wall slip, similar to Equation 1.6;

$$\frac{8V}{D} = \frac{8V_S}{D} + \frac{4n}{3n+1}\left(\frac{\sigma_W}{K}\right)^{1/n} \tag{1.15}$$

Where D is the capillary diameter, V and V_S are the average flow velocity and slip velocity, respectively. σ_w is the pressure corrected wall shear stress, and K and n are the power law parameters evaluated under no-slip conditions. It is noted that $8V/D$ is equal to the uncorrected (apparent) shear rate.

Hatzikiriakos and Dealy (1991) carried out shear experiments for a high-density polyethylene using the sliding plate rheometer. They found that above a critical shear stress, polymer melt slips and the slip velocity, V_S is a power-law function of wall shear stress written as;

$$V_S = a\sigma_w^{\ m} \tag{1.16}$$

Their results showed that the slip coefficient, *a* increases strongly with temperature, while the slip power law exponent, *m* is practically independent of temperature.

Lau and Schowalter (1986) suggested a model to take into account the shear stress and temperature dependence of wall slip velocities. They applied the concept of junctions at the polymer/wall interface as well as in the bulk of the polymer fluid, and they combined their model with a kinetic equation describing a reaction between bonded and free macromolecules at the interface. The developed expression can be written as;

$$V_S = c_1(\sigma_w)^m \left[1 - c_2 \tanh\left(\frac{E - c_3\sigma_w}{kT}\right)\right] \tag{1.17}$$

Where E is the activation energy, T is the absolute temperature, k is the Boltzman constant, and c_1, c_2, and c_3 are the empirical fitting parameters. At constant temperature, a power-law constitutive equation relating the wall slip velocity to the wall shear stress is valid in agreement with other studies [Ramamurthy (1986); Kalika and Denn (1987)]. Model predictions were found to be consistent with data for an ethylene-propylene copolymer reported by Vinogradov and Ivanova (1967). Hatzikiriakos and Dealy (1992a) conducted capillary experiments for a series of high density polyethylenes. They proposed a similar slip velocity model using similar concepts to include the effect of temperature, first normal stress difference and molecular characteristics. The equation can be written as;

$$V_S = \xi_0 f_1(T)\left[1 - c_2 \tanh\left(\frac{E + c_3\sigma_n/\sigma_w}{RT}\right)\right]\left(\frac{\sigma_w}{\sigma_c PI^{1/4}}\right)^m \tag{1.18}$$

where ξ_0, c_2, and c_3 are empirical constants. $f_1(T)$ is either the WLF or the Arrhenius equation that models the temperature dependence of rheological properties, R is the universal gas constant, σ_c is the critical shear stress for onset of slip, σ_n is the normal stress at the wall, and PI is the polydispersity index.

1.1.4.2 Dynamic slip models

The aforementioned slip velocity models imply that the slip velocity adjusts instantaneously to the wall shear stress and they do not consider slip relaxation effects observed in transient flows. Therefore, dynamic models must be used in transient conditions to address these slip relaxation effects. Pearson and Petrie (1965) first proposed a memory (dynamic) slip model in which the slip velocity depends on the past states of the wall shear stress as;

$$V_S + \lambda_S \frac{dV_S}{dt} = f(\sigma_w) \tag{1.19}$$

Where λs is the slip relaxation time, and $f(\sigma_w)$ shows the slip dependency on wall shear stress based on the considered static slip model. If a power-law slip model is used [Kalika and Denn (1987); Hatzikiriakos and Dealy (1991)], Equation (1.19) becomes;

$$V_S + \lambda_S \frac{dV_S}{dt} = A' {\sigma_w}^m \tag{1.20}$$

Where *A'* is the slip coefficient and *m* is the slip power law exponent.

Hatzikiriakos and Dealy (1991) studied the slip behavior of a high-density polyethylene in steady and dynamic shear experiments using a sliding plate rheometer. Their observations have suggested the dependency of slip velocity to the past states of shear and normal stresses. Hatzikiriakos and Kalogerakis (1994) simulated the behavior of a polymer/wall interface by using a network kinetic theory, and performed Brownian dynamics, and thus developed a dynamic slip velocity model. Using this model, they predicted the steady-state slip of a high-density polyethylene satisfactorily. However, they could only describe the slip dynamics qualitatively. Hatzikiriakos (1994) extended this single-mode model to a multimode one to improve the predictions of the slip dynamics.

Graham (1995) studied large amplitude oscillatory shear flows of polymer melts between parallel plates and used a power-law dynamic slip model with non-zero slip yield stress. Its two-mode generalization reproduced experimental data reported by Hatzikiriakos and Dealy (1991). They suggested that both viscoelasticity and a dynamic slip model are necessary to explain the instabilities and nonlinear dynamics of polymer melts in oscillatory shear.

Lan *et al*. (2000) coupled the dynamic slip models with different nonlinear viscoelastic constitutive models, such as Wagner and Liu models [Wagner (1976); Liu *et al.* (1981)], to study slip of a linear low-density polyethylene in both steady and unsteady flows using a sliding plate

rheometer. The models gave good predictions of slip data in steady shear but showed insufficient gap dependence in exponential shear. They modified the slip model by raising the time derivative in Equation (1.20) to a power *p* as follows;

$$V_S + \lambda_S \left(\frac{dV_S}{dt} \right)^p = A' \sigma_w{}^m \tag{1.21}$$

Kazatchkov and Hatzikiriakos (2010) have extended Equation (1.20) by analogy to the derivation of the generalized Maxwell model for viscoelasticity;

$$V_{S,i} + \lambda_{S,i} \frac{dV_{S,i}}{dt} = A'_i \sigma_w{}^m \qquad \text{and} \qquad V_S = \sum_i V_{S,i} \tag{1.22}$$

Where $\sum_i A'_i = A'$

They combined this modified slip model with Wagner's constitutive equation to solve the transient shear response of a linear low-density polyethylene and observed improvement in predicting experimental data.

Kaoullas and Georgiou (2015) derived analytical solutions for the start-up of Newtonian Poiseuille and Couette flows with dynamic wall slip. Their results revealed that under dynamic slip conditions, the slip velocity depends not only on the instantaneous value of the wall shear stress, but also on its past states.

1.2 Knowledge gap

Despite many efforts on the measurement and prediction of wall slip velocity of polymer melts, the following gaps/concerns still remain:

- Limited studies are available on wall slip velocity of polymer melts considering the effect of polymer MW and more importantly the effect of MWD.
- There are very few studies on the effect of surface migration on slip velocity of polymer melts.

- There are few studies to systematically address the effects of surface roughness and energy on slip violations in polymer melts.
- The rheological behavior and wall slip of polymer melts need to be investigated thoroughly in transient flows.

It is important to comprehensively study the wall slip of polymer melts, considering the parameters such as MW, MWD, migration effects, surface roughness and energy, and slip relaxations in transient flow for fully understanding the true rheological behavior of polymer flows over solid surfaces. It is also equally important to include all these effects in a comprehensive, fully predictive model.

1.3 Research objectives

The main goal of this project is to fully explore and understand the effects of molecular weight and its distribution on the slip mechanism of polymers and propose a reliable model to address these effects. Moreover, it is important to study surface fractionation effects on the slip of polydisperse polymer melts. The effects of surface topology and energy would also be addressed as a part of this research. Although polyethylene is the main polymer of interest in this study, it is necessary to verify the reliability of the proposed model in predicting the slip velocity of other linear polymer melts. The objectives can be further detailed as follows:

1. To identify a suitable rheological model that can accurately capture the effect of molecular weight and its distribution on polymer wall slip quantitatively. This was addressed by studying the applicability of double reptation mixing rule of viscoelasticity.
2. To study surface fractionation effects on slip of polydisperse polymer melts particularly bimodal polymers. This was done by using a segregation model previously proposed in the literature to calculate the surface-MWD which dominates the slip.
3. To perform a series of slit experiments using dies with various surface topographies and treatments in order to study the effect of different physical and chemical characteristics of solid substrates on the slip velocity of entangled polymer melts.

4. To conduct a series of rheological experiments using a rotational rheometer equipped with a partitioned plate in order to study slip of polymers in transient flows at high shear rates and develop a reliable dynamic slip model to predict the rheological behavior and slip relaxation of polymers.

1.4 Thesis organization

The organization of this dissertation is as follows. A brief introduction to polymer wall slip is presented in Chapter 1. Literature review on experimental methods for quantifying slip, the mechanisms of slip, and the critical factors in polymer slip are also discussed in this chapter. Moreover, the gaps in knowledge and the thesis objectives are provided in Chapter 1. Materials and details of the apparatuses used in this study, including a rotational rheometer (AntonPaar MCR 502 or AntonPaar MCR 702 with parallel plate geometry and partitioned plate fixture), a capillary rheometer (Bohlin RH 2000), laser ablation and silanization and the methodology associated with these experimental techniques are described in Chapter 2. The molecular dependence of slip velocity for a series of commercial HDPEs of various MWs and polydispersities previously studied by Ansari et al. (2011, 2013b) is described in Chapter 3. The dependence of slip velocity of other families of polymers on the molecular characteristics is also discussed in this chapter. Furthermore, using the double reptation mixing rule, an equation is developed to calculate the slip velocity of linear polymers for any given MWD once the MW dependence of slip of their monodisperse counterparts is determined (Objective 1). Chapter 4 reports surface fractionation effects on slip of polydisperse polymer melts. In this chapter, the slip behavior of several high-density polyethylenes with broad range of molecular weight (MW) including bimodals is studied as a function of molecular weight (MW) and its distribution. A model of surface MW fractionation is used to predict the surface MWD, and a formulation similar to the double reptation theory is used to predict the slip velocity of the studied polymers as a function of surface-MWD (Objective 2). Chapter 5 presents the slip behavior of high-density polyethylenes (HDPEs) over surfaces of different topology and surface energy. Roughness and surface energy effects were incorporated into the double reptation slip model to predict the slip velocity of studied polymers on different substrates (Objective 3). Chapter 6 includes a series of rheological experiments using a rotational rheometer

equipped with a partitioned plate fixture in order to study slip of polymers in transient flows and develop reliable dynamic slip models (Objective 4). Finally, chapter 7 summarizes the concluding remarks of this thesis and provides recommendations for future studies.

Chapter 2: Materials and Experimental Methods

This chapter describes the materials and the experimental methods used in this study. The instruments include a rotational rheometer equipped with parallel plate and parallel partitioned plate fixtures, and a pressure driven capillary rheometer to fully study the rheological behavior of the materials. Moreover, in order to study effect of surface characteristics on polymer wall slip, femtosecond laser irradiation was used to pattern die surfaces. Some of the substrates were also subjected to silanization to reduce their surface energy.

2.1 Materials

In this study, several industrial grade HDPEs with different MW and MWD supplied from ExxonMobil Chemical Company are used. Moreover, the slip velocity data of two groups of HDPEs provided by Chevron Phillips Chemical Company, namely Ziegler-Natta (ZN-HDPEs) with unimodal MWD and metallocene (m-HDPEs) with bimodal distribution, reported by Ansari *et al*., (2013b) is investigated in the present study. The rheological characterization of these resins and their processability in terms of their melt fracture performance have been reported by Ansari *et al*., (2011) and Ansari (2012d). Furthermore, the slip data for a linear bimodal HDPE studied by Inn (2013) is analyzed. The slip data for nearly monodisperse polybutadienes (PBDs) reported by Mhetar and Archer (1998b, 1998c) and the slip data for nearly monodisperse polystyrenes (PSs) studied by Awati *et al.* (2000) are also used in our analysis. TABLE 2.1 lists the polymers used in the experimental part of this study along with their MW characteristics.

TABLE 2.1: List of HDPEs used in this study and their different moments of molecular weight.

Resin	M_n (kg/mole)	M_w (kg/mole)	$PI=M_w/M_n$
HDPE-1	16.2	51.8	3.2
HDPE-2	9.1	223.8	24.6
HDPE-3	8.2	212.4	26.0

2.2 Rotational rheometer

Rotational rheometry is a powerful technique for measuring the rheological behavior of polymer melts and other complex fluids. It can be used to determine different rheological characteristics of the sample by rotating, oscillating or applying a step function either by controlling the torque (stress controlled) or angular motion (strain controlled). Studied polymers are characterized using stress/strain controlled AntonPaar MCR502 and MCR702 TwinDrive rheometers. Small amplitude oscillatory shear (SAOS) or frequency tests were performed using MCR502 with the 25-mm parallel disk geometry and a gap of 1 mm. However, due to the well-known edge fracture instability, it is impossible to obtain reliable rheological data of viscoelastic polymer melts at high shear rates and strains using the conventional parallel plate geometries [Larson (1992); Macosko (1994); Dealy and Wissbrun (2012)]. Therefore, the start-up of shear experiments were conducted using the parallel partitioned plate geometry mounted on MCR702 TwinDrive rheometer. All experiments were run under nitrogen gas to avoid any thermal degradation. More details of the different types of fixtures used are given below.

2.2.1 Parallel plate (PP) geometry

Parallel plate geometry is the most extensively used rheological fixture to produce simple shear flows. As depicted in FIGURE 2.1, it consists of two parallel concentric disks with specific diameter and distance between them (gap). The upper disk can rotate with respect to the other to produce shear flow. This geometry is essentially used to measure the linear viscoelastic properties of polymer melts. Advantages of a parallel plate (PP) system is that relatively small amount of material is required and cleaning and preparation are quick and easy. Also, due to the adjustable gap, various measuring conditions can be set. On the other hand, non-uniform shear strain and inability to reach high shear rates and strains due to edge fracture are its disadvantages [Dealy and Wang (2013); Macosko (1994)]. Important equations for this geometry are listed below by using cylindrical coordinates [Macosko, 1994].

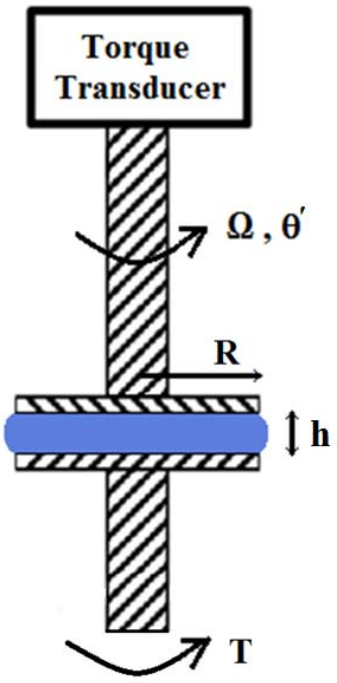

FIGURE 2.1: Schematic representation of parallel plate geometry.

Shear stress,

$$\sigma_{12} = \sigma_{\theta Z} = \frac{T}{2\pi R^3}[3 + \frac{d \ln T}{d \ln \dot{\gamma}_R}] \tag{2.1}$$

$$\sigma_A = \frac{2T}{\pi R^3}, \qquad \text{Newtonian shear stress} \tag{2.2}$$

Shear strain at radial distance r,

$$\gamma = \frac{\theta' r}{h} \tag{2.3}$$

Shear rate at $r=R$,

$$\dot{\gamma}_R = \frac{R\Omega}{h} \tag{2.4}$$

Where, T is the torque, R is the disk radius and h is the distance between parallel disks. θ' and Ω are rotation angle and rate, respectively.

Anton Paar, MCR-502 with parallel-plate geometry was used to study the linear viscoelastic (LVE) properties of the HDPEs. The frequency sweep tests were carried out over a wide range of temperatures from 150 to 230ºC. The curves at various temperatures were shifted using the time-temperature superposition (TTS) to generate the master curves at the reference temperature of 190ºC.

2.2.2 Parallel partitioned plate (PPP) geometry

This geometry allows measuring the non-linear shear flow behavior of polymer melts, which suffer from edge fracture in regular parallel plate geometries. Reliable data can be obtained with this system at high shear rates and strains by avoiding effects of edge fracture [Meissner *et al.* (1989), Snijkers and Vlassopoulos (2011)]. In this fixture, another partition has been added, only to shield off the edge fracture. As shown in FIGURE 2.2, the top geometry consists of a standard 8 mm plate attached to the transducer (center plate), and a coaxial stationary ring (partitioned plate). The transducer takes into account only torque contributions from the center plate. Therefore, the effects of the edge fracture will be postponed to higher shear rates and strains. Small amount of sample, and no need for sample trimming are other advantages of this fixture. It is worth mentioning that the present setup is specifically made for rheometers with two motors. AntonPaar MCR 702 TwinDrive with partitioned parallel plate geometry is used to study the non-linear viscoelastic behavior and dynamic slip of HDPEs by conducting step-strain stress relaxation experiments for shear strains ranging from 0.05 to 10 and the start-up of steady shear experiments for shear rates in the range of 0.05 to 20 s^{-1}.

FIGURE 2.2: Schematic representation of the partitioned parallel plate geometry.

2.3 Capillary rheometer

Capillary rheometer is an effective instrument for measuring the viscosity of polymer melts at high shear rates comparable to industrial processing conditions. FIGURE 2.3 shows the schematic representation of the capillary rheometer. It consists of a reservoir/barrel with a die connected to its bottom using a die holder. The polymer melt in the barrel is forced to move through the die by pressure imposed from the plunger. The force needed for moving the plunger (pressure drop) and the velocity of the plunger are the raw data obtained from this rheometer. Apparent shear rate, $\dot{\gamma}_A$ and wall shear stress, σ_w can be calculated based on the following relations [Macosko (1994)];

$$\dot{\gamma}_A = \frac{4Q}{\pi R^3} \tag{2.5}$$

$$\sigma_w = \frac{R\Delta p}{2L} \tag{2.6}$$

Where Q, Δp, R and L are volumetric flow rate, applied pressure, die radius and die length, respectively. Similarly, for a rectangular channel (slit) of height H and width W with $W >> H$, so that end effects can be neglected, the following expressions can be derived;

$$\dot{\gamma}_A = \frac{6Q}{WH^2} \tag{2.7}$$

$$\sigma_w = \frac{H\Delta p}{2L} \tag{2.8}$$

In this project, extrusion experiments were performed using a pressure-driven constant-speed capillary rheometer (Bohlin RH 2000). The HDPE melts were extruded at 190 ºC in order to study their slip behavior.

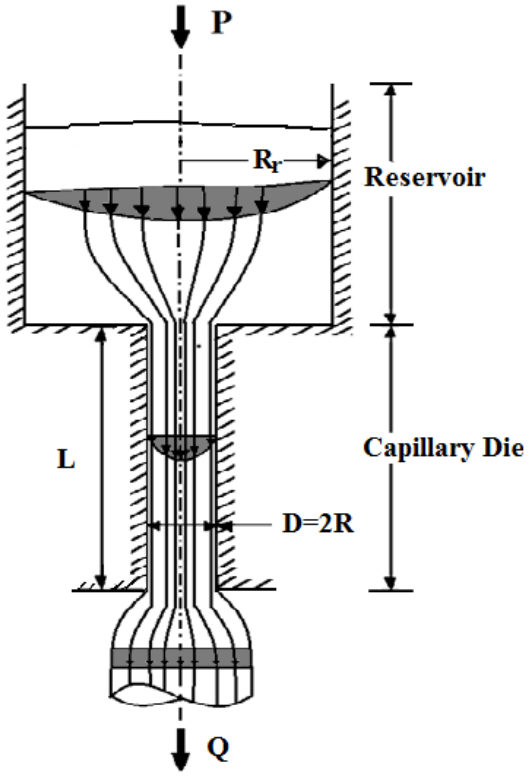

FIGURE 2.3: Schematic representation of the capillary rheometer [adapted from Macosko (1994)].

2.4 Surface laser irradiation

In order to study the effect of surface characteristics on polymer wall slip, laser irradiation was used to ablate the surfaces of the slit dies to produce different micro/nano structured patterns [Kietzig *et al.* (2009); Moradi *et al.* (2013, 2015)]. In particular, ultrashort laser pulses generated by an amplified all solid-state Ti:Sapphire laser were used to irradiate various substrates in this case stainless steel (SS) surfaces. The laser system includes a Ti:Sapphire seed laser Coherent Mira HP and an amplifier Coherent Legend to produce amplified femtosecond laser pulses with center wavelength of 800 *nm* and a linear translation stage. The beam profile from this regenerative amplifier system has a Gaussian distribution with a beam average wave length of 10 *mm*. Neutral density (ND) filters were used to adjust the laser energy and a lens with 300 *mm* focal length was used to focus the beam on the sample. The focused beam spot size ($2\omega_0$) was 30 μm that has been calculated using following equation;

$$2\omega_0 = \left(\frac{4\lambda'}{\pi}\right)\left(\frac{F}{D'}\right) \tag{2.9}$$

Where λ' is laser wavelength, F is the focal length of the lens (300 *mm* in this set up) and D' is the beam waist (10 *mm*). The schematic representation of this set up is displayed in FIGURE 2.4. In order to move the samples under the laser beam, the SS slit dies were mounted on a computer-controlled ZABER T-LS80 X-Y translation stage with a maximum linear speed of 4000 and step resolution of less than 0.1 μm. By changing the power of the laser beam, Φ and the scanning speed, V', different surface patterns with different height and diameter of the asperities, pitch size and amount of nano-scale features are produced. The samples were irradiated in air environment and then subjected to an ultrasonic bath for 2 min in acetone to remove all the debris off the patterned surfaces.

Using this technique, various patterns of controlled microstructure morphology can be produced consisting of microbumps covered with superposed submicron size nano-features. Figure 2.5. shows such a typical surface whose effect on slip is examined in chapter 5.

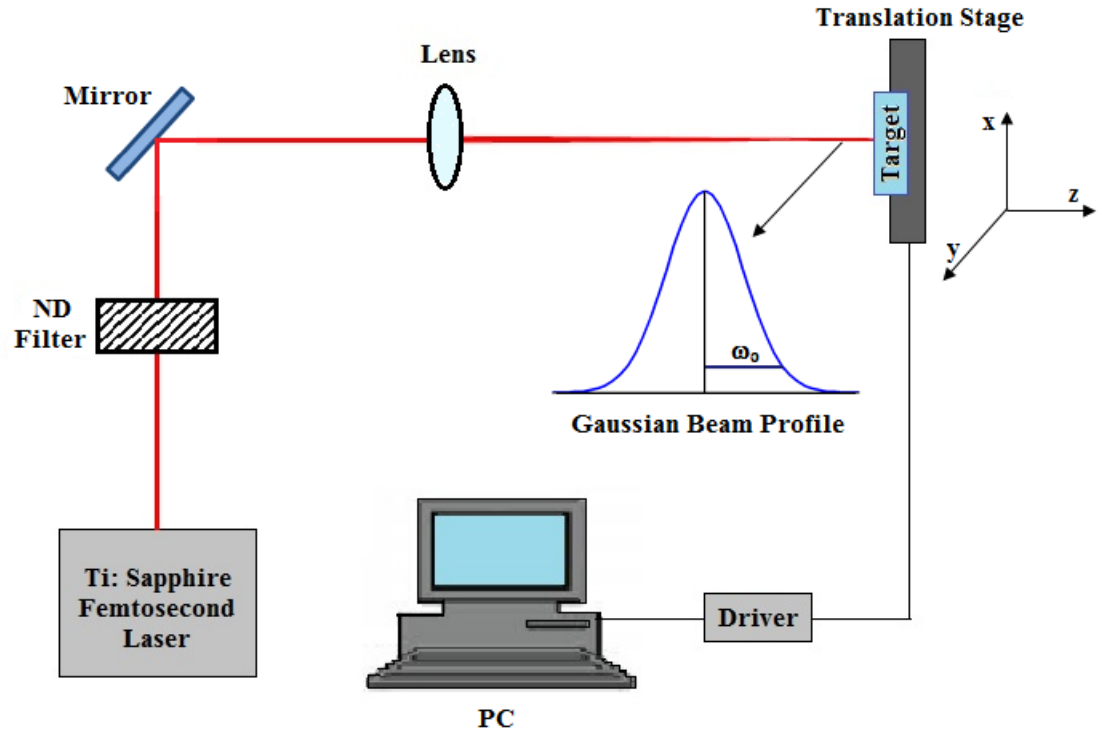

FIGURE 2.4: Schematic representation of the laser irradiation set-up [adapted from Moradi (2014)].

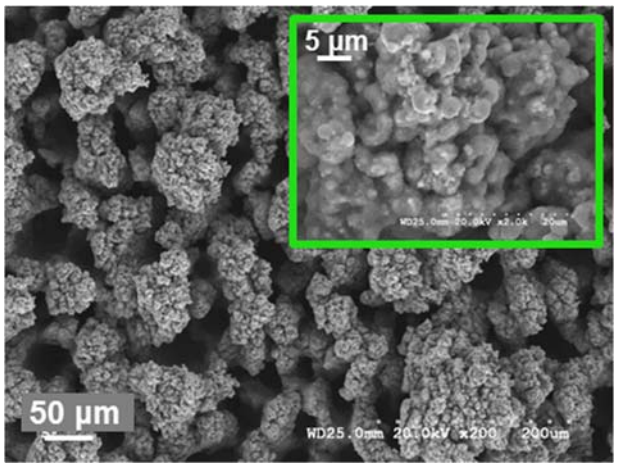

FIGURE 2.5: SEM images of the fabricated micro/ nano-patterned stainless steel (SS) surface with $\Phi = 465$ J/cm^2, and $V' = 370$ µm/s.

2.5 Silanization coating

To alter the surface energy of the nanopatterns such as that depicted in Figure 2.5, solution based dip-coating method was used to coat the surfaces of the slit dies. By this technique, fluoro groups have been deposited on the surface, resulting in reduction of surface energy [Moradi (2014)]. By acid treatment, hydroxyl groups are exposed on the metal substrates. The silanization process occurs by hydrogen bonding between silane solution and hydroxyl groups on the substrates [Chovelon *et al.* (1995)]. The alkylsilane coatings used in this study are rather stable due to the cross-polymerization of alkylsilane chains [Sagiv (1980)]. The fluoroalkylsilane used in this study is trichloro (1,1,2,2-perfluorooctyl) silane ($C_6F_{13}CH_2CH_2$ Si Cl_3), FTS, 97%.

This method consists of four steps discussed below. First, the fluorinated alkyl silane is hydrolyzed by absorbing water. Second, the SS slit dies were immersed in a Pirhana solution composed of H_2SO_4/H_2O_2 (4:1 v/v) for 1 hour at room temperature to remove any contamination and expose the hydroxyl groups on metallic surfaces. After acid treatment, the surfaces were rinsed with distilled water, acetone and ethanol, respectively for 10 minutes in ultrasonic bath. Third, the pretreated dies were immersed in 0.5% wt. FTS in n-hexane (0.075 *gr* per 10 *ml* of n-hexane) for 1 hour at 70°C. In this step, hydrogen bonds form between hydroxyl groups on the substrate and hydrolyzed fluorinated alkyl silane groups. Moreover, cross-links between silane groups form in this step. Finally, in the last step, the samples were heated at 120°C for 30 mins and then at 70°C over night to remove water molecules and stabilize the coating. FIGURE 2.6 displays these steps [Moradi (2014)].

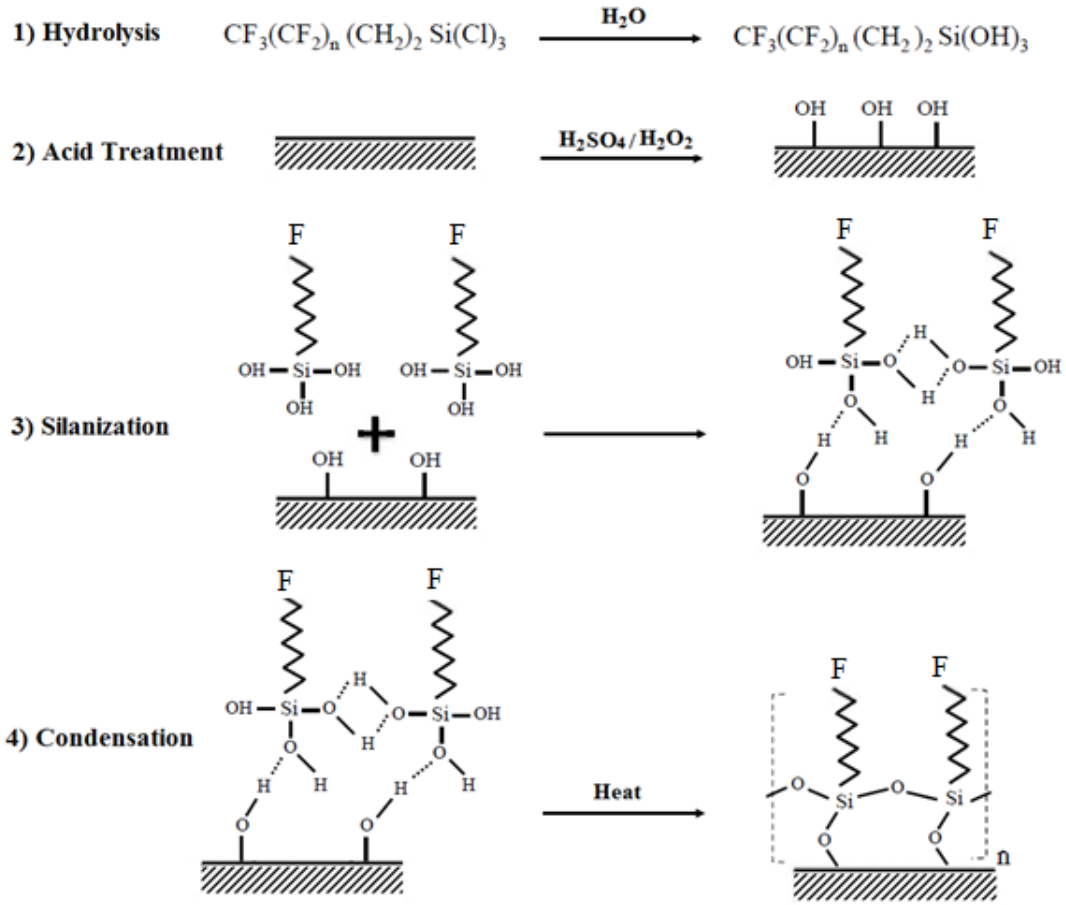

FIGURE 2.6: Schematic diagram of the four steps of coating a metallic substrate using fluorinated alkylsilane [adapted from Moradi (2014)].

Chapter 3: Wall Slip of Linear Polymers Using Double Reptation Mixing Rule

In this chapter, the slip behavior of different linear polymers is analyzed in term of their MW characteristics to fully understand their effects. Studying the slip data for nearly monodisperse PBDs reported by Mhetar and Archer (1998b, 1998c) and nearly monodisperse PSs studied by Awati *et al.* (2000) shows that the slip velocity, V_S, increases with decrease of molecular weight. It scales with weight or number average molecular weight (due to monodispersity) as $V_S \propto M_w^{\beta}$, where β is related to the flexibility of the polymer and ranges between 1.9 to 3.2 [Chatzigiannakis *et al*. (2017)]. Moreover, in this chapter, several polydisperse high-density polyethylenes (HDPEs) reported by Ansari *et al.* (2012d, 2013b) are studied as a function of molecular weight (MW) and its distribution for a broad range of molecular weight distributions (MWDs). Concepts from double reptation theory [Tuminello (1986), des Cloizeaux (1988, 1990), Tsenoglou (1991)] are used to develop a theoretical expression to relate slip velocity with molecular weight and its distribution for these polymers. Moreover, the slip velocity of linear polymers scales nonlinearly with the wall shear stress, namely, $V_S \propto \sigma_W^m$ [Hill *et al*. (1990); Hatzikiriakos and Dealy (1992a)]. Using de Gennes' theory (1992) for slip, the values of m reported in the literature are explained on a theoretical basis and they are found to be equal to $1/n$, where n is the local slope of the flow curve of the corresponding polymer, $n \equiv d\log(\sigma_w)/d\log(\dot{\gamma}_w)$, which changes from 1 (Newtonian flow regime) to n in the power law flow regime.

3.1 Results and discussion

3.1.1 Slip of monodisperse polymers

There are only a few sets of experimental data on the slip velocity of monodisperse polymers having various MWs, namely PBDs [Mhetar and Archer (1998b, 1998c)] and PSs [Mackay and Henson (1998), Awati *et al*. (2000)]. Mhetar and Archer (1998b, 1998c) using a tracer particle velocimetry technique in simple shear flow, studied the slip behavior of a series of narrow molecular weight distribution PBD melts of various molecular weights ranging from 70.0 to 540.8 *kg/mol* (see TABLE 3.1).

FIGURE 3.1 (a) shows plots of slip velocity, *Vs* versus wall shear stress, σ_w for these polymers in the weak slip regime adopted from Mhetar and Archer (1998b). As expected, in this regime the slip velocity is dependent on MW of polymers and it decreases by increasing MW. Using the scaling, $V_S \propto M_w^{-1.94}$, the slip data of various PBD melts can be superposed well resulting a master curve as illustrated in FIGURE 3.1 (b).

Awati *et al.* (2000) investigated slip velocity of nearly monodisperse polystyrenes of various molecular weights, ranging from 24.5 to 393 *kg/mol* (reported in TABLE 3.2), in a parallel plate geometry using the gap-dependence technique. Their results in the weak slip regime, are shown in FIGURE 3.2 (a). Similarly, their reported slip data can be brought to a master curve by assuming $V_S \propto M_w^{-3.2}$ as depicted in FIGURE 3.2 (b). Therefore, for monodisperse polymers, the slip velocity can be written as;

$$a_T a_p V_S = A M_w^{\beta} \sigma_w^m \tag{3.1}$$

Where V_S is the slip velocity, a_T is the temperature dependence of slip velocity, similar to that of viscosity [Ansari *et al*. (2013b)], a_p is the pressure dependence of slip velocity [Hill *et al*. (1990); Hatzikiriakos and Dealy (1992b)], A and β are constants which depend on the polymer structure and the entanglement molecular weight (the origin of slip due to partial disentanglement), M_w is the weight average molecular weight and σ_W is the wall shear stress. The dependence of slip velocity on shear stress; $V_S \propto \sigma_W^m$ and the exponent m are explained and discussed in detail later. The values of A and β calculated from FIGUREs 3.1 (b) and 3.2 (b) for the cases of monodisperse PBD and PS respectively, are listed in TABLE 3.3. The entries in TABLE 3.3 for the case of HDPEs are the calculated values using the slip velocity data of polydisperse HDPEs and after performing necessary corrections for the polydispersity effects using a method explained later. The difference in the exponent β between PBD and HDPE with that of PS might be due to the difference in the flexibility of their chains (as described by the molecular weight between entanglements, M_e). At a given M_w, the number of entanglements, M_w/M_e, in PS melts is much smaller (weakly entangled polymers) and since slip depends on M_w/M_e, it is perhaps expected to

depend strongly on M_w. For flexible polymer macromolecules, such as PBD, and HDPE, $V_s \propto M_w^{-2}$ can show the MW dependence of slip velocity. However, for stiffer macromolecules such as PS, $V_s \propto M_w^{-3.2}$ is the accurate scaling in agreement with experimental data. These findings are compared with theoretical models on slip later in this Chapter.

TABLE 3.1: List of PBDs analyzed in this study and their different moments of molecular weight [Mhetar and Archer (1998b)].

Resin	M_n (kg/mol)	M_w (kg/mol)	$PI=M_w/M_n$
PBD67	67.3	70.0	1.04
PBD86	86.5	90.0	1.04
PBD129	129.3	133.2	1.03
PBD176	176.4	181.7	1.03
PBD253	207.0	215.3	1.04
PBD315	285.0	296.4	1.04
PBD650	515.0	540.8	1.05

TABLE 3.2: List of PSs analyzed in this study and their average molecular weight [Awati *et al.* (2000)].

Resin	$M_n \sim M_w$ (kg/mol)
25k	24.5
100k	104
200k	198
400k	393

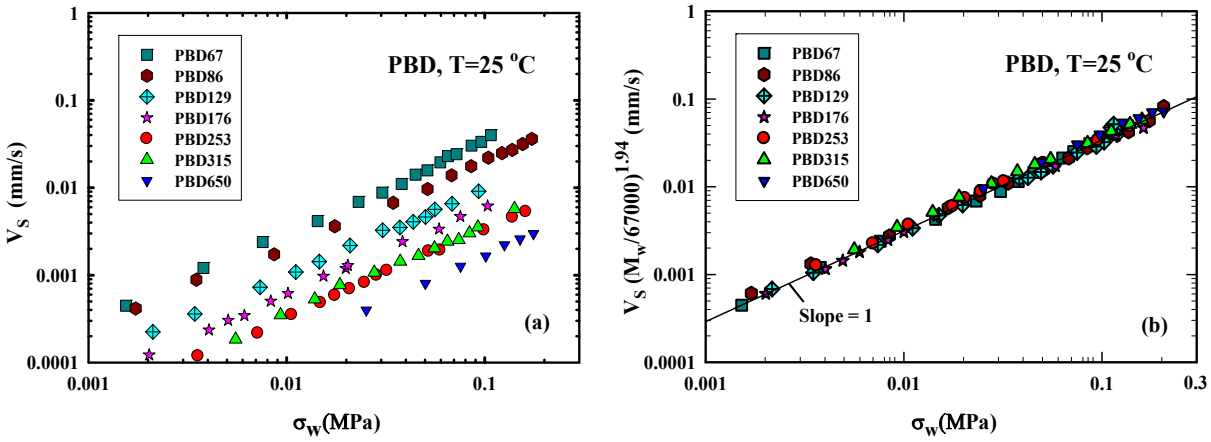

FIGURE 3.1: **(a)** Plots of slip velocity, *Vs* versus wall shear stress, σ_w in weak slip regime for PBD melts reported by Mhetar and Archer (1998b, 1998c). **(b)** Normalized slip velocity versus wall shear stress, showing a dependence of $V_S \propto M_w^{-1.94}$.

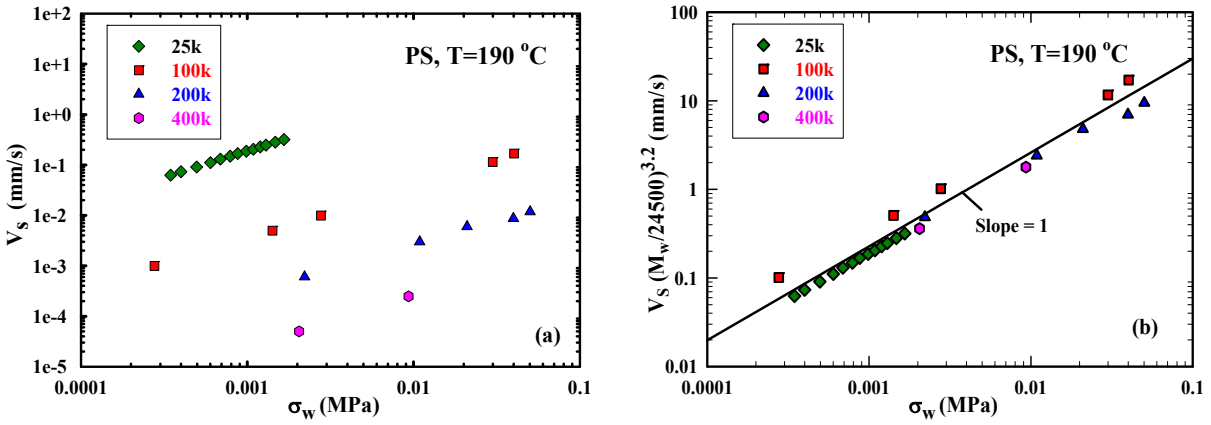

FIGURE 3.2: **(a)** Plots of slip velocity, *Vs* versus wall shear stress, σ_w in weak slip regime for PS melts reported by Awati *et al.* (2000) **(b)** Normalized slip velocity versus wall shear stress, showing a dependence of $V_S \propto M_w^{-3.2}$.

TABLE 3.3: List of parameters for the molecular weight dependence of slip velocity.

Polymer	A (mm.MPa^{-m} s^{-1})	β	m	T (°C)	p	M_e [a] (g/mol)
***PBD*[b]**	8.50×10^{8}	-1.94	1.03	25	1 atm	1,850
***PBD*[c]**	1.06×10^{10}	-1.94	1.03	190	1 atm	1,850
PS	3.80×10^{16}	-3.20	1.06	190	1 atm	14,900
***HDPE*[d]**	1.00×10^{10}	-2.00	2.5 – 3.3	190	p	1,200
HDPE	2.90×10^{10}	-2.00	2.5 – 3.3	190	1 atm	1,200

[a] *The values of M_e for PE and PS were obtained from Vega et al. (2004), essentially calculated from: $M_e = 4\rho RT / 5G_N^0$ at 190 °C, for PBD was obtained from Struglinski and Graessley (1985) where ρ is density and G_N^0 is plateau modulus.*

[b] *The slip velocity of PBDs were determined on glass surfaces, while those of PS and HDPE refer to metallic ones (Stainless Steel and Tungsten Carbide respectively).*

[c] *The value A for PBD was corrected for the effect of temperature based on the Arrhenius equation [Ngai and Plazek (1985)].*

[d] *The value of pressure, p, corresponds to a capillary die of L/D=16. The value of A for HDPE was corrected for the effect of pressure (listed in the above Table and entered in the last row) based on results reported by Hatzikiriakos and Dealy (1992a).*

3.1.2 Slip of polydisperse HDPEs

FIGURE 3.3 (a) plots the slip velocity data of several HDPEs studied and reported by Ansari *et al*. (2013b). Some of these polymers have different molecular weights and about the same polydispersity and thus the effect of M_w on slip could be studied independently. The slip velocity increases with decrease of molecular weight, M_w consistent with observations for PBDs reported by Mhetar and Archer (1998b, 1998c) and PSs reported by Awati *et al.*, (2000). Analysis of these data revealed the scaling $V_S \propto M_W^{-2}(PI)^3$ that superposes the data well, where PI is the polydispersity index defined by $PI \equiv M_w / M_n$ [Ansari *et al.* (2013b)]. An overall good

superposition is obtained with most points to fall within ±40% of the line passing through the data (FIGURE 3.3 (b)). However, the scaling $V_S \propto M_w^{-2}(PI)^3$ is not very helpful in revealing the exact dependence of slip velocity on details of the MWD (tails at either end of the distribution or other deviations from the log-normal distribution) and therefore a different method is needed to take into account the details of the MWD. In addition, the line with slope of 1 in FIGURE 3.3 (b) (note that data is plotted versus σ_w^3) passes through the experimental data and seems to describe them well (represents a master curve in view of the scaling $V_S \propto M_w^{-2}(PI)^3$). However, as it will be discussed below the slope of V_S versus σ_w depends on the rheology of the individual polymers. Therefore, the double reptation mixing rule is used to calculate the fundamental constants of A and β for the case of HDPE (describe the effect of MWD and listed in TABLE 3.3) in the absence of slip data for monodisperse HDPEs to fully understand MWD dependency of slip velocity. Moreover, the procedure outlined below is also a method to calculate the slip velocity of any HDPE polymer possessing an arbitrary MWD once the A and β values are determined.

For the studied HDPEs, a log normal distribution was found to describe the detailed MWD quite well as seen from FIGURE 3.4. The weight fraction distribution is expressed as follows;

$$w(M) = \frac{1}{(2\pi)^{1/2}} \frac{1}{\sigma_{std}} \frac{M^{A^*}}{B\overline{M}_m^{A^*+1}} \exp\left[\frac{-(\ln M - \ln \overline{M}_m)^2}{2\sigma_{std}^2}\right] \tag{3.2}$$

Where

$$B = \exp\left[\frac{\sigma_{std}^2}{2}(A^*+1)^2\right] \tag{3.3}$$

σ_{std} is the standard deviation for this distribution, $\overline{M}_m$ is the median value, M is the molecular weight, and A^* is a constant. These parameters along with the MW characteristics of these polymers are listed in TABLE 3.4.

TABLE 3.4: List of MW characteristics and log normal parameters for MWD of studied unimodal HDPEs.

Resin	M_n (kg/mol)	M_w (kg/mol)	PI=M_w/M_n	σ_{std}	A^*	$\overline{M_m}$(kg/mol)
ZN-HDPE-0	23.0	328.4	14.3	1.82	0.86	187.3
ZN-HDPE-5	18.7	328.7	17.6	1.87	0.8	189
ZN-HDPE-6	26.8	296.2	11.1	1.63	1.31	232.5
ZN-HDPE-10	29.6	320.3	10.8	1.72	1.01	272.6
ZN-HDPE-11	26.6	290.4	10.9	1.73	1.10	180.1
ZN-HDPE-12	22.8	291.0	12.8	1.74	1.00	222.5
ZN-HDPE-13	21.8	270.4	12.4	1.77	1.02	137.4
ZN-HDPE-14	21.7	259.6	12.0	1.78	0.94	154.6
ZN-HDPE-15	18.0	228.3	12.7	1.77	0.80	197.7
ZN-HDPE-16	16.0	193.3	12.1	1.69	0.85	211.9

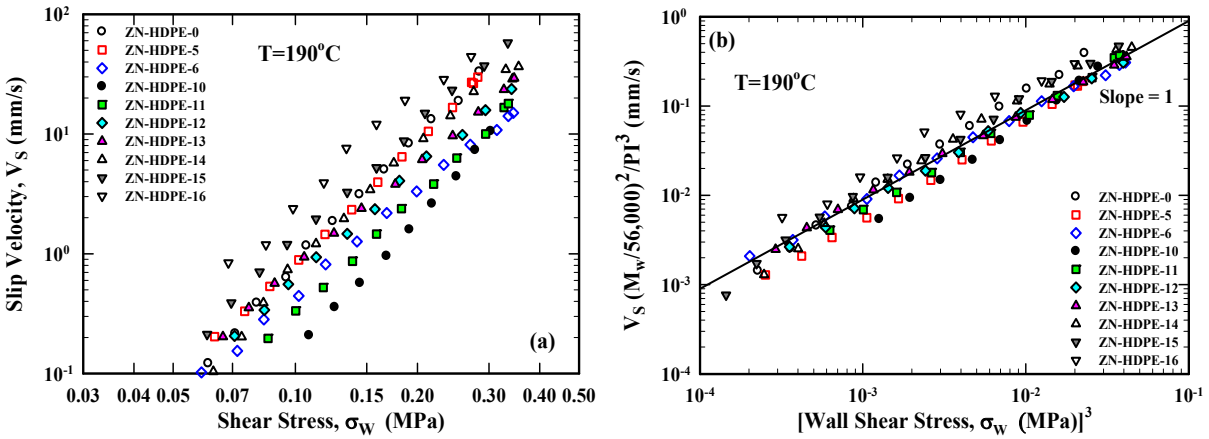

FIGURE 3.3: **(a)** The slip velocity of polydisperse HDPEs studied by Ansari *et al.* (2013b). **(b)** Using the scaling, $V_S \propto M_w^{-2}(PI)^3$, a master curve is produced [adopted from Ansari *et al.* (2013b)].

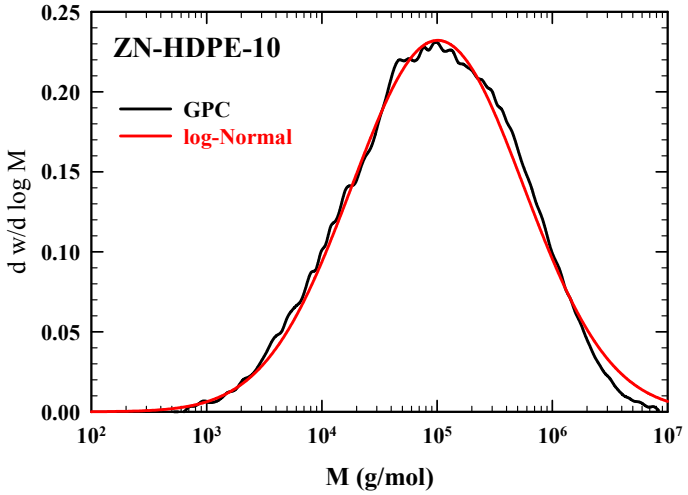

FIGURE 3.4: Typical molecular weight distribution of a polydisperse HDPE and its representation using the log normal distribution (Equation 3.2).

3.1.3 Power law exponent in slip law

As discussed above, several published data (most of them for PEs) have correlated the slip velocity with wall shear stress using Equation 3.1, $a_T a_p V_S = A M_w^{\beta} \sigma_w^m$, where m is the power-law exponent of slip velocity model. The power-law dependence of the slip velocity on wall shear stress and the exact value of the exponent m are discussed in this section. The starting point to determine the exponent m is the expression for the slip velocity for a given temperature and pressure in terms of the extrapolation length, b (Equation 3.4), based on an interfacial rheological law for the case of a passive polymer/wall interface (no interaction between the polymer and solid surface) proposed by Navier (1823) as follows;

$$V_S = b\left[\frac{dV}{dy}\right]_{y=0} = b\dot{\gamma}_w = \left[\frac{b}{\eta}\right]\sigma_w \tag{3.4}$$

Where V_S is the slip velocity, b known as extrapolation or slip length, $\dot{\gamma}_w$ is the wall shear rate (slope of the velocity profile at the wall), η is the melt viscosity at $\dot{\gamma}_w$ and σ_w is the wall shear stress (refer FIGURE 3.5).

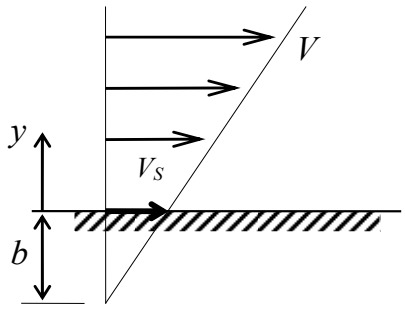

FIGURE 3.5: Navier's idealized view of wall slip in shear flow of molten polymers.

Experimental evidence has shown that the extrapolation length, *b* is constant at small values of the wall shear rate i.e. for small slip velocities (weak slip regime). At higher shear rate values, it is proportional to wall shear rate in the marginal regime, where stick-slip transition occurs before it becomes again constant when complete disentanglement occurs (strong slip regime) [Leger *et al*. (1997), Durliat *et al*. (1997)]. Similar results have been reported for PBDs [Sabzevari *et al*. (2014)] where *b* is independent of shear rate in weak and strong slip regimes.

In the present work, we consider weak slip regimes of flow in which extrapolation length, *b* is independent of shear rate and nearly constant. FIGURE 3.6 shows that the extrapolation length is constant for several studied HDPEs as a function of the shear rate corrected for the effect of slip, $\dot{\gamma}_{A,S}$. The data shows that *b* may be taken as a constant over a wide range of shear rates span over two decades. Using that $b = b_0 = constant$, Equation 3.4 becomes;

$$V_S = \left[\frac{b_0}{\eta}\right]\sigma_w \tag{3.5}$$

At small wall shear rate values, the viscosity is a constant and equal to zero-shear viscosity, η_o (Newtonian regime). In these cases, the slip velocity from Equation 3.5 becomes $V_s = \left(b_o / \eta_o\right)\sigma_w$, which implies $V_s \propto \sigma_w$ typically reported for PBDs [Mhetar and Archer (1998b, 1998c)], and PS [Awati *et al*. (2000)] where slip measurements were performed at conditions where the viscosity is close to its Newtonian value and nearly constant. However, at higher shear

rates, the viscosity strongly depends on shear rate and typically exhibits shear thinning behavior. Assuming a power law dependence of viscosity on the shear rate ($\eta = K\dot{\gamma}_w^{n-1}$ or $\sigma_w = K\dot{\gamma}_w^n$) and substituting to Equation (3.5), the following relationship can be easily derived;

$$V_S = \left[\frac{b_0}{K^{1/n}}\right]\sigma_w^{1/n} \tag{3.6}$$

Therefore, the exponent of the shear stress power-law dependence of slip velocity is 1/*n*, which is the inverse exponent of the power-law dependence of shear stress on shear rate. In the general case *n* represents the local slope of the flow curve, $n \equiv d\log(\sigma_w)/d\log(\dot{\gamma}_w)$. Viscosity power law exponents *n* of typical polyethylenes studied in terms of their slip velocity, are in the range from 0.3 to 0.4. Thus, the expected slip power law exponents are *m*=1/*n*=2.5 to 3.3, values typically reported in the literature (see TABLE 3.5) [Blyler *et al.* (1970), Funatsu and Kawijara (1988), Lupton and Regester (1965), Worth *et al.* (1977), Hatzikiriakos and Dealy (1992a), Ansari *et al.* (2013b)].

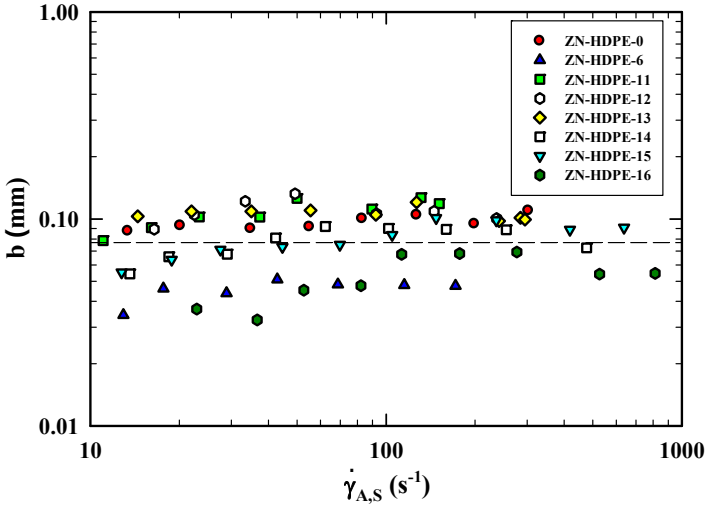

FIGURE 3.6: The extrapolation length of several HDPEs as a function of the true shear rate at 190°C.

TABLE 3.5: The power-law exponent of slip velocity model reported in the literature.

Resin (Type of Polymer)	Reference	*m*
HDPE	Blyler and co-workers (1970)	3.18, 2.90, 2.62 (various MWs)
	Funatsu and Kawijara (1988)	3.65
	Lupton and Regester (1965)	1.92
	Worth and co-workers (1977)	2.31
	Hatzikiriakos and Dealy (1992a)	2.86-3.58 (various MWs)
	Ansari *et al*. (2013b)	3

FIGURE 3.7 simulates the slip velocity of ZN-HDPE-6 (Equation 3.6) using its complex viscosity as a function of shear stress/complex modulus in a single graph. At small shear stress values, where the behavior of the polymer is almost Newtonian (n=0.92) and the viscosity approaches the Newtonian plateau, the slip velocity scales linearly with the wall shear stress ($V_s \sim \sigma_w$). Experimental data for HDPEs at these small shear rates is not available. However, the slope of 1 has been typically reported in slip studies for other systems such as PDB and PDMS at diminishingly small values of shear rate [Migler *et al*. (1993, 1994); Leger *et al*. (1997); Mehtar and Archer (1988a, 1988b, 1988c)]. As shear stress increases, shear thinning occurs. In this region, there is a power law relationship between the slip velocity and shear stress ($V_s \sim \sigma_w^{1/n} = \sigma_w^m$) with the value of m increasing gradually from 1 to about 3 (value depends on n). Experimental results are also shown in the graph that are in good agreement with the calculations. Therefore, the reported values of m in the literature depend on the rheological power-law exponent n as well as on the range of wall shear stress values over which the slip velocity has been studied and reported.

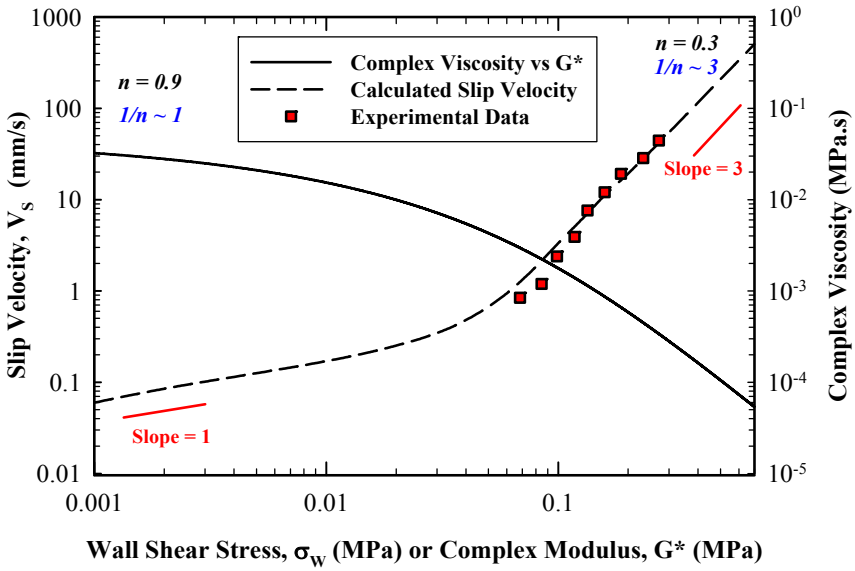

FIGURE 3.7: Slip velocity and complex viscosity versus wall shear stress/ complex modulus for ZN-HDPE-6 melt.

3.1.4 Double reptation theory for calculating slip

The double reptation (mixing rule) theory for stress relaxation in polydisperse entangled melts presents a relationship between molecular weight distribution and dynamic viscosity as well as other rheological material functions [Tuminello (1986), des Cloizeaux (1988,1990), Tsenoglou (1991)]. Using this theory, the rheological properties of polydisperse polymers can be calculated once the corresponding values of monodisperse polymers and the detailed molecular weight distribution are known. For example, the zero-shear viscosity of a polydisperse linear polymer can be expressed as a function of the integral of the stress relaxation function and can be written as [Milner (1996)];

$$\eta_0 \propto \int_0^\infty \left[\tau(N) w(N) \int_N^\infty w(N') dN' \right] dN \tag{3.7}$$

Where $\tau(N)$ is the reptation time of chains length N and $w(N)$ is the volume fraction of chains of length N. The double integral represents the concept of double reptation mechanism, which assumes that the entanglement ability of polymers is defined by the presence of heteropolymer neighbors and the associated entanglement stresses could relax whenever the shorter chain is able

to reptate its free end through the entanglement [des Cloizeaux (1988,1990); Tsenoglou (1991)]. Since $\tau(N)$ scales with N to the power of 3 ($\tau(N) \propto N^3$), the zero-shear viscosity has also a power law dependence, which is in agreement with the fundamental relation for the viscosity of polymers that the zero-shear viscosity scales with $\eta_0 \propto M_w^{3.4}$ (monodisperse linear polymers).

As discussed above, it has been demonstrated that the slip velocity is a strong function of molecular weight and its distribution [Mhetar and Archer (1998b, 1998c), Wang and Drda (1996a, 1996b), Awati *et al*. (2000), Hatzikiriakos and Dealy (1992a), Ansari *et al*. (2013b)]. The origin of the molecular weight dependence of slip arises from the strong molecular weight dependence of the melt viscosity in the entanglement regime. Based on a theory proposed by Brochard *et al*. (1992), the extrapolation length, *b* relates to melt viscosity as follows [Wang and Drda (1996a, 1996b)];

$$b = \left[\frac{\eta}{\eta_i}\right]\alpha \tag{3.8}$$

Where η_i is the viscosity of the melt in the interfacial layer, and α is the layer thickness of the order of monomer length. Using this relation, Equation 3.4 becomes;

$$V_S = \left[\frac{\eta}{\eta_i}\right]\alpha\dot{\gamma}_w = \left[\frac{\eta}{\eta_i}\right]\alpha\frac{\sigma_w}{\eta} = \frac{\alpha\sigma_w}{\eta_i} \tag{3.9}$$

where η_i depends on the number of entanglements between the moving and adsorbed chains and decreases with increasing stress due to stretching of the chains at the interface. Experimental results have proven that by increasing the molecular weight, the number of entanglements increases and the slip of polymer chains decreases [Mhetar and Archer (1998b, 1998c), Mackay and Henson (1998), Awati *et al*. (2000), Ansari *et al*. (2013b), Inn (2013)]. Based on these experimental results, the fact that both the slip velocity and the viscosity are functions of the number of entanglements and in view of Equation 3.9, it is reasonable to conclude that there is a relationship between the viscosity and slip velocity and therefore the concept of double reptation for calculating slip velocity seems applicable. Moreover, double reptation can be viewed as a mixing rule, which is simply applied to calculate the slip velocity of polydisperse polymers.

The starting point for developing the expression for the slip velocity of polydisperse system (excluding the effects of temperature and pressure) is Equation 3.1, that is $a_T a_p V_S = A M_w^{\beta} \sigma_w^m$ and in particular the scaling $V_S \propto M_w^{\beta}$. As discussed above, both the viscosity and slip velocity are related to the number of entanglements. Thus, the molecular weight dependence of slip velocity can be analogous to that of viscosity. Using the double reptation blending rule for calculating the zero-shear viscosity (Equation 3.7) and taking the slip dependence of monodisperse polymers on M_w to be $\sim M_w^{\beta}$ as Equation 3.1 implies, Equation 3.10 can be derived for the slip velocity of a polydisperse system having a molecular weight distribution given by *w(M);*

$$a_T a_P V_S = A\left\{\int_0^{\infty}\left[M^{\beta} w(M)\int_M^{\infty} w(M')dM'\right]dM\right\}\sigma_w^{1/n} = Af(M)\sigma_w^{1/n} \tag{3.10}$$

This relation includes the dependence of the slip velocity on both the molecular weight and its distribution in place of the scaling $V_S \propto M_w^{-2}(PI)^3$ reported by Ansari *et al.* (2013b). Equation 3.10 is tested in this section to identify how well it represents the slip velocity data of the polydisperse HDPEs presented above. To test this, the optimum values of A and β are calculated to result a master curve for the slip velocity of studied HDPEs independent of their molecular weight distributions. These values are listed in TABLE 3.3 with A=1.0×10^{10} mm.MPa^{-m} s^{-1} and $\beta = -2.0$. These values can be used to calculate the slip velocity of monodisperse HDPEs through Equation 3.1. In fact, Equation 3.10 is reduced to Equation 3.1 for monodisperse polymers. Once the A value is corrected for the effect of pressure [Hatzikiriakos and Dealy (1992a)] to calculate its value at atmospheric pressure (the A values for PS and PBD refer to atmospheric pressure) results a value of 2.90×10^{10} (also listed in TABLE 3.3).

The reduced slip velocities of all HDPEs for which the MWD were available to perform the calculations, are plotted in FIGURE 3.8. The slip velocity data shown in FIGURE 3.3(a) are shifted vertically by an amount equal to Af(M) (exact form seen in Equation 3.10) and the resulted curve is plotted as a function of $\sigma_W^{1/n}$. Most of the points are falling on the line with slope equal to 1, indicating that Equation 3.10 represents the data well, within ±30%. This is satisfactory as an error in wall shear stress of 10% can reflect an error in the calculated slip velocity value of ~ $(1.1)^3$

that is 33%. Moreover, since the power-law dependence of slip velocity on wall shear stress is different for different HDPEs (exponent is 1/*n*), the single values of A and β represent the data very well. Note the difference between FIGURE 3.3 (b) and FIGURE 3.8. Obviously, Equation 3.10 provides a better representation of the data compared to the simple empirical scaling of $V_S \propto M_w^{-2}(PI)^3\sigma_w^3$. This will be more evident below when the predictions of Equation 3.10 are compared directly with the slip velocity of the various HDPEs (see FIGURE 3.9).

Comparing the slip velocity of the three classes of polymers, at a given shear stress and molecular weight value, PS melts slip more due to the lower number of entanglements. The magnitude of the slip is indicated by the function AM_w^{β}. For example, for $M_w = 50\ kg/mol$, AM_w^{β} gives values for the three classes of polymers, which as ratios are PS/HDPE/PBD =35/11.8/8.2. These ratios become smaller with increase of M_w and for $M_w = 100\ kg/mol$, they are PS/HDPE/PBD =3.8/2.9/2.1. Overall, HDPE and PBD slip about the same (similar M_e and thus similar number of entanglements), while PS melts slip more (M_e of PS is 12.5 times higher than that of HDPE and thus the number entanglements are significantly lower that causes the higher slip).

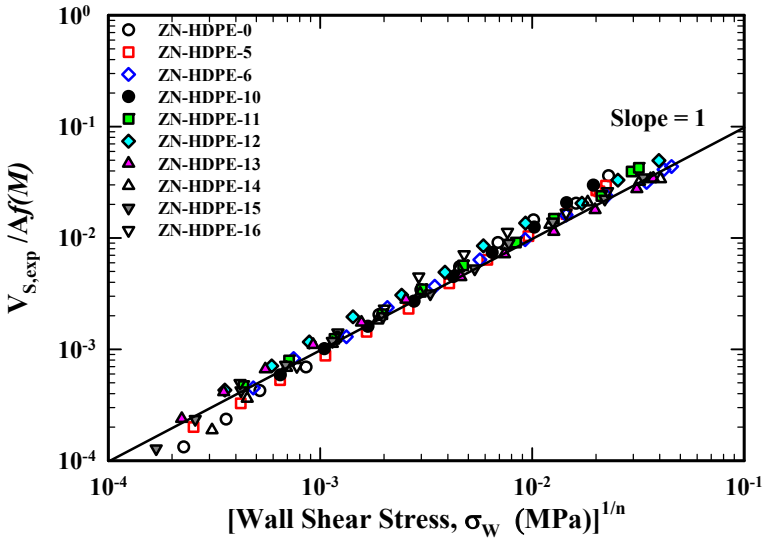

FIGURE 3.8: The reduced slip velocity of several polydisperse HDPEs studied by Ansari *et al.* (2013b) versus $\sigma_W^{1/n}$.

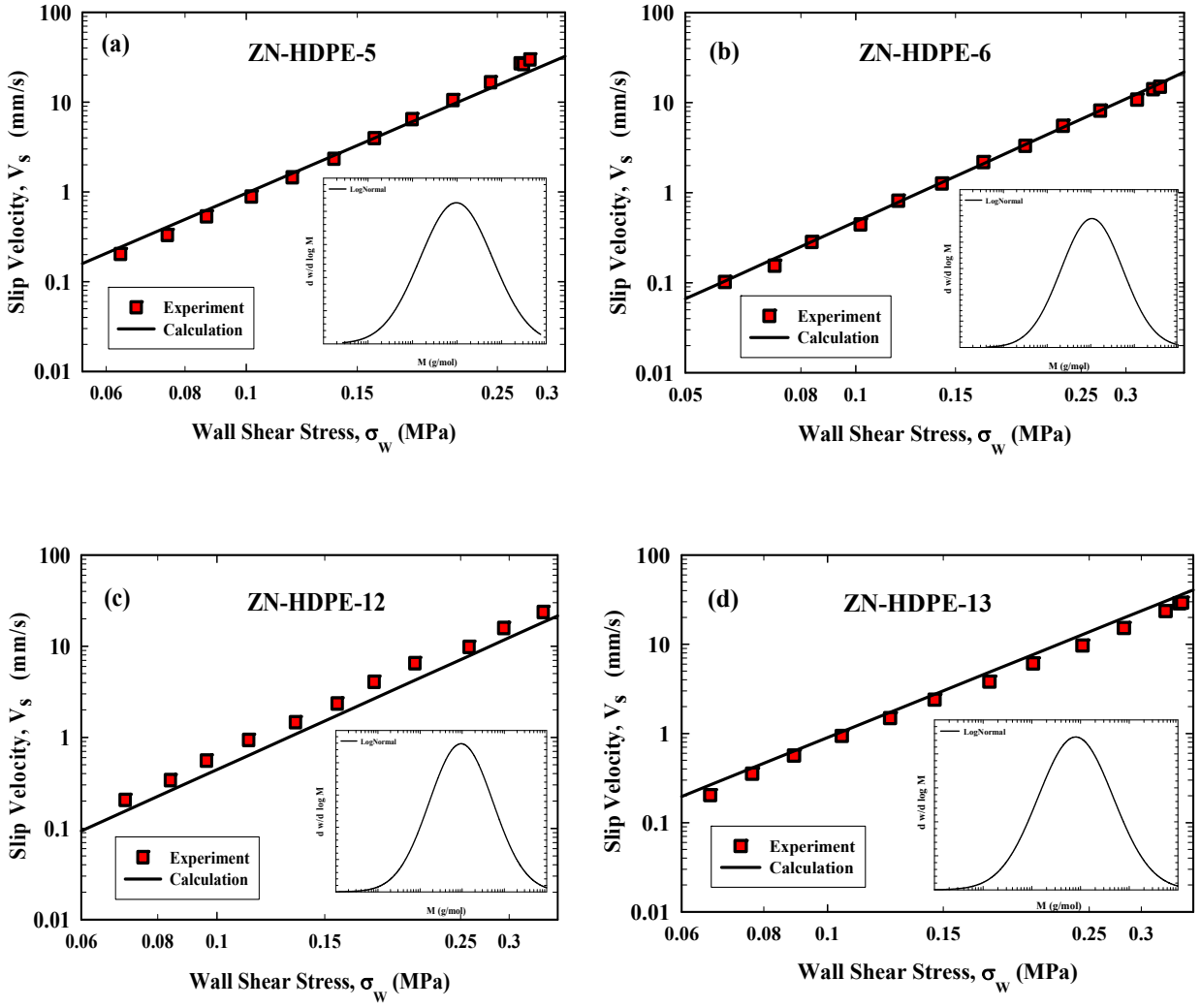

FIGURE 3.9: The slip velocities of some of the HDPEs with different MW and MWD **(a)** ZN-HDPE-5, **(b)** ZN-HDPE-6, **(c)** ZN-HDPE-12, and **(d)** ZN-HDPE-13. Experimental results are shown with symbols and the calculated slip velocity using Equation 3.10 is shown by solid line. The inset shows the MWD based on log normal distribution.

3.1.5 Sensitivity of slip to MW and MWD

In order to study the sensitivity of our proposed model to M_w and its distribution, Equation 3.2 (the log normal distribution) was used to generate five different molecular weight distributions with the same polydispersity (PI=10) and various M_w ranging from 50 to 250 kg/mol. TABLE 3.6

lists the parameters of Equation 3.2 to generate these distributions. Furthermore, five different molecular weight distributions with the same weight average molecular weight (M_w=200 kg/mol) and different PIs (from 6 to 18) were generated in a similar manner. The parameters of Equation 3.2 to generate these MWDs are listed in TABLE 3.7.

TABLE 3.6: The log normal distribution coefficients (Equation 3.2) of polymers with different Mws and same PI=10

Mw	**50k**	**100k**	**150k**	**200k**	**250k**
A^*	0.9	0.9	0.9	0.9	0.9
σ_{std}	1.52	1.52	1.52	1.52	1.52
$\overline{M}_m$ *(kg/mol)*	195.36	390.71	468.85	586.06	781.42

TABLE 3.7: The log normal distribution coefficients (Equation 3.2) of polymers with different PIs and same Mw=200 kg/mol.

PDI=M_w/M_n	**6**	**9**	**12**	**15**	**18**
A^*	0.9	0.9	0.9	0.9	0.9
σ_{std}	1.048	1.339	1.482	1.576	1.646
$\overline{M}_m$ *(kg/mol)*	14319.87	2713.12	1025.29	514.04	300.89

The viscosity material functions needed for the slip velocity calculations (to calculate the exponent 1/*n* only) were generated using double reptation theory [des Cloizeaux (1988,1990), Tsenoglou (1991)] and specifically the method illustrated by Jam *et al*. (2012) was used. The generated viscosity curves for the two series of HDPEs with MWD coefficients listed in TABLEs 3.6 and 3.7 are depicted in FIGUREs 3.10 (a) and 3.11 (a). Equation 3.10 is used to predict the slip velocity of these polymers at different shear stress values (FIGUREs 3.10 (b) and 3.11 (b)). As seen, the slip velocity increases by decreasing the M_w (FIGURE 3.10 (b)) and broadening the MWD (increasing the PI) (FIGURE 3.11 (b)). At small shear stress values, the slope of V_s with shear stress is 1, in agreement with the 1/*n* law (Newtonian plateau), and gradually increases to 3 or higher depending on the power law exponent, *n*, of the viscosity curve of the corresponding

polymer [Mhetar and Archer (1998b, 1998c); Awati *et al*. (2000); Hatzikiriakos and Dealy (1992a); Inn (2013); Ansari *et al*. (2013b)].

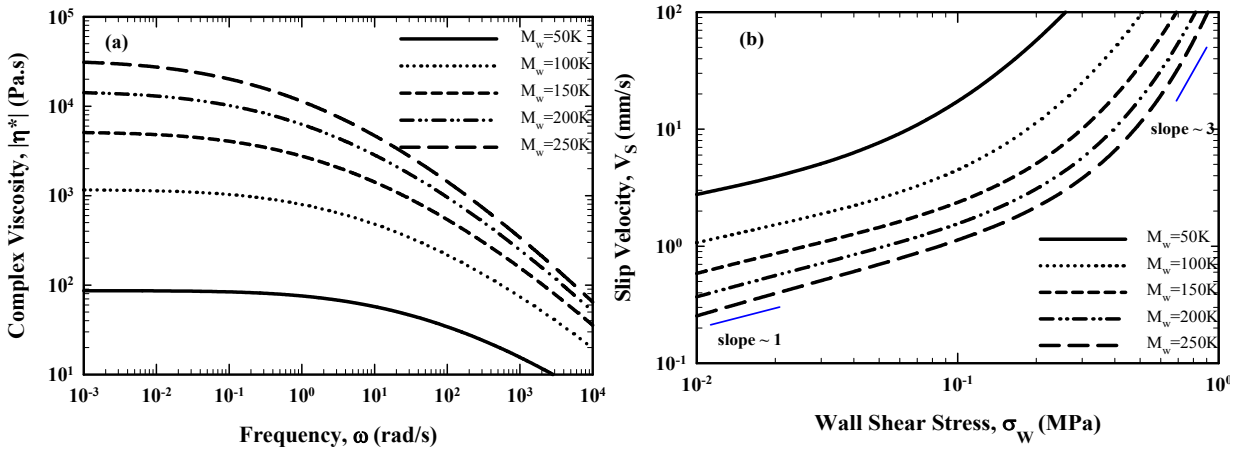

FIGURE 3.10: **(a)** The simulated viscosity curve of HDPEs with different M_w listed in TABLE 3.6 predicted by double reptation [Jam *et al*. (2012)]. **(b)** The calculated slip velocity based on Equation 3.10 using the viscosity curves depicted in FIGURE 3.10 (b).

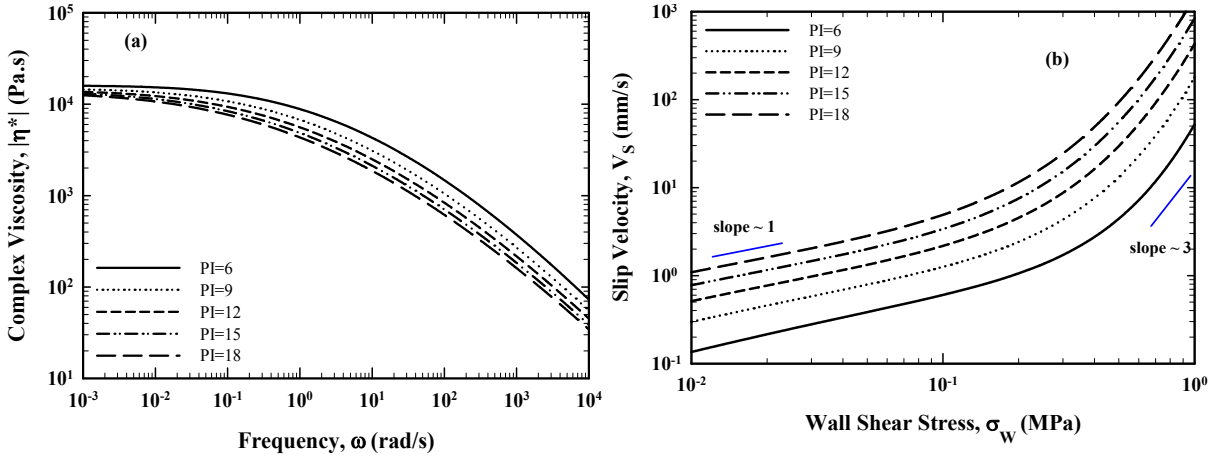

FIGURE 3.11: **(a)** The simulated viscosity curve of HDPEs with different polydispersities in TABLE 3.7 predicted by double reptation [Jam *et al*. (2012)]. **(b)** The calculated slip velocity based on Equation 3.10 using the viscosity curves depicted in FIGURE 3.11 (a).

Another interesting case worthwhile of examining is how tails at the two ends of a MWD affects the slip velocity of HDPEs. To study this, the following distributions were generated with details listed in TABLE 3.8. Starting with a log normal molecular weight distribution (first entry in TABLE 3.8, labelled as HDPE A), a 10 wt% of a small molecular weight HDPE (second entry in TABLE 3.8 labelled as HDPE B) was added, producing a distribution with a shoulder at the low end (see inset of FIGURE 12 (b)) whose molecular weight characteristics listed in TABLE 3.8 (labelled as 90%A+10%B). Finally, a 10 wt% of a high molecular weight HDPE (third entry in TABLE 3.8 labelled as HDPE C) was added to HDPE A, producing a distribution with a shoulder at the high end (see inset of FIGURE 12 (b)) whose molecular weight characteristics listed in TABLE 3.8 (labelled as 90%A+10%C). The addition of 10% of small molecules does not change significantly the viscosity material function, as it is the case with the addition of larger molecules. In spite of this, the addition of small molecules increases more dramatically its slip behavior at high shear stress values, which are of more interest to practical applications. On the other hand, large molecules decrease the slip of polymers more dramatically at relatively small shear stress values causing processability problems (large pressure drops needed for their flow).

TABLE 3.8: The log normal distribution parameters (Equation 3.2) and the molecular characteristics of polymers whose viscosity and slip velocity curves are simulated in FIGUREs 12 (a) and (b).

Resin	**Log normal Distribution Coefficients**			**MWD moments**		
	A^*	σ_{std}	$\overline{M}_m$ [kg/mol]	M_n [kg/mol]	M_w [kg/mol]	$PI=M_w/M_n$
HDPE A	1	1.6	500	23	300	13
Low Mw HDPE (B)	1	0.8	1300	3.4	6.5	1.9
High Mw HDPE (C)	1	0.8	415000	1084	2055	1.9
90% A + 10%B	--	--	--	14.7	270	19
90% A + 10%C	--	--	--	25.8	475	19

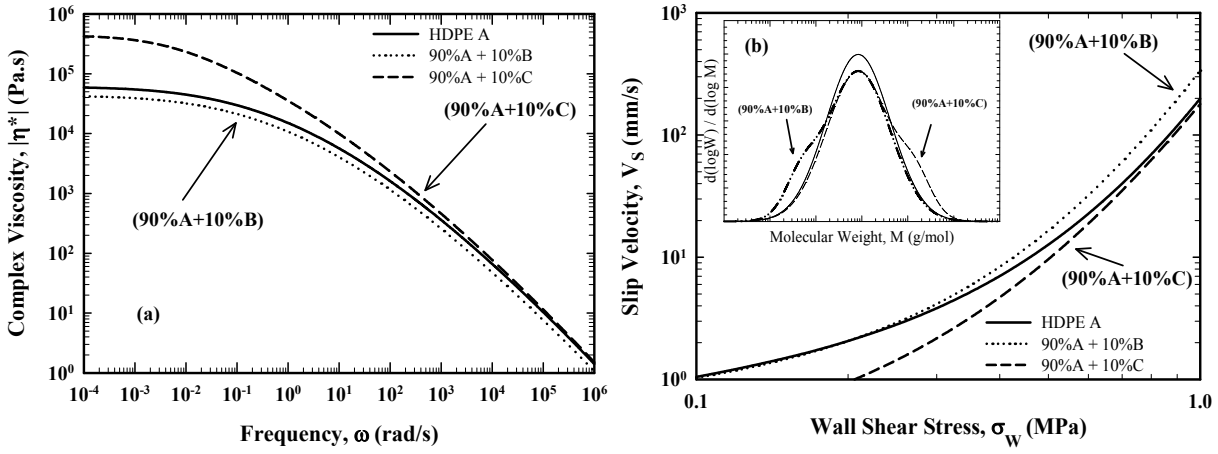

FIGURE 3.12: **(a)** The simulated viscosity curve of HDPEs with MW distributions depicted in the inset of FIGURE 3.12 (b) with the coefficients of the distributions listed in TABLE 3.8. **(b)** The calculated slip velocity of HDPEs based on Equation 3.10 using the viscosity curve depicted in FIGURE 3.12 (a). Note how a small shoulder at the low end of the MWD increases the slip velocity of the polymer.

3.1.6 Theoretical models on dependence of slip velocity on molecular weight

Most of the molecular models on slip of polymers on grafted surfaces are based on the assumption that slip velocity depends on the characteristic relaxation time of the bulk and grafted chains [Adjari *et al*. (1994), Mhetar and Archer (1998a), Joshi *et al*. (2001), Joshi and Lele (2002), Tchesnokov *et al*. (2005)]. Adjari *et al.* (1994) considered deformation of grafted chains in the flow and proposed three different relations between the applied shear stress and slip velocity at different flow regimes. In the intermediate regime, which is of interest in polymer processing, the grafted chains can relax by arm retraction (AR) and/or constraint release (CR) (in a way similar to star polymers), but not with reptation mechanism as they are tethered (FIGURE 3.13) [Mhetar and Archer (1998a. 1998b), Joshi *et al*. (2001), Joshi and Lele (2002), Tchesnokov *et al*. (2005)].

In this section, the origin of the scalings $V_s \propto M_w^{-2}$ that has been found experimentally for flexible macromolecules such as HDPE, and PBD [Ansari *et al.* (2013b), Mhetar and Archer (1998a, 1998b)] and $V_s \propto M_w^{-3.2}$ reported by Awati *et al.* (2000) for stiffer PS macromolecules are examined based on theoretical models [Chatzigiannakis *et al.* (2017a)].

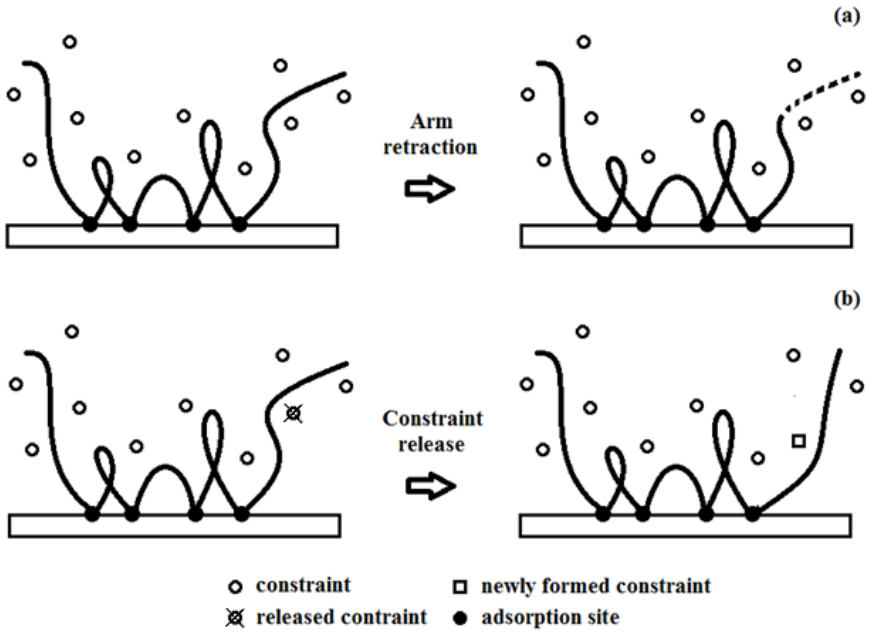

FIGURE 3.13: The two main relaxation mechanisms of an adsorbed chain: (a) Arm retraction and (b) Constraint release. An adsorbed chain is assumed to develop multiple contacts with a high energy surface, thus creating multiple segments that relax independently [adopted from Chatzigiannakis *et al.* (2017a)].

3.1.6.1 Arm retraction mechanism

In the Arm Retraction (AR) case, it is assumed that the melt chains are extremely long, and behave as a permanent network [Adjari *et al*. (1994)]. In this case, the head of the chain is stretched and forms a straight tube (stick consisting of z* monomers) followed by a ball consisting of z monomers, with number of monomers of the whole chain, $N = z + z^*$. The friction that the stick experiences is monomeric and the friction force required to cause disentanglement is equal to $F_e = kT/D_e$, where $D_e \cong \alpha N_e^{1/2}$ is the diameter of the tube, α is the monomer length, and N_e the number of monomers between entanglements. Therefore, the grafted chain can only relax by arm retraction and the slip velocity is given by:

$$V_s = \frac{D_e}{\tau_{AR}(z)} \tag{3.11}$$

where $\tau_{AR}(z)$ is the characteristic relaxation time due to arm retraction of the ball consisting z monomers. According to Adjari *et al*. (1994);

$$\tau_{AR}(z) \cong \tau_1 N^2 \exp\left(\frac{\mu z^2}{N_e N}\right) \tag{3.12}$$

where τ_1 is a microscopic jump time, μ is a numerical coefficient ($\mu=15/8$), and N is the number of monomers of the whole chain. In high energy surfaces, it is assumed that only 5% of the grafted chain monomers are directly attached to the surface [Scheutjens and Flreer (1979, 1980), Tchesnokov *et al*. (2005)]. Therfore, the length of the ball that is not stretched and contribute to relaxation is much smaller than that of the whole chain $N >> z$. In this case the exponential part of Equation 3.12 simplifies to unity as follows;

$$\tau_{AR}(z) \propto N^2 \tag{3.13}$$

By considering that the tube's diameter in the intermediate regime is independent of chain length, N [Adjari *et al*. (1994)], and combining Equations 3.11 and 3.13, the scaling $V_s \propto N^{-2}$ or $V_s \propto M_w^{-2}$ is obtained for monodisperse polymers.

The values of A, and β for different polymers are listed in TABLE 3.3. The exponent β is equal to -1.94 for PBD and -2 for HDPE. Therefore, it implies $V_s \propto M_w^{-2}$ for these polymers similar to $V_s \propto N^{-2}$, showing that arm retraction can be a possible relaxation mechanism for these polymers' slip. However, CR is also expected to occur in parallel with AR and, the analysis of the CR relaxation mechanism is essential in order to fully understand the mechanisms contributing to MW dependence of slip velocity.

3.1.6.2 Constraint release mechanism

If the melt chains are not too long, they can relax at a much faster rate than arm retraction due to constraint release mechanism [Adjari *et al*. (1994)]. In this case (chain pulled through a melt), the grafted chain forms the shape of a Zimm-like trumpt and a ball and, the tail can only relax by constraint release. The slip velocity is given by [Adjari *et al*. (1994)];

$$V_s \cong \frac{R(z)}{\tau_{CR}(z)} \tag{3.14}$$

where $R(z) \cong \alpha(z)^{1/2}$ is the radius of the coil (ball) relaxing with constraint release and $\tau_{CR}(z)$ is the characteristic relaxation time due to the constraint release mechanism given by;

$$\tau_{CR}(z) = \tau_{rep}(N)\left(\frac{z}{N_e}\right)^2 = \tau_1 \frac{N^3}{N_e}\left(\frac{z}{N_e}\right)^2 \propto N^3 z^2 \tag{3.15}$$

where z is the number of monomers of the grafted chain that relax by CR, N the number of monomers of the chains in bulk and $\tau_{rep}(N)$ their relaxation time due to reptation. Combining Equations 3.14, 3.15, and $R(z) \propto z^{0.5}$ results in following relation;

$$V_s \propto N^{-3} z^{-1.5} \tag{3.16}$$

By taking into account that the length of the tail is much smaller than that of the whole chain $N >> z$, the dependency of slip velocity on z becomes negligible. Therefore, relaxation is dominated by the reptation of bulk chains, and the scaling $V_S \propto N^{-3}$ or $V_S \propto M_w^{-3}$ is obtained similar to the experimental findings for PS [Awati *et al.* (2000)].

3.2 Conclusions

In this chapter, the slip velocity of several linear polymers, namely, PBD, PS and HDPE was studied in an attempt to elucidate the effects of molecular weight and its distribution. The double reptation mixing rule was used to develop a general expression to calculate the dependence of the slip velocity on molecular weight and its distribution. The derived relation was used to calculate the slip velocity of several polydisperse HDPEs (with different MW and MWD) and good agreement between experimental and calculated results was observed. It was further explained that the slip velocity is a function of the wall shear stress to an exponent *m* which is equal to inverse of the local slope of the flow curve of the corresponding polymer, *n*. Moreover, the dependence of slip velocity on molecular weight was explained based on theoretical models. For highly entangled flexible polymers such as PBD and HDPE, arm retraction is the dominant

mechanism of relaxation resulting in scaling $V_s \propto M_w^{-2}$. However, for stiff polymers with high entanglement molecular weights such as PS, constraint release is the main relaxation mechanism leading to the relation $V_S \propto M_w^{-3}$. The significance of this work is as follows: For any linear unimodal PS, PBD, or HDPE melts, once the two slip parameters of A and β of Equation 3.10 are known (dependence of slip on MW), by having the viscosity curve (only the local slope n) and the MWD, their slip velocity can be predicted by using this equation.

Chapter 4: Surface Fractionation Effects on Slip of Polydisperse Polymer Melts

In this chapter, the slip behavior of several high-density polyethylenes (HDPEs) with broad range of molecular weight distribution including bimodals is studied as a function of molecular weight (MW) and its distribution (MWD). As explained in the first chapter, entropy driven migration of polymer chains complicates the analysis of slip data in the case of polydisperse polymer melts. For example, the slip velocity model developed in the previous chapter does not work to predict the slip velocity of very broad molecular weight distribution polymers due to significant migration effects. Therefore, a formulation similar to the double reptation theory is used to predict the slip velocity of the studied polymers as a function of MWD coupled with a model of surface molecular weight fractionation. While surface fractionation has a minor effect on slip of narrow to moderate MWD polymers (particularly unimodal), its role is significant for broad bimodal MWD polymers. The entropy driven migration of short chains towards the die wall has a profound effect and should be considered in order to calculate the effective MWD on the boundary layer and thus the correct magnitude of wall slip.

4.1 Results and discussions

4.1.1 Migration effects on unimodal HDPEs

For a polydisperse melt, the entropy loss of the longer chains in the vicinity of the surface is greater than that of shorter ones. Thus, shorter chains would segregate to the surface to reach the maximum entropy for the system. Therefore, the composition of the polymer close to the surface is different from that in the bulk [Hariharan *et al.* (1990)]. As discussed in the first chapter, Van der Gucht et al. (2002) investigated the effects of polydispersity on the behavior of polymer melts near the surface. They used self-consistent field theory simulations based on Scheutjens and Fleer lattice model (1979, 1980) and proposed a simple model that relates the surface excess, θ_N^{ex} and bulk volume fraction, φ_N^b, of each component of a polydisperse polymer melt as follows;

$$\frac{\theta_N^{ex}}{\varphi_N^b} = A_C\left(1 - \frac{N}{N_w}\right) \tag{4.1}$$

Where N and N_w are the chain length and the weight average chain lengths respectively, and A_C is a universal prefactor, which has been reported to be equal to 0.195 [Van der Gucht et al. (2002)]. For monodisperse distribution, Equation 4.1 is reduced to $\theta_N^{ex} = 0$, that implies the absence of migration effects.

Using Equation 4.1, the molecular weight distribution next to the surface, $w_s(M)$, can be calculated from the bulk molecular weight distribution, $w_b(M)$ by assuming constant chain density, ρ (a reasonable assumption for high enough molecular weights [Fetters *et al.* (1994)]) as follows;

$$\frac{\theta_N^{ex} \times \rho}{\varphi_N^b \times \rho} = A_C\left(1 - \frac{N \times M_m}{N_w \times M_m}\right) \rightarrow \frac{\nu_{ex}(M)}{w_b(M)} = A_C\left(1 - \frac{M}{M_w}\right) \tag{4.2}$$

$$w_s(M) = w_b(M) + \nu_{ex}(M) \tag{4.3}$$

Where M_m is the monomer molecular weight and $\nu_{ex}(M)$ and $w_b(M)$ represent the excess and bulk weight fractions, respectively. In our case both bulk and surface have molecular weights higher than the entanglement molecular weight, so it is rational to assume a constant density. This model (Equation 4.2) predicts negative values for $M/M_W > 6.13$ by taking into account that A_C is equal to 0.195 [Van der Gucht et al. (2002)]. Therefore, it is modified by considering the surface molecular weight fraction to be zero for fractions resulting $M/M_W > 6.13$.

$$w_s(M) = 0 \quad \textit{for} \quad \frac{M}{M_w} > 6.13 \tag{4.4}$$

This assumption has a negligible effect on the slip calculations since the smaller molecular weight species dominate the slip behavior ($V_s \propto M_w^{-2}$) and the segregation of these are calculated correctly, not affected by this assumption.

FIGURE 4.1(a) shows the bulk MWD, $w_b(M)$ and surface MWD, $w_s(M)$ calculated based on Equation 4.3 for a unimodal distribution HDPE of relatively moderate MWD with PI of 12.4 (ZN-HDPE-13). As it was expected [Busse (1964), Schreiber and Storey (1965), Schreiber *et al*. (1966), Hariharan *et al.* (1990), Van der Gucht et al. (2002), Shelby and Caflisch (2004), Rorrer and Drogan (2014)], the molecular weight distribution of the surface is shifted to lower molecular weights, resulting in a distribution with increased fraction of the low molecular weight chains.

The slip velocity based on the surface distribution, $w_s(M)$, can be calculated based on our proposed model using double reptation mixing rule (Equation 3.10). Figure 4.2 (a) depicts the predicted slip velocities based on the bulk, $w_b(M)$ (no migration effects), and surface, $w_s(M)$, molecular weight distributions as well as the experimental slip velocity results. The slip velocity calculated based on $w_s(M)$ is slightly higher than that based on $w_b(M)$. However, the difference is within ±15 %, which is within experimental error, thus the migration (segregation) effects are not significant for this case. Although the surface MWD, has lower M_w which increases the slip velocity, its polydispersity decreases as well compared to that of the bulk. These two competing effects result into a minor effect on the predicted slip velocity. Similarly, calculations of slip velocities for a broader unimodal distribution HDPE i.e. ZN-HDPE-5 having a PI of 17.6 (TABLE 2.1) with and without consideration of the segregation effects resulted in small differences of ±15 % (FIGUREs 4.1(b) and 4.2(b)). Therefore, Equation 3.10 can still be used for such polymers (narrow to broad unimodal MWD HDPEs) to predict their slip velocity.

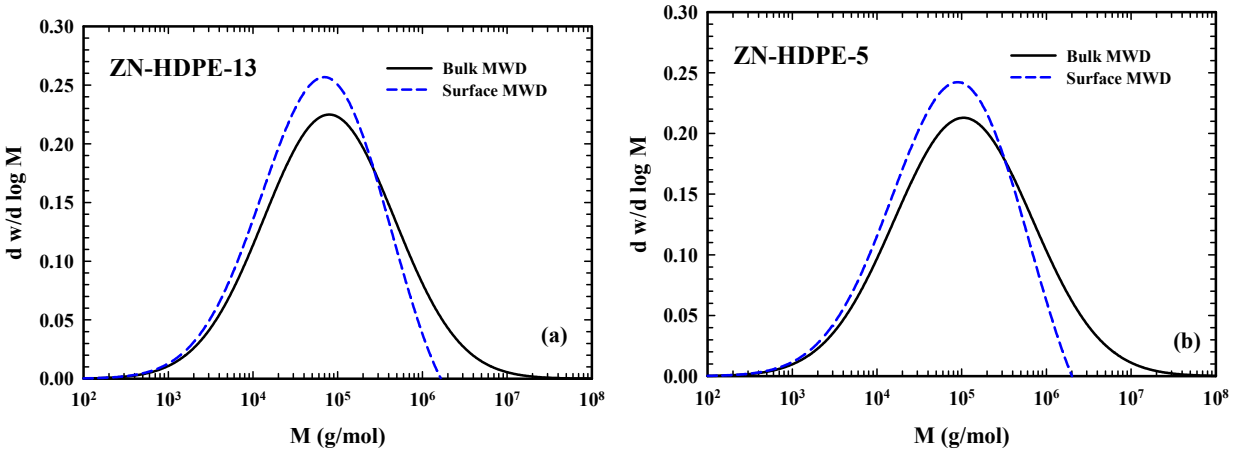

FIGURE 4.1: Molecular weight distribution of bulk, $w_b(M)$ (solid line) and surface, $w_s(M)$ (dashed line) of: **(a)** ZN-HDPE-13 and **(b)** ZN-HDPE-5.

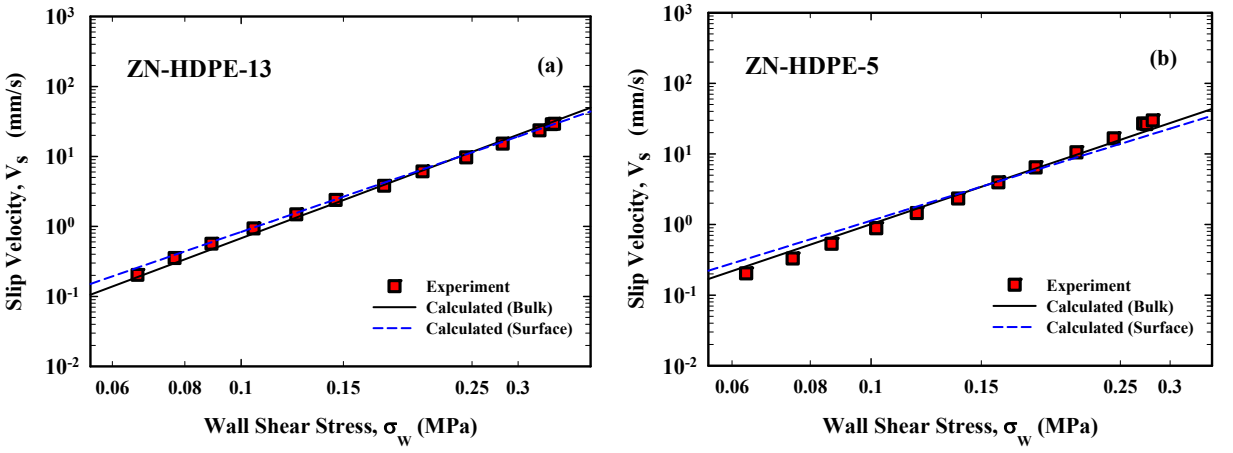

FIGURE 4.2: The slip velocity of ZN-HDPE-13. Experimental results are shown with symbols and the calculated slip velocity using Equation 4 based on the bulk, $w_b(M)$ and surface, $w_s(M)$, molecular weight distributions are shown by solid and dashed lines respectively: **(a)** ZN-HDPE-13 and **(b)** ZN-HDPE-5.

4.1.2 Migration effects on bimodal HDPEs

Experimental and theoretical studies have shown that migration effects become more pronounced with increase in the difference between the molecular weights of the chains [Hariharan *et al.* (1990), Lee and White (1974, 1975)]. For bimodal distribution resins studied by Ansari *et al.* (2013b) and Inn (2013), Equation 3.10 is used to calculate the slip velocity. For these polymers, it is desirable to describe MWD in terms of the summation of two unimodal MWD resins, namely a low-MW and a high-MW distribution as shown in FIGURE 4.3 for resin m-HDPE-8 studied by Ansari *et al.* (2013b). The bimodal distribution is a linear combination of the two unimodal distributions and it can be written as follows;

$$w(M) = \varphi_{LM} w(LM) + (1 - \varphi_{LM}) w(HM) \tag{4.5}$$

Where φ_{LM} is the weight fraction of the low-MW resin, and $w(LM)$ and $w(HM)$ show log normal distribution of low-MW and high-MW components respectively. The MW characteristics and the parameters of log normal distributions for bimodal HDPEs studied in this work are listed in TABLEs 4.1 and 4.2 respectively.

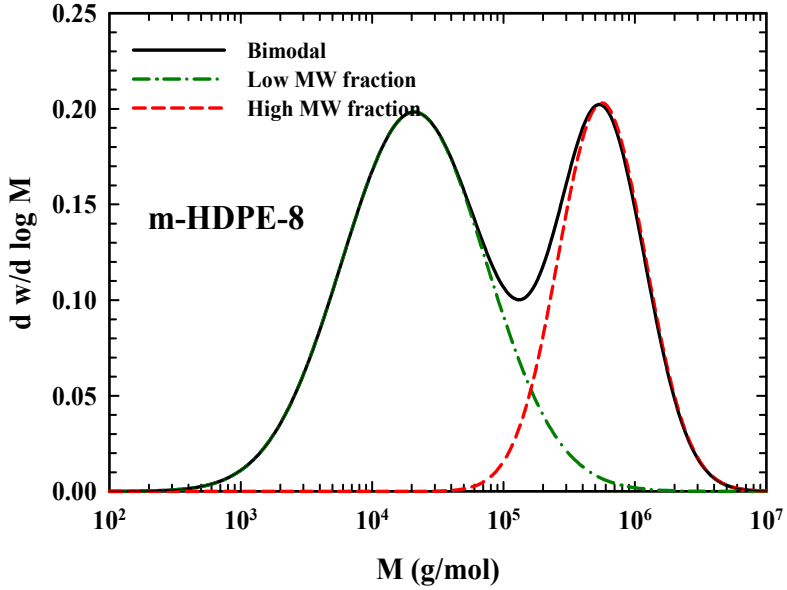

FIGURE 4.3: Typical molecular weight distributions of a bimodal HDPE that can be represented by a combination of two log-normal distributions of its Low-MW and High-MW fractions (Equation 4.5).

TABLE 4.1: List of MW characteristics of studied bimodal HDPEs.

Resin	M_n (kg/mol)	M_w (kg/mol)	$PI=M_w/M_n$
m-HDPE-8	10.8	272.4	25.2
m-HDPE-9	12.8	269.9	21.1
m-HDPE-10	12.5	266.2	21.3
m-HDPE-11	13.0	248.5	19.1
m-HDPE-12	11.6	229.8	19.8
L3H1	8.2	250	30.5

TABLE 4.2: List of log normal parameters for MWD of bimodal HDPEs.

Resin	φ_{LM}	$\sigma_{std\ (LM)}$	A^{*} $_{(LM)}$	$\overline{M_{m(LM)}}$(kg/mol)	$\sigma_{std\ (HM)}$	A^{*} $_{(HM)}$	$\overline{M_{m(HM)}}$(kg/mol)
m-HDPE-8	0.628	1.26	1.72	271.4	0.76	13.79	108.6
m-HDPE-9	0.680	1.26	1.72	271.4	0.76	13.79	108.6
m-HDPE-10	0.682	1.26	1.72	271.4	0.76	13.79	108.6
m-HDPE-11	0.715	1.26	1.72	271.4	0.76	13.79	108.6
m-HDPE-12	0.748	1.26	1.72	271.4	0.76	13.79	108.6
L3H1	0.640	1.37	2.98	8.61	0.74	10.79	673.2

For bimodal distribution resins studied by Ansari *et al.* (2013b), Equation 3.10 is used to calculate the slip velocity. The results for m-HDPE-8 are shown in FIGURE 4.4. A large discrepancy of several orders of magnitude exist between experimental slip velocity results and the model prediction using Equation 3.10 based on bulk MWD. This discrepancy can be attributed to migration of shorter chains to the surface, which increases the slip velocity [Musil and Zatloukal (2011, 2012a, 2012b), Inn (2013), Ansari *et al.* (2013b)]. As discussed above, MWD of bimodal HDPEs can be described as a summation of two unimodal resins [inset of FIGURE 4.5]. TABLE 4.3 shows the molecular weight characteristics of these resins.

TABLE 4.3: MW characteristics of Low-MW and High-MW components and their weight fraction in bimodal m-HDPEs.

MW Characteristics	Low-MW resin	High-MW resin
M_n (kg/mol)	9.4	420.0
M_w (kg/mol)	46.3	748.7
PI=M_w/M_n	4.9	1.8

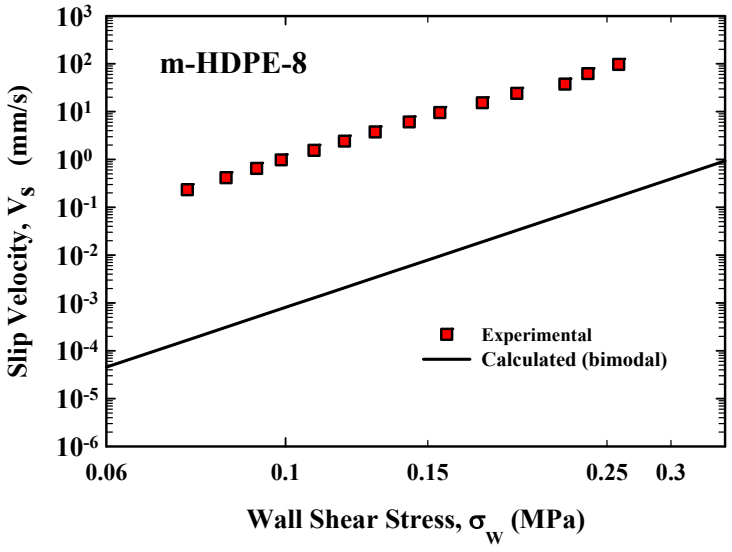

FIGURE 4.4: The slip velocities of m-HDPE-8. Experimental results are shown with symbols and the calculated slip velocity using Equation 3.10 is illustrated by solid line.

For Low and High-MW resins, double reptation method [des Cloizeaux (1988, 1990), Tsenoglou (1991), Jam *et al*. (2012)] is used to generate viscosity material functions needed for slip velocity calculations. Their simulated viscosity curves are illustrated in FIGURE 4.5.

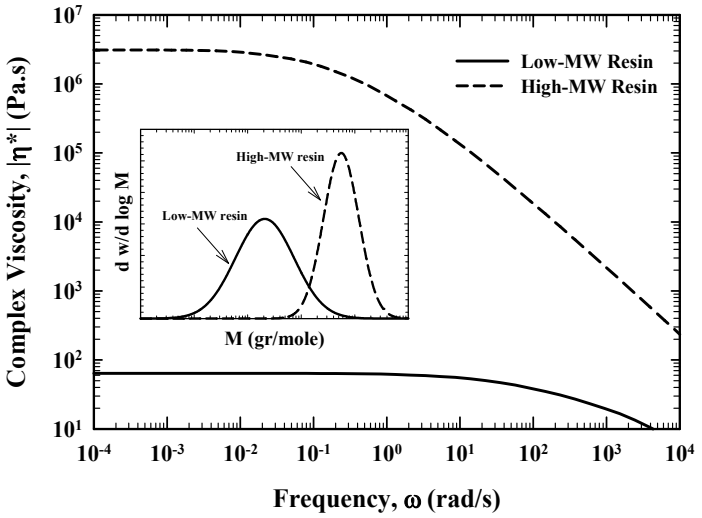

FIGURE 4.5: The simulated viscosity curves of Low and High-MW resins with different MWD depicted in the inset, predicted by double reptation method [Jam *et al*. (2012)].

The slip velocities of these resins are calculated based on Equation 3.10 by having their MWD and viscosity curves. FIGURE 4.6 shows these results along with experimental velocities of m-HDPEs reported by Ansari *et. al*. (2013b). All experimental data falls in between the predicted slip velocities for high-MW and low MW resins, and it is evident that low-MW resin dominates the slip behavior. Furthermore, by increasing the weight fraction of low-MW resin from m-HDPE-8 to 12, the slip velocity increases and becomes closer to the simulated slip velocity of low-MW resin. These observations confirm that migration of low MW chains to the surface plays an important role in slip behavior of bimodal polymers, thus migration effects should be taken into account to predict the correct magnitude of slip.

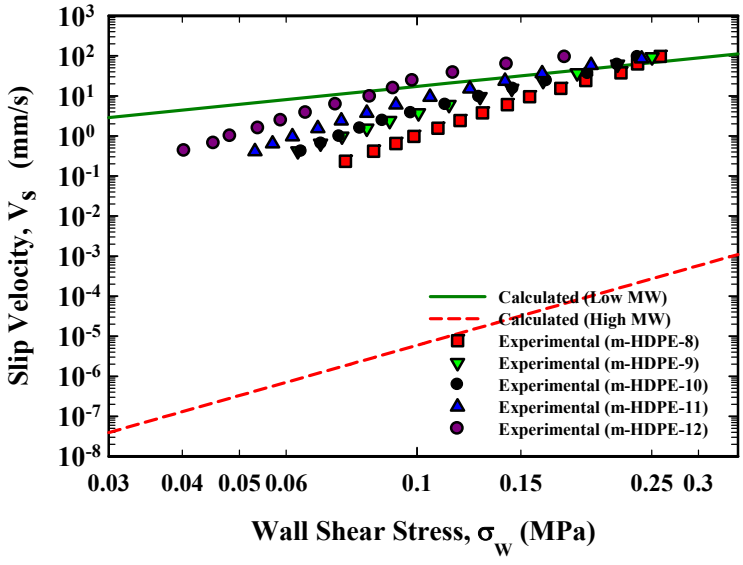

FIGURE 4.6: The calculated slip velocity based on Equation 3.10 using the viscosity curves depicted in FIGURE 4.5 and experimental slip velocities for m-HDPEs shown by symbols.

For resin m-HDPE-8, the surface-MWD, $w_s(M)$, is first calculated based on Equation 4.3 (plotted in Figure 4.7(a)), and based on this the corresponding slip velocity is calculated and plotted in Figure 4.7(b) (long-dashed line labeled as MWD (surface, $w_s(M)$). The agreement is significantly better compared to the case of "no migration" (MWD (bulk, $w_b(M)$). Remarkably the agreement is excellent at low values of the wall shear stress and the difference gradually increases at higher shear stress values. This disagreement is due to the effect of shear-induced migration (additional effect) which the used segregation model of Equation 4.3 does not take into account. Molecular simulation of cross flow migration in polymer melts performed by Rorrer and Dorgan (2014), showed similar segmental density distribution for quiescent case and simple shear flow. Therefore, under simple shear flow, where there is no shear rate gradient, no additional migration other than that caused by the walls occurs. However, for parabolic flow with shear rate gradient, strong chain migration was observed. In Van der Gucht equation for calculating the surface MWD, shear rate gradient and thus the flow induced migration are not taken into account causing higher slip velocities in the experiment at high shear rates compared to the model.

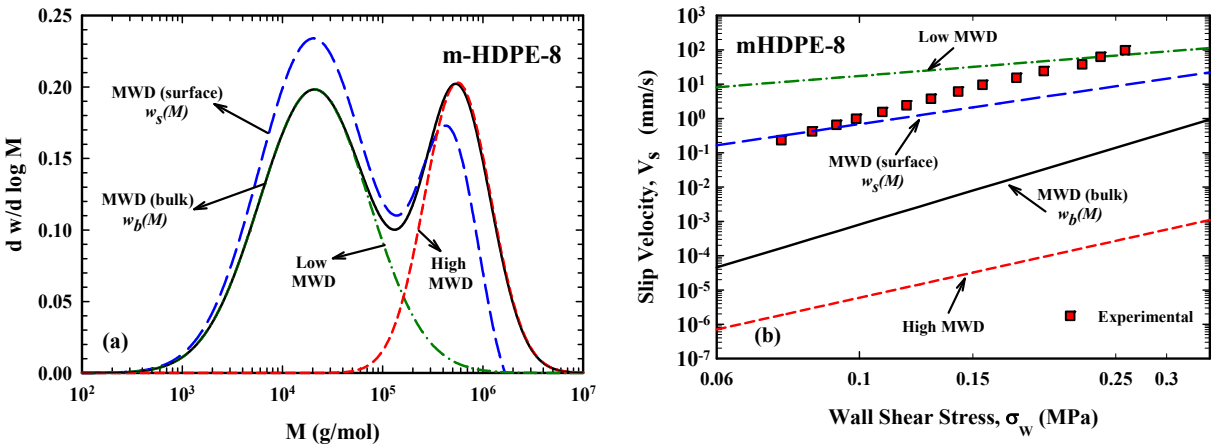

FIGURE 4.7: **(a)** Molecular weight distribution of bulk, $w_b(M)$, (solid line) and surface, $w_s(M)$, (long dashed line) and the molecular weight distributions of the two fractions of the low-MWD and high-MWD that make up the bimodal distribution. **(b)**The slip velocity of m-HDPE-8. Experimental results are shown with symbols and the calculated slip velocity using Equation 3.10 is illustrated for the cases with and without migration effects.

To further study migration effects on slip, all bimodal m-HDPEs were analyzed and tested. FIGUREs 4.8 (a)-(d) depicts the bimodal MWD distributions, $w_b(M)$, as a summation of a low- and high-MWDs, as well as the surface-distributions, $w_s(M)$, of m-HDPE-9, m-HDPE-10, m-HDPE-11 and m-HDPE-12 respectively. The corresponding slip velocity of these resins are calculated based on Equation 3.10 by using the low, the high, the bulk, $w_b(M)$, and the surface, $w_s(M)$, MWDs and plotted in FIGUREs 4.9 (a)-(d) respectively. Similar comments apply here to those discussed for the results of FIGURE 4.7. Neglecting the effect of migration, the difference between the calculated and experimental slip velocity is significant, in fact the differences are of several orders of magnitude due to the scaling $V_S \propto M_w^{-2}$. The experimental data lies between the predicted slip velocities that correspond to the high-MWD and low-MWD fractions of $w_b(M)$, with the low-MWD dominating the overall slip behavior. When migration/segregation effects are considered by using Equation 4.3, the agreement is remarkable at low shear stress. As discussed before at higher stress values, shear-induced migration causes an additional effect which is not taken into account by Equation 4.3 [Rorrer and Dorgan (2014)].

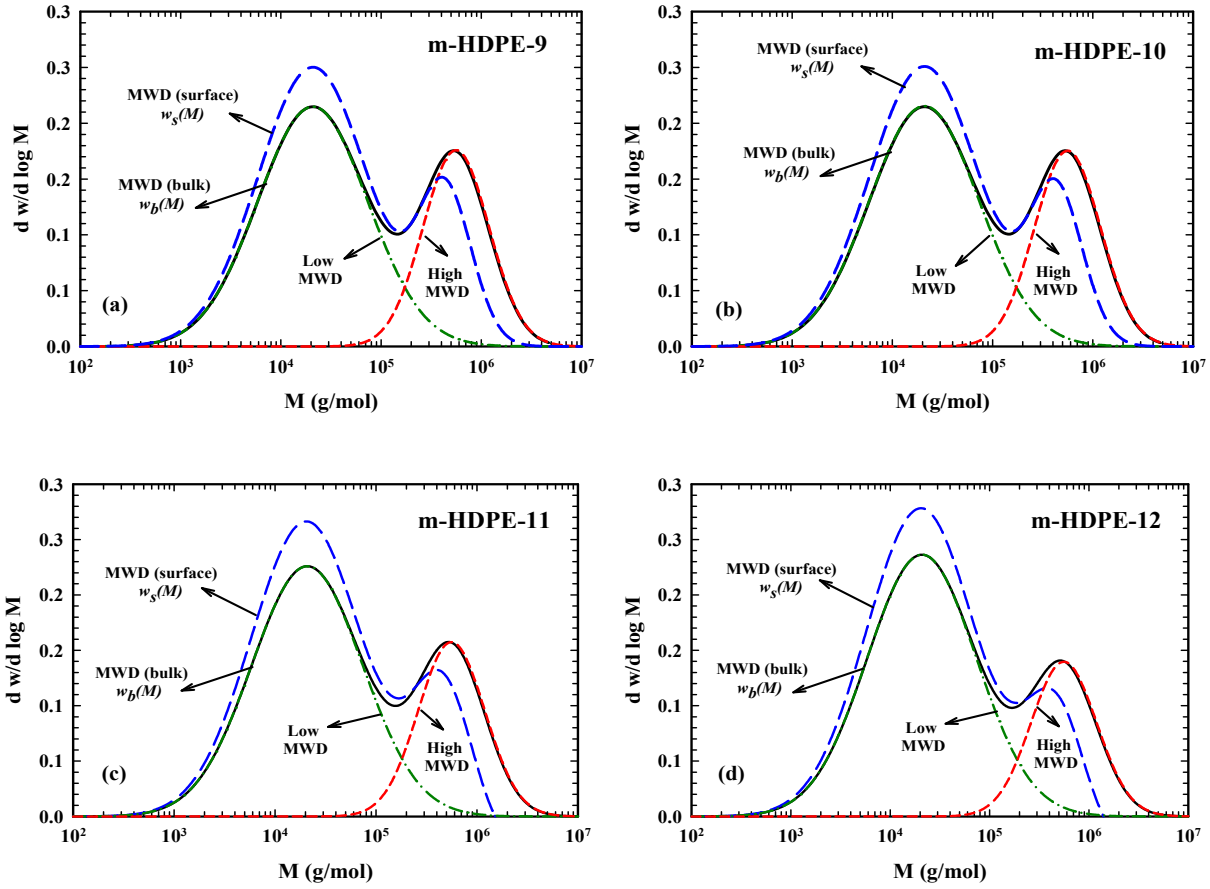

FIGURE 4.8: Molecular weight distribution of bulk, $w_b(M)$, (solid line) and surface, $w_s(M)$, (long dashed line) and the molecular weight distributions of the two fractions of the low-MWD and high-MWD that make up the bimodal distribution of: **(a)** m-HDPE-9, **(b)** m-HDPE-10, **(c)** m-HDPE-11, and **(d)** m-HDPE-12.

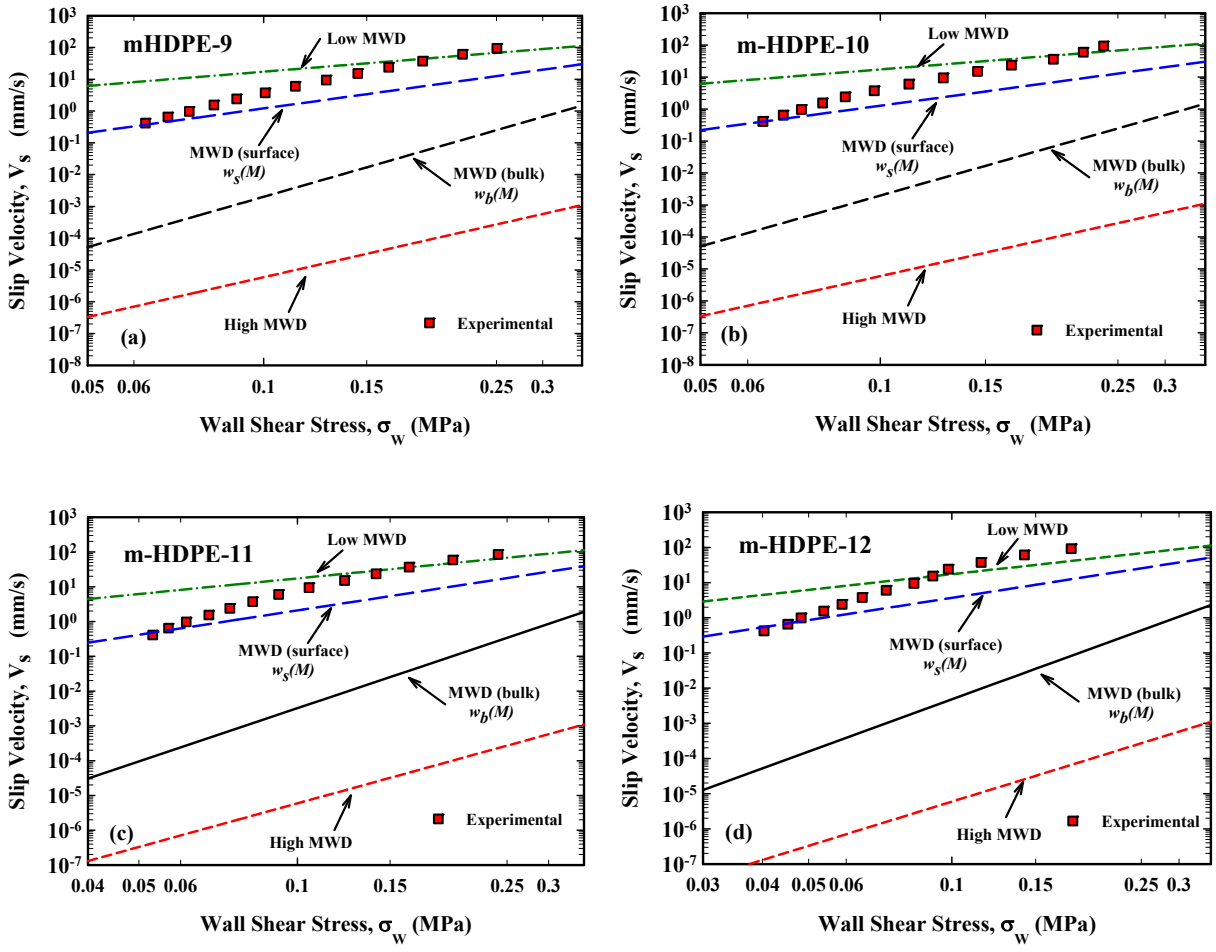

FIGURE 4.9: The slip velocity of: **(a)** m-HDPE-9, **(b)** m-HDPE-10, **(c)** m-HDPE-11, and **(d)** m-HDPE-12. Experimental results are shown with symbols and the calculated slip velocity using Equation 4 is illustrated for the cases with and without migration effects.

Melt fracture and wall slip behavior of bimodal polyethylene resins in capillary flow were also investigated by Inn (2013). To further examine our model, the slip behavior of a bimodal HDPE studied by Inn (2013) (L3H1 reported in TABLEs 4.1 and 4.2) was also investigated. Viscosity curves of low and high-MW components of this polymer are simulated using double reptation theory [Jam *et al*. (2012)] depicted in FIGURE 4.10, and their MW characteristics are reported in TABLE 4.4. The MWD and slip behavior of this resin was also analyzed and plotted in FIGUREs 4.11 (a) and (b). One more time similar comments can be made. Coupling of

Equations 3.10 and 4.3 predicts the behavior of bimodal distribution resins well (compare the experimental data with the line labelled as MWD-surface, $w_s(M)$). These observations confirm the importance of surface segregation on the slip velocity of broad molecular weight bimodal polymers.

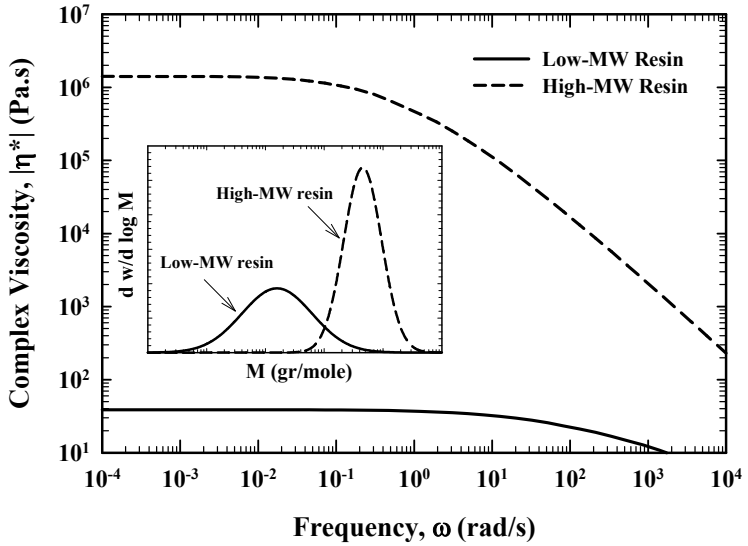

FIGURE 4.10: The simulated viscosity curves of Low and High-MW resins with different MWD depicted in the inset, predicted by double reptation method [Jam *et al*. (2012)].

TABLE 4.4: MW characteristics of Low-MW and High-MW components and their weight fraction in L3H1 reported by Inn (2013).

MW Characteristics	Low-MW resin	High-MW resin
M_n (kg/mol)	6.5	341.5
M_w (kg/mol)	40.3	591.4
PI=M_w/M_n	6.5	1.7

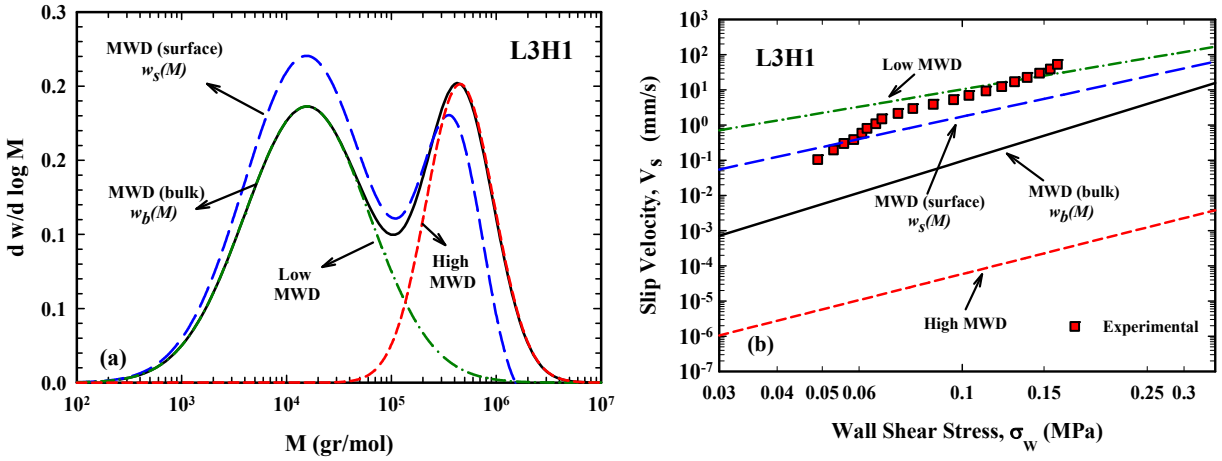

FIGURE 4.11: **(a)** Molecular weight distribution of bulk, $w_b(M)$, (solid line) and surface, $w_s(M)$, (long dashed line) and the molecular weight distributions of the two fractions of the low-MWD and high-MWD that make up the bimodal distribution. **(b)** The slip velocity of L3H1. Experimental results are shown with symbols and the calculated slip velocity using Equation 4 is illustrated for the cases with and without migration effects.

4.1.3 Experimental verification of migration

As it is difficult to analyze the samples obtained from capillary extrusion (small diameter samples), pipe extrusion experiments were performed for a bimodal distribution HDPE from Chevron Phillips Chemical Company LP extruding an 8 inch-diameter pipe. Microtome was applied on the surface of the sample, shaving about $1\mu m$ off its surface. GPC analysis was performed to obtain the MWD of the sample harvested from the pipe surface [Johnson *et al.* (2000)]. This was compared with the MWD of the bulk of the material. These results reported from Chevron Phillips are plotted in FIGURE 4.12 [Ebrahimi *et al.* (2016)]. The surface has been enriched with low molecular weight species relative to the bulk. Smaller molecular weight species dominate the slip behavior ($V_s \propto M_w^{-2}$) and the segregation of these to the surface is important in slip analysis which is observed in surface MWD in FIGURE 4.12. Although the qualitative features are similar, the predictions of the Van der Gucht expression are not particular compelling. However, it must be pointed out that this might be due to several reasons (i) experimental error from GPC analysis (ii) the microtomes were only $1\mu m$ in depth and migration as reflected by slip

velocity measurements should be affected by a surface layer only a few *nm* (same order of magnitude with radius of gyration of the molecules) (iii) the Van der Gucht expression does not include shear induced effects.

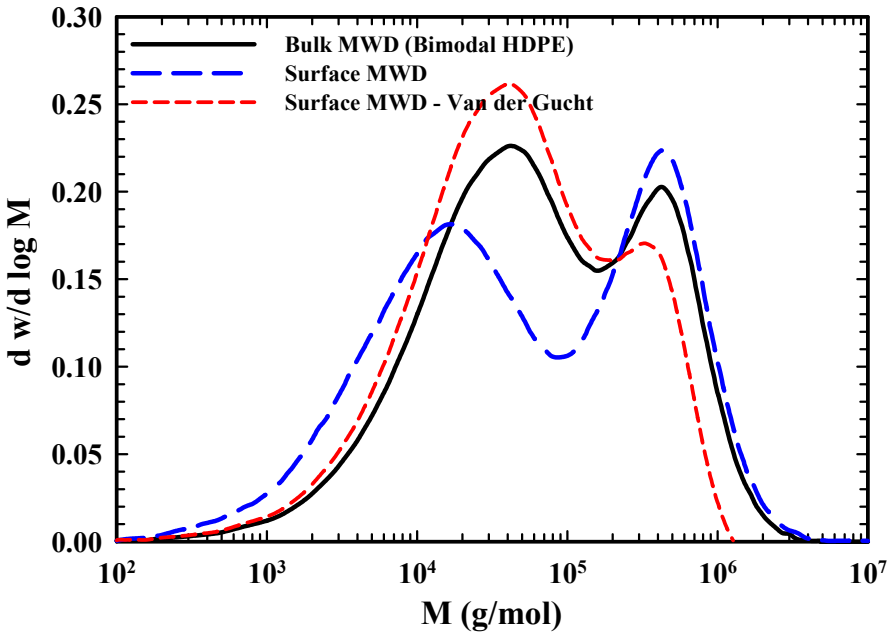

FIGURE 4.12: Molecular weight distribution of a bimodal HDPE samples obtained from pipe extrusion. MWD of the bulk, wb(M), (solid line), MWD of the surface (1 μm depth), $w_s(M)$, (long dashed line) reported by Chevron Phillips and MWD of the surface predicted by the Van der Gucht's expression (Equation 4.3).

Musil and Zatloukal (2012a) analyzed the die drool phenomenon during extrusion of linear HDPE melts and found that die drool sample has narrower MWD containing lower molecular weight chains compared to the bulk. They reported that the flow induced fractionation takes place only in a very thin layer near the die (i.e., within less than 8% of the channel radius). FIGURE 4.13 depicts the calculated surface MWD using Van der Gucht's expression from the bulk MWD of HDPE-1 reported by Musil and Zatloukal (2012a). As it can be seen, there is qualitatively good agreement between this predicted MWD and die drool MWD as they both have more short chains and the difference can be attributed to the effect of shear-induced migration (additional effect) which the used segregation model does not consider.

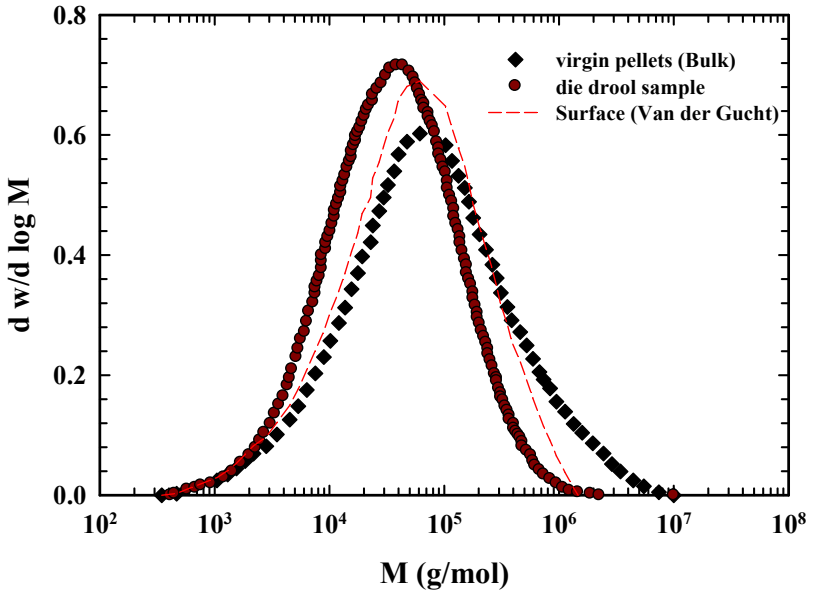

FIGURE 4.13: MWD curves for material HDPE 1 in the form of die drool sample and virgin pellet (bulk) reported by Musil and Zatloukal (2012a) and surface MWD calculated using Van der Gucht's expression.

4.2 Conclusions

In this chapter, the slip velocity of several HDPEs with different MW and MWD including unimodal and bimodal distribution was studied in an attempt to elucidate the effects of surface segregation on slip velocity of polymers. A model is proposed based on Van der Gucht (2002) method to calculate quantitatively the MWD of the surface. For the case of unimodal HDPEs, the predicted slip velocity for bulk and surface is similar. However, for bimodal HDPEs, where the surface fractionation is profound, the difference is considerable. Good predictions are obtained by using the segregation model to calculate the surface-MWD which dominates the slip. These calculated surface-MWDs are used to calculate the slip based on our proposed double reptation slip model. The difference between the experimental results and model prediction at high values of shear stress can be attributed to the flow-induced molecular weight fractionation which is not included in Van der Gucht's expression and enhances the concentration of shorter chains in the surface.

Chapter 5: Slip of Polymer Melts over Micro/ Nano-Patterned Metallic Surfaces

In this chapter, the slip behavior of high-density polyethylenes (HDPEs) is studied over surfaces of different topology and energy. Two HDPEs with different MW characteristics are studied in this Chapter (HDPE-1 and HDPE-2, TABLE 2.1). Laser ablation is used to micro/nano-pattern the surface of dies to examine the effect of surface roughness on slip. In addition, fluoroalkyl silane-based coatings on smooth and patterned substrates are used to understand the effect of surface energy on slip. Surface roughness and surface energy effects are incorporated to the double reptation slip model in order to predict the slip velocity of studied polymers on different substrates. It was found that for rough dies, polymer melt penetrates the cavities of the substrate (depending on the depth and distance of the asperities), thus decreasing slip velocity. Moreover, silanization of the surface increases the slip velocity of polymers in the case of smooth die, although it has a negligible effect on rough dies. Interestingly, the slip velocity of the studied polymers on various substrates of different degrees of roughness and surface energy, were brought into a mastercurve by modifying the proposed double reptation slip velocity model.

5.1 Results and discussions

Depending on the surface structure, flow conditions and chemistry, there are two different states of wetting, namely Wenzel and Cassie states [Wenzel (1936), Cassie and Baxter (1944)] as illustrated in FIGURE 5.1. In the Wenzel state, the liquid droplet completely wets the surface, filling up the valleys between the asperities, typically expected in polymer flow due to high pressure**,** normal and shear stresses [Granick *et al*. (2003), Cottin-Bizonne *et al*. (2003, 2004), Reyssat *et al*. (2006), Bartolo *et al*. (2006), Joseph *et al*. (2006), Lee and Choi (2008), Rothstein (2010), Forsberg *et al*. (2011), Tretyakov and Müller (2013)]. On the other hand, in the Cassie state, liquid does not fully wet the surface and is suspended by trapped air pockets between roughness features. This second state can give rise to a phenomenon known as superhydrophobicity, also called the lotus effect [Quéré (2002), Gao *et al*. (2009)]. To systematically change the surface roughness and modify the surface energy, we fabricated slit dies

that consist of two (halves) pieces as seen in FIGURE 5.2(a) that could be held together by means of two screws and an O-ring (FIGURE 5.2(b)).

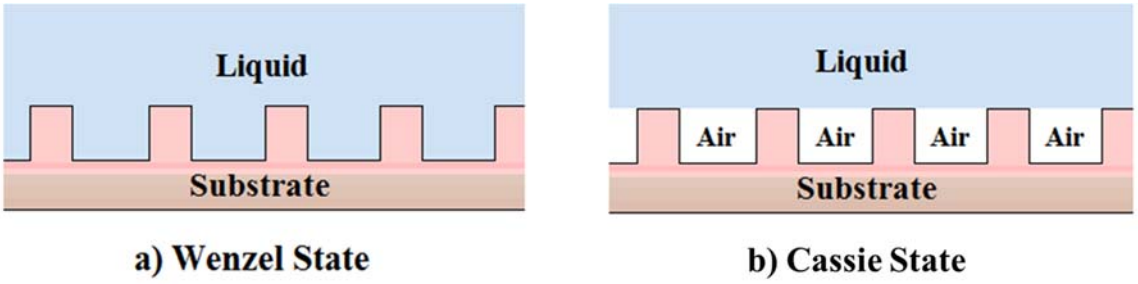

FIGURE 5.1: Schematic diagram of two distinct wetting states **(a)** The Wenzel state **and (b)** The Cassie state.

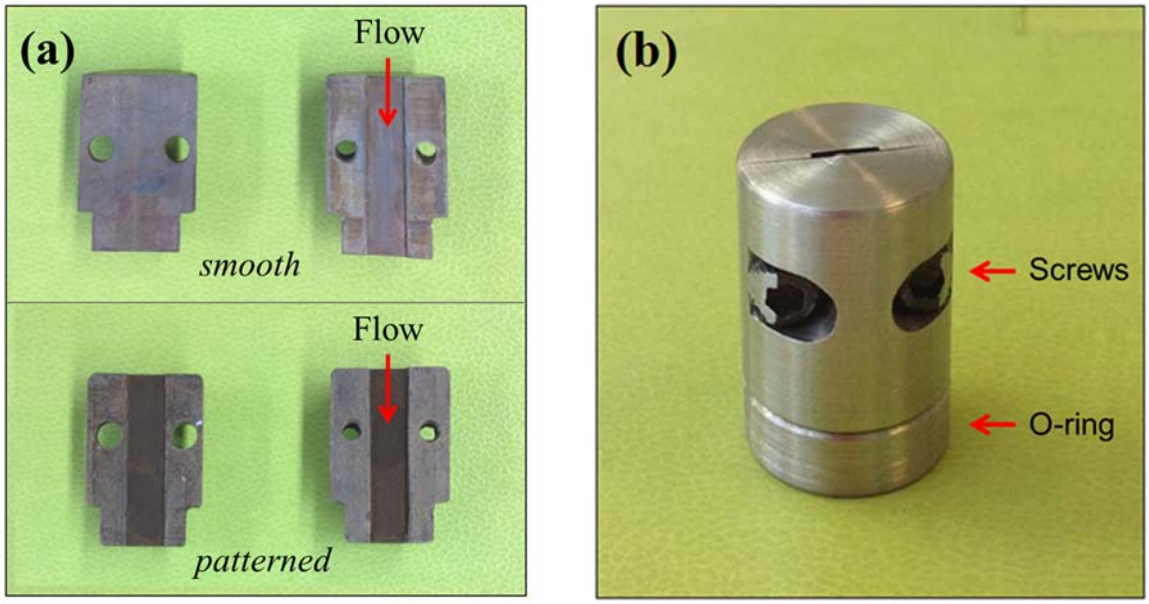

FIGURE 5.2: Images of the fabricated slit dies **(a)** slit die disassembled showing the flow field. The upper is the slit die with unmodified surface and the lower part is the die with the laser ablated surface (dark) **(b)** The slit die assembled with O-ring and screws, as used in the flow experiments.

5.1.1 Surface morphology

Laser ablation was used to fabricate roughness on the slit die surfaces by using different combinations of laser fluence (energy), Φ and scanning speed, V', a variety of different surface patterns, specifically microbumps with different height and diameter, pitch size and amount of nano-scale features were produced. The morphology of the fabricated surfaces was analyzed using a variable-pressure Scanning Electron Microscope (Hitachi S-3000N SEM) and an Optical Profilometer (Wyko NT3300) in order to determine the mapping of the geometrical characteristics of the structures precisely. FIGURE 5.3 presents the SEM images of smooth and laser ablated surfaces referred to as paraboloidal, cauliflowered and scaly [Moradi *et al.* (2013, 2014, 2015)]. It can be observed that all these micro/nano-patterns produced by laser ablation, possess dual scale roughness of a few microns superposed by submicron scale roughness (please refer to the insets of FIGUREs 5.3(b)-(d)). FIGURE 5.4 shows the 3-D maps of the smooth and fabricated rough surfaces obtained from Profilometry. The geometric information in the plane such as average peak to valley distance, G and pitch size (distance between asperities, D) was measured using Vision and ImageJ softwares and these values are listed in FIGURE 5.4 along with the corresponding images.

Laser irradiation has altered the dimensions of the originally fabricated slit dies and this is the reason that the dies have different dimensions. The new dimensions have been measured using a Nikon Confocal Microscope and are listed in TABLE 5.1. The dimensions of interest are the width, W, the gap or height, H and the L/H needed for analyzing the rheological data.

TABLE 5.1: List of slit dies fabricated along their characteristics dimensions.

Die # (type of pattern)	***W* (mm)**	***H* (mm)**	***L/H***
Die #1 (Smooth)	4.80	0.40	54.5
Die #2 (Paraboloidal)	4.80	0.48	45.4
Die #3 (Cauliflowered)	4.80	0.84	25.9
Die #4 (Scaly)	4.80	1.30	16.8

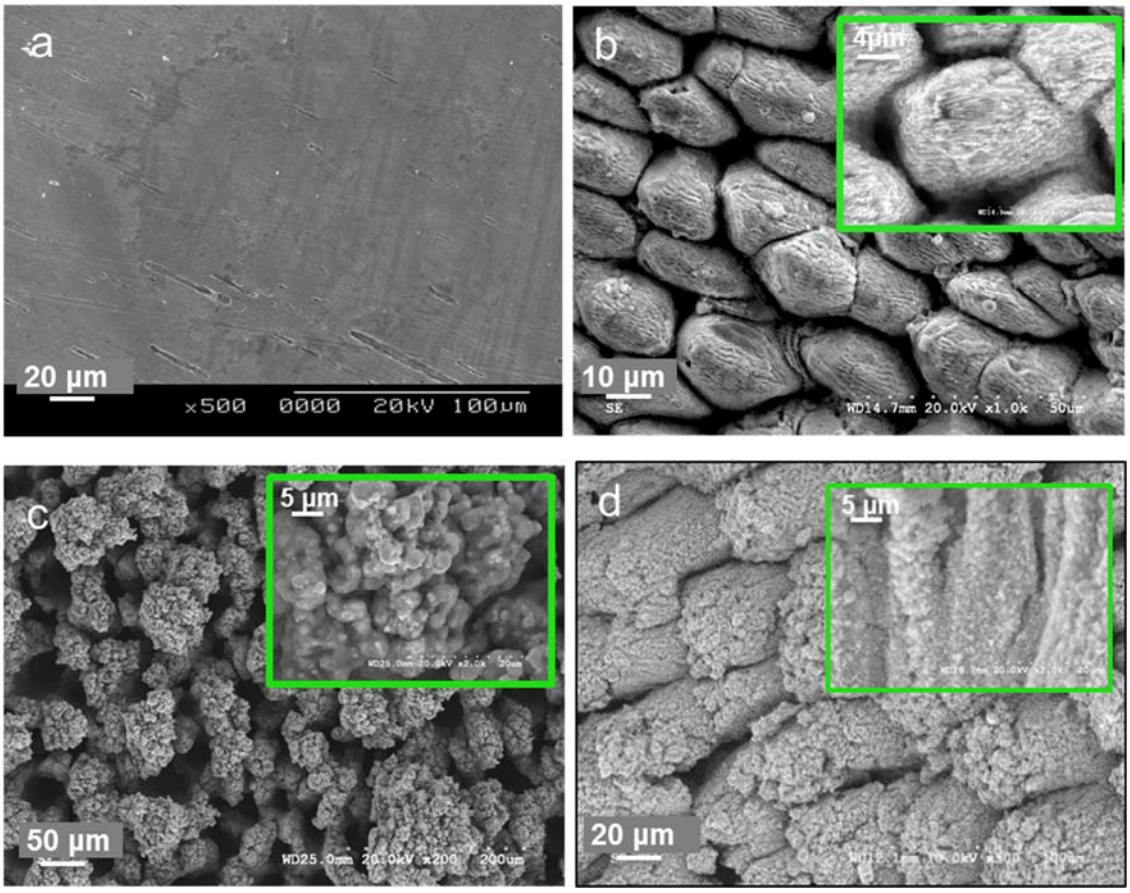

FIGURE 5.3: SEM images of the smooth and fabricated micro/ nano-patterned stainless steel (SS) surfaces used in the flow experiments **(a)** Smooth SS surface **(b)** Paraboloidal pattern with Φ = 16 J/cm2, V' = 930 µm/s, **(c)** Cauliflowered pattern with Φ = 465 J/cm2, V' = 370 µm/s, and **(d)** Scaly pattern with Φ = 175 J/cm2, V' = 150 µm/s.

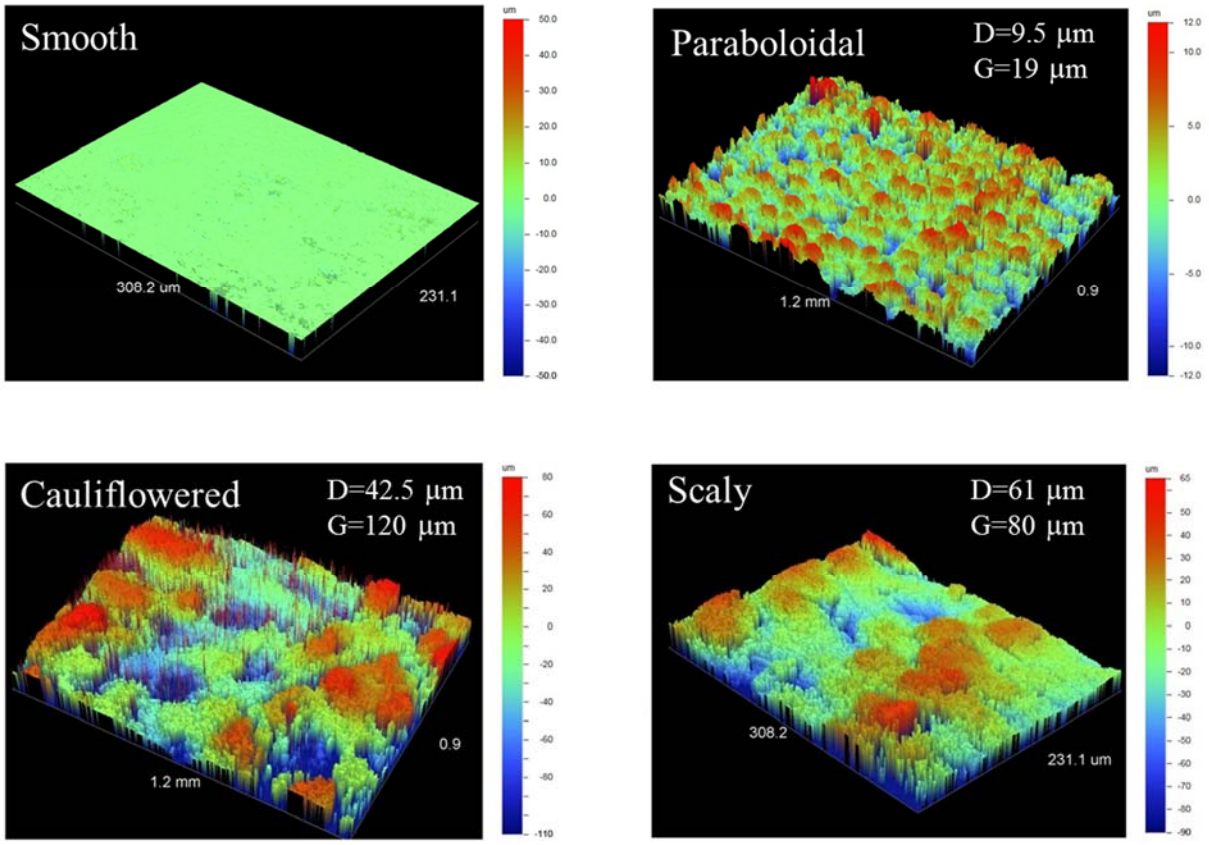

FIGURE 5.4: Surface topography of the smooth and fabricated micro/nano-patterned stainless steel (SS) surfaces and their corresponding characteristic dimensions; peak to valley, *G* and the pitch size, *D*, of the first order bump of the patterned surfaces.

A matter of concern is the mechanical stability of the microbumps as polymer flows over them at high pressure and stresses. Due to the high viscosity of these fluids, the pressures developed are high and these may alter the geometrical characteristics of the microbumps. However, as FIGURE 5.5 shows, these micro/nano patterns are mechanically stable as they appear to be nearly the same before and after flow.

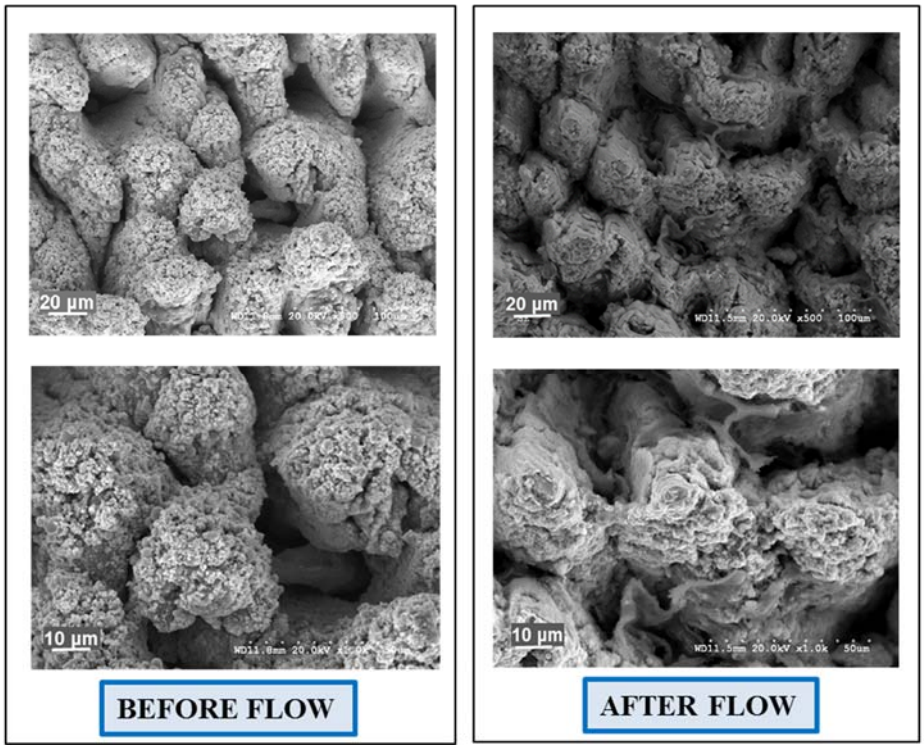

FIGURE 5.5: SEM images of a cauliflowered die showing the excellent mechanical stability of the fabricated micro/nano patterns at two different magnifications. The micro/nano patterns appear to be nearly the same before and after flow.

5.1.2 Surface energy

To alter the surface energy, all the studied dies have been coated with fluoroalkyl silane using solution based dip-coating method. As discussed in Chapter 2, fluoro groups are deposited on the surface by this method. Therefore, silanization reduces the surface energy of a metallic surface rendering it hydrophobic. Hydrophobicity in combination with micro/nano-patterning produces superhydrophobic surfaces. The sessile drop method was used to measure the contact angle (CA) and contact angle hysteresis (CAH) of all surfaces with and without silanization [Moradi *et al.* (2013)]. Droplets of distilled, deionized water of volume 4 μL were dispensed on the surfaces and the contact angles were determined by analyzing droplet images with the image processing method of ImageJ. Measuring the advancing and receding contact angles of a growing

and shrinking droplet resulted in CAH [Moradi *et al.* (2013, 2014)]. TABLE 5.2 lists these data; it is evident that silanization and microstructures both play important roles in the wettability of the surfaces.

TABLE 5.2: The CA and CAH of all surfaces used in this study.

Type of Surface	**Non-silanized**		**Silanized**	
	CA °	**CAH °**	**CA °**	**CAH °**
Pristine/ Smooth	80 ± 1	50 ± 2	105 ± 3	35 ± 2
Paraboloidal	<5	180	148 ± 8	40 ± 3
Cauliflowered	<5	180	>150	12 ± 1
Scaly	<5	180	>160	<5

5.1.3 Linear viscoelasticity of HDPEs

The frequency sweep tests were carried out using a rotational rheometer (Anton Paar, MCR-502) with parallel-plate geometry over a wide range of temperatures from 150 to 230°C. The curves at various temperatures were shifted using the time-temperature superposition (TTS) to generate the master curves at the reference temperature of 190°C at which flow experiments were performed. FIGUREs 5.6(a) and (b) present the master curves of the linear viscoelastic moduli, *G'* and *G"* and complex viscosity, η^*, of the two studied HDPEs (HDPE-1 and HDPE-2) at the reference temperature of 190ºC. Moreover, the complex viscosity data was fitted with the Carreau-Yasuda model, Equation 5.1;

$$\eta(|\dot{\gamma}|) = \eta_0[1 + (\lambda|\dot{\gamma}|)^a]^{(n'-1)/a} \tag{5.1}$$

where η_0, is zero shear viscosity, $|\dot{\gamma}|$ is the local shear rate or magnitude of the strain rate tensor, defined as $\sqrt{\text{II}}$, where II is the second invariant of the strain rate tensor, a, n' and λ are empirically determined constants. The parameters a and n' are dimensionless, and the parameter λ has units

of *s*. The corresponding Carreau-Yasuda model parameters of HDPE-1 and HDPE-2 are listed in TABLE 5.3.

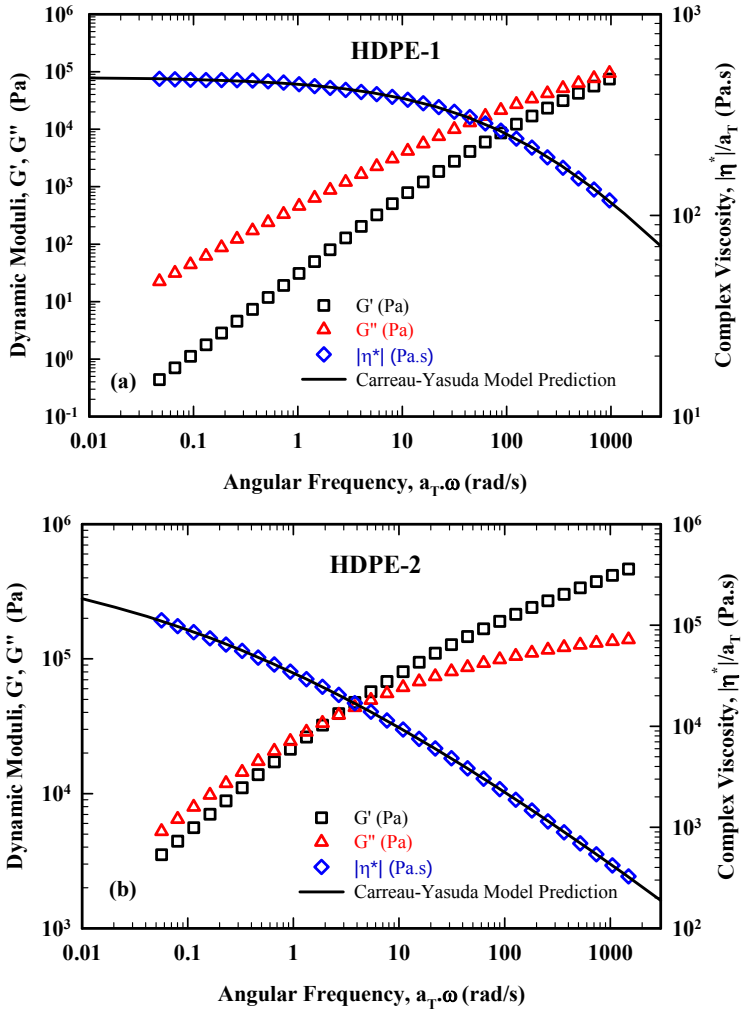

FIGURE 5.6: The master curves of storage (*G'*), loss moduli (*G"*), complex viscosity (*η**) and the corresponding fit of the Carreau-Yasuda model for the studied resins **(a)** HDPE-1 and **(b)** HDPE-2 at the reference temperature of 190ºC.

TABLE 5.3: The corresponding Carreau-Yasuda model parameters of HDPE-1 and HDPE-2.

Carreau-Yasuda parameters	HDPE-1	HDPE-2
η_0 (Pa.s)	486	627050
a	0.51	0.25
n'	0.40	0.16
λ (s)	0.005	3.586

5.1.4 The flow curves and slip velocities

Capillary extrusion experiments were performed using a piston-driven constant-speed capillary rheometer (Bohlin RH 2000). The HDPE melts were extruded at 190 °C using a series of slit dies listed in TABLE 5.1. FIGURE 5.7(a) presents the flow curves of HDPE-1 using all the slit dies before and after silanization. Similar curves have been plotted for HDPE-2 in FIGURE 5.7(b). The wall shear stress σ_w is defined as $\sigma_w \equiv \Delta p / 2(L/H)$, which neglects the excess entry pressure drop, which is negligible considering the large *L/H* values (see TABLE 5.1). The apparent shear rate, $\dot{\gamma}_A$, is defined as, $\dot{\gamma}_A \equiv 6Q/(H^2 W)$, where Q is the volumetric flow rate, H is the height of the slit die and W is its width. The continuous solid line indicated as LVE represents the complex modulus of the polymer plotted as flow curve, namely $G^*(\omega) = |\eta^*(\omega)| \times \omega$. As discussed before, the surface chemistry of the die surfaces is modified by silanization to produce low surface energy surfaces for the nanopatterned dies. As shown in FIGURE 5.7 (a), the flow curve of HDPE-1 extruded through smooth salinized die has changed and deviates more from LVE data because of its lower surface energy and thus the polymer exhibits a higher slip. However, for the cases of patterned dies, silanization has no effect on the flow curves (the differences are within experimental error). These results, show that no trapped air pockets exist between micro/nano structures of the patterned dies due to the high pressures in capillary flow, resulting in Wenzel state, at which the polymer melt fills the asperities. These asperities are sufficiently large comparing to the trapped HDPE chains (few nanometers) [Sanchez-Reyes and Archer (2003)]. Therefore, interactions between unbound chains and trapped chains within asperities replace

chain/wall interactions and polymer/wall interactions are only confined to the peaks of asperities. Similar results are observed for HDPE-2 (FIGURE 5.7 (b)). Similar results were reported for flow of a highly entangled linear PE on smooth and treated smooth and rough dies [Wang and Drda (1997)].

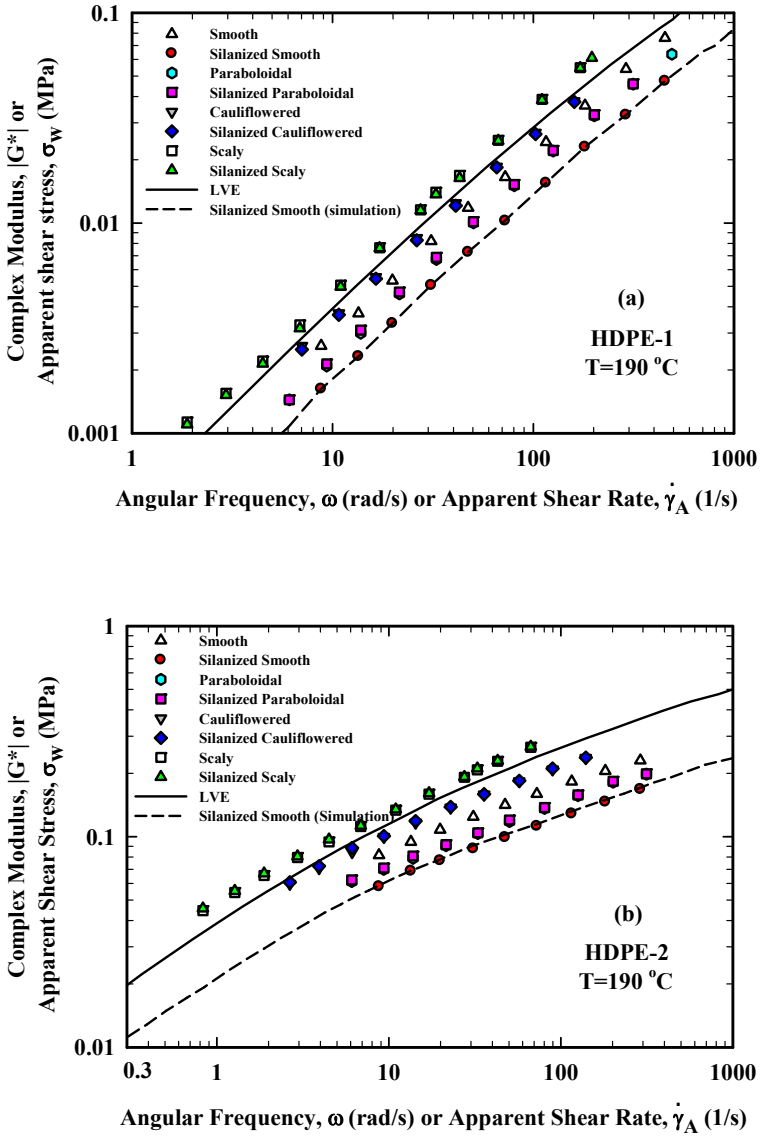

FIGURE 5.7: The flow curves of resins **(a)** HDPE-1 and **(b)** HDPE-2 using the various slit dies listed in TABLE 5.1 (before and after silanization) at the reference temperature of 190ºC. The continuous line is the LVE data, and the dashed line is the FEM based flow simulation for silanized smooth die discussed in a following section.

For both polymers, for the slit dies with high aspect ratio, *W/H*, of more than 10, i.e. smooth, and paraboloidal dies, the end effects are negligible and there is no need to apply any correction [Migler *et al*. (1994)]. The significant deviation from the LVE data (failure of the Cox-Merz rule) is clear and is due to the occurrence of slip [Ansari *et al.* (2013a, 2013b)]. For these cases, slip velocities were calculated from the deviation of each flow curve from LVE curve using the following relationship;

$$\dot{\gamma}_A = \frac{3n}{2n+1}\omega + \frac{6V_S}{H} \tag{5.2}$$

where n is the local slope of the flow curve of the corresponding resin, $n \equiv d\log(\sigma_w)/d\log(\dot{\gamma}_w)$, V_S is the slip velocity, and H is the die gap [Ansari *et al.* (2013a)]. This technique has been successfully applied for studying wall slip of HDPEs [Ansari *et al.* (2013a)] and polylactides [Othman *et al*. (2012)], while a similar method was also used for polybutadienes [Park et al. (2008)]. For the slit dies with low aspect ratio (*W/H* < 10*)*, namely the cauliflowered and scaly patterned dies, the end effects are significant. Therefore, appropriate corrections should be applied to the data to have rheological meaning. This is done by using a 3-D finite element analysis as described in the next section. The flow data are determined for each experimental point separately to calculate the slip velocity as explained below.

5.1.5 Finite element analysis to calculate slip

The governing equations for the 3-D flow simulation of an incompressible viscous fluid under steady-state, isothermal and creeping flow conditions are given as follows;

The continuity equation:

$$\nabla \bullet \mathbf{v} = 0 \tag{5.3}$$

The momentum balance equation:

$$-\nabla p + \nabla \cdot \boldsymbol{\tau} = 0 \tag{5.4}$$

where v is the velocity vector, p is the pressure, $\boldsymbol{\tau}$ is the stress tensor of the viscous fluid. The general relationship between the stress tensor and rate of the deformation tensor is, $\tau = 2\eta(|\dot{\gamma}|)\boldsymbol{D}$. The rate of deformation tensor **D** is defined as: $\mathbf{D}=(\nabla\mathbf{v}+\nabla\mathbf{v}^{\mathrm{T}})/2$, where $\nabla\mathbf{v}$ is the velocity gradient tensor. The well-known generalized non-Newtonian model described by Carreau-Yasuda equation (Equation 5.1) is used to represent HDPE-1 and HDPE-2 in the present simulations.

The typical slit/flat die geometry and mesh of a silanized cauliflowered die used in this study are shown in FIGURE 5.8. Only one-quarter of the total flow channel has been used in the simulations that were performed using the commercial package ANSYS POLYFLOW®. The following boundary conditions have been used: Along the inlet and outlet boundaries, fully developed flow with constant flow rate; at the symmetric planes, zero traction condition are imposed; finally, at the walls, a nonlinear slip condition that relates slip velocity (V_S) to the wall shear stress (σ_w) of the following form as discussed in Chapter 3;

$$V_S(mm/s) = A'[\sigma_W(MPa)]^{1/n} \tag{5.5}$$

note that n is the local slope of the flow curve of the corresponding polymer, $n \equiv d[\log(\sigma_w)]/\mathrm{d}[\log(\dot{\gamma}_w)]$, thus fixed and independent of the surface conditions and characteristics, and *A'* is a parameter that consolidates the effects of molecular weight of the polymer, temperature and pressure and the interfacial characteristics and conditions. Therefore, any different *A'* values calculated for each polymer will be because of the effect of interface since all other factors are kept constant.

Initially, 3-D finite element method (FEM) simulations were performed for polymers HDPE-1 and HDPE-2 for the smooth die using the slip coefficients (refer TABLE 5.4) obtained directly from experimental measurements by using Equation 5.2. As can be seen from FIGURE 5.7(a) and 5.7(b), the simulation results (dashed lines) are in excellent agreement with the flow curve data of both HDPE-1 and HDPE-2, asserting the use of 3-D FEM analysis to represent the experimental data. The good agreement also asserts that the end effects are negligible for these dies with aspect ratio greater than 10.

For the cases with aspect ratio less than 10, to determine the coefficient *A'* of the slip velocity each experimental point was simulated separately. The value of *A'* was determined in order the simulations to match the experimental pressure drop. These values were averaged to represent the slip behavior of the polymers for each set of data i.e. different interfacial conditions and characteristics. This was the case for the cauliflowered and scaly dies that have an aspect ratio much less than 10 where the end effects are significant, and thus Equation 5.2 could not be used. The average values of the slip coefficient *A'* of HDPE-1 and HDPE-2 for Silanized/unsilanized cauliflowered and scaly dies are listed in TABLE 5.4. A representative result of pressure contour plot of HDPE-1 in Silanized Cauliflowered die using the slip parameters listed in TABLE 5.4 at a flow rate of 58 mm^3/s (i.e., at an apparent shear rate of 103 s^{-1}) is given in FIGURE 5.9. As discussed above for the case of smooth surfaces, silanization decreases the work of adhesion and thus slip increases accordingly. For the roughened surfaces, silanization does not play any significant role, as polymer chains are trapped at the dales between the asperities to various degrees and thus the slip occurs at the polymer/polymer interface.

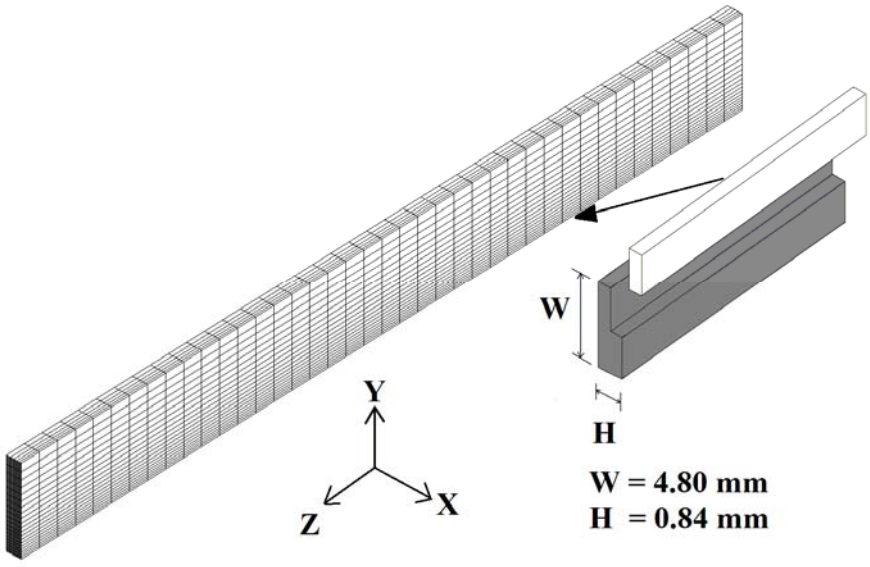

FIGURE 5.8: Finite Element (FE) mesh of Silanized Cauliflowered die with 4000 number of elements and 5166 number of nodes. The flow direction is in positive Z-axis.

TABLE 5.4: The slip parameters obtained from experiments (Silanized/unsilanized Smooth and Paraboloidal) and FEM simulations (Silanized/unsilanized Cauliflowered and Scaly).

Type of Surface	HDPE-1		HDPE-2	
	A' (mms^{-1}MPa^{-n})	*n*	*A' (mms^{-1}MPa^{-n})*	*n*
Clean unsilanized Smooth	170.25	0.88	3751.56	0.26
Silanized Smooth	582.26	0.88	13093.02	0.26
Silanized/unsilanised Paraboloidal	338.65	0.88	7318.10	0.26
Silanized/unsilanized Cauliflowered	125.03	0.88	3071.91	0.26
Silanized/unisilanised Scaly	97.47	0.88	2115.28	0.26

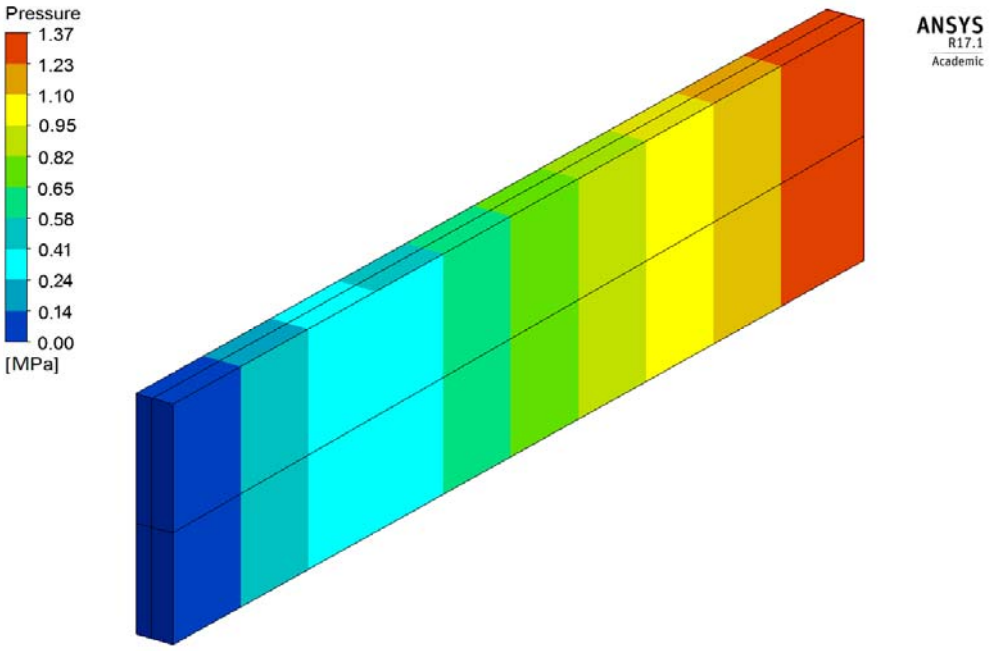

FIGURE 5.9: Pressure contours of HDPE-I in Silanized Cauliflowered die obtained from FEM simulation at a flow rate of 58 mm^3/s (i.e., an apparent shear rate of 103 s^{-1}).

5.1.6 Slip on smooth surfaces and its modelling

As discussed in Chapter 3, elements from the theory of double reptation were used to relate the slip velocity of several HDPEs with their molecular weights and their distributions. Thus, for a given MWD of a HDPE melt, Equation 3.10 can be used to generate its slip velocity versus shear stress relationship without performing any additional experiments. The predictions solely depend on the two parameters A and β, which are fixed for the same family of polymers. Consolidating the effects of all parameters the constant A' can be recovered as defined in Equation 5.5. The values of A' for the two polymers are also listed in TABLE 5.4. FIGURE 5.10(b) shows the experimental and calculated slip velocities of the studied polymer on smooth dies before silanization based on their MWD (depicted in FIGURE 5.10(a)). As can be seen from FIGURE 5.10(b), excellent agreement between experimental and calculated velocities is observed.

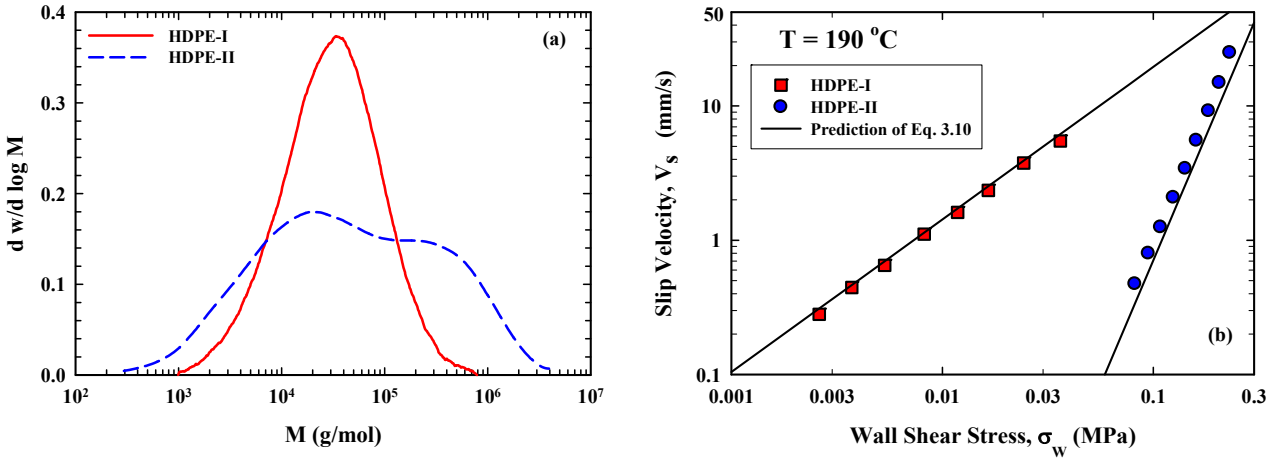

FIGURE 5.10: (a) Molecular weight distribution of the studied polymers. **(b)** The slip velocity versus wall shear stress. Experimental results are shown with symbols and the calculated slip velocity using Equation 3.10 is shown by solid line.

5.1.7 Slip on rough and treated surfaces and its modelling

For treated and roughened surfaces, the constant A in Equation 3.10 has a different value which should be a function of the roughness and surface energy. We denote these new values of A as A_e and A_s related to surface energy and surface topology/structure, respectively. These can be realized once we plot the slip velocity for the various cases. FIGURE 5.11 shows that roughness reduces the slip velocity of HDPEs to various degrees depending on the type of nanopatterning for both polymers in a similar fashion. Also, the slip velocity of the silanized smooth surface is higher compared to the slip velocity of the clean/ unsilanized smooth surface for both polymers (FIGUREs 5.11(a) and (b)). Thus, silanization (low surface energy) increases the slip significantly. Using these data and some arguments based on scaling laws below, we derive how A of Equation 3.10 is related to surface energy and roughness of the surface.

To study first, the effect of surface energy on slip velocity, the slip velocity of polymers over smooth and silanized smooth surfaces are compared (FIGURE 5.11). These results show that slip velocity of both HDPEs are significantly higher over the silanized dies. The ratios of the proportionality constants of slip velocity on silanized smooth die over that of the clean/ unsilanized one (A_e/A) is equal to 3.4 and 3.5 for HDPE-1 and HDPE-2, respectively. Previous experimental evidence has also shown that the presence of fluoropolymer-based coatings increases the slip velocity by a certain amount, which is a function of the work of adhesion defined by Israelachvili (2011);

$$W_{adh} = \gamma_{LV}(1+\cos\theta) \tag{5.6}$$

where γ_{LV} is the interfacial tension between the molten polymer and its vapor (air) and θ is the contact angle of the polymer in the melt state over the solid interface. When a polymer melt slips over a solid surface under shear stress σ_w, the ratio $k' = \sigma_w / V_S$ is defined as the friction coefficient [Navier (1823)]. The velocity profile next to the interface can be described in terms of the extrapolation length, b defined by the distance to the wall at which the velocity extrapolates to zero [Navier (1823), Brochard and de Gennes (1992)]. This can be written as follows;

$$b = \frac{V_S}{\dot{\gamma}_w} = \frac{\eta}{k'} \tag{5.7}$$

where $\dot{\gamma}_w$ is the shear rate at the wall, and η is the melt viscosity at $\dot{\gamma}_w$. The friction coefficient, *k'* can be evaluated via the Green-Kubo relation [Bocquet and Barrat (1993, 1994), Barret (1999)]. Barret (1999) proposed that *k'* is proportional to the square of the attraction between substrate and liquid, ε_s as $k' \approx \varepsilon_s^{\,2}$, thus $b \approx \varepsilon_s^{\,-2}$. Previous studies have confirmed the applicability of this relationship [Léonforte *et al*. (2011), Tretyakov and Müller (2013)] Tretyakov and Müller (2013) observed this dependence by using molecular dynamic simulations for slippage of a polymer liquid. On the other hand, the work of adhesion, W_{adh} depends linearly on ε_s [Servantie and Muller (2008)], resulting in the proportionality of extrapolation length, *b* to inverse of the square of work of adhesion, as $b \approx W_{adh}^{\,-2}$ [Huang *et al*. (2008), Sendner *et al*. (2009)]. By combining these relations, we obtain;

$$V_S \approx W_{adh}^{-2} \tag{5.8}$$

$$A_e / A \equiv (W_{adh} / W_{adh,e})^2 \tag{5.9}$$

where *A* is the proportionality constant of slip velocity on clean unsilanized smooth surface (Equation 3.10) and subscript *e* shows the modified surface applying a coating that changes its work of adhesion from W_{adh} to $W_{adh,e}$. This ratio can also be related to the contact angle of polymer over the clean and treated (silanized in this case) surfaces through Equation 5.6.

Anastasiadis and Hatzikiriakos (1998) have studied the interfacial characteristics of a variety of polymer/wall interfaces, including HDPEs and clean and fluoropolymer coated stainless steel substrates, and calculated the work of adhesion of these surfaces. Their results showed that the work of adhesion decreases by modifying stainless steel surfaces with fluoropolymer coatings. They have reported the work of adhesion of different HDPEs with various molecular weight characteristics, on clean and fluoropolymer coated stainless steel surfaces (the fluoropolymer used has similar structure to fluoroalkyl silane coating used in this study). The value of $(W_{adh} / W_{adh,e})^2$

based on their study is reported to be 3.3 which is close to our results confirming the applicability of the proposed relationship (Equation 5.9).

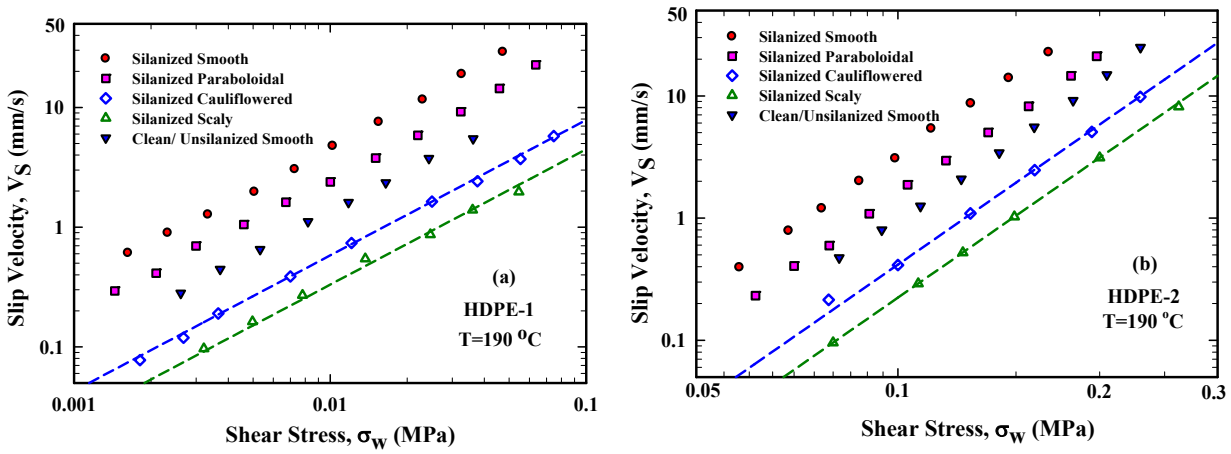

FIGURE 5.11: The slip velocities versus wall shear stress for **(a)** HDPE-1 and **(b)** HDPE-2 using different dies listed in TABLE 5.1 at reference temperature of 190 ºC. The solid symbols represent the slip data obtained from experimental measurements and the open symbols represent the slip data determined using the 3-D FEM simulations, and the dashed lines are plotted using the average values of slip coefficients obtained from FEM simulations.

As depicted in FIGURE 5.11, roughness reduces slip velocity of HDPEs to various degrees. As mentioned before, for such rough surfaces, the polymer melt enters the cavities of the substrate and many chains can be trapped in the space between asperities resulting in the replacement of polymer/wall interface with corresponding polymer/polymer interface. This definitely depends on the depth and width of the dales between the asperities. For deep and narrow dales, the interface can be flat. However, for wide and narrow dales the interface may be curved, thus the streamlines may deep slightly inside these areas, increasing the pressure drop that is reflected as a decrease in slip. The slip velocity decreases with degree of surface roughness from paraboloidal to scaly patterns for both studied HDPEs (FIGURE 5.11). Tretyakov and Müller (2013) compared the flow of a polymer liquid in channels with patterned walls with that in channels with flat walls by non-equilibrium molecular dynamics simulations. Their results have shown that the difference between

patterned and flat substrates is rather controlled by the area fraction, not the size of the grooves. Therefore, we defined the ratio of the substrate covered by cavities to the projected flat surface as the "free surface fraction", φ. These values were calculated for each patterned die using ImageJ analysis and are reported in TABLE 5.5. By ablating dies to fabricate patterns, laser energy creates active sites which affect surface energy [Moradi et al (2013, 2014)]. Thus, the slip velocity obtained from the silanized dies are examined/compared in order to keep surface energy constant to solely study the effect of surface topology. The ratio of proportionality constants of slip velocity of silanized patterned surface to silanized smooth die (A_s/A_e) versus the free surface fraction, φ is plotted in FIGURE 5.12 for both HDPEs. For smooth surface, φ is zero and A_s/A_e equals to 1. It is evident that by increasing the φ of the surface, the slip velocity decreases resulting in decrease of A_s/A_e. An exponential function seems to fit the data well as follows;

$$A_s / A_e = \exp(-4.6\varphi) \tag{5.10}$$

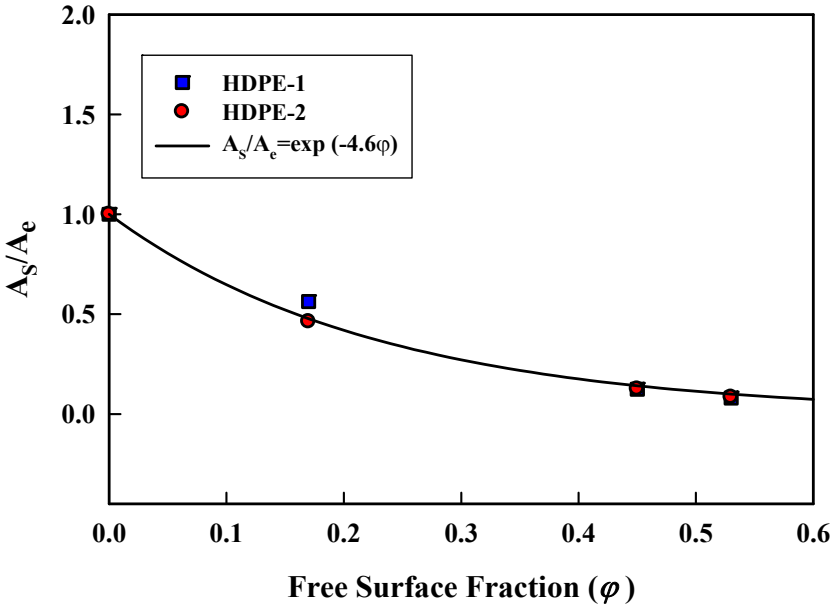

FIGURE 5.12: A_s/A_e as a function of free surface fraction, φ for different dies. The solid line represents the exponential law given by Equation 5.10.

Incorporating Equations 5.9 and 5.10 into Equation 3.10, the slip velocity that includes the effects of surface treatment and roughness on slip velocity can now be written as follows;

$$a_T a_p V_S = A\left(\frac{W_{adh}}{W_{adh,e}}\right)^2 \exp(-4.6\varphi)\left\{\int_0^{\infty}\left[M^{\beta} w(M)\int_M^{\infty} w(M')dM'\right]dM\right\}\sigma_w^{1/n} \qquad (5.11)$$

Where the 5.11(a) and (b) for HDPE-1 and HDPE-2 are shifted vertically by an amount equal to $\left(\frac{W_{adh}}{W_{adh,e}}\right)^2 \exp(-4.6\varphi)\left\{\int_0^{\infty}\left[M^{\beta} w(M)\int_M^{\infty} w(M')dM'\right]dM\right\}$ (to correct for the effects of polydispersity, surface energy and topology) and is plotted versus $\sigma_w^{1/n}$ for each polymer and surface roughness. The resulted master curve is shown in FIGURE 5.13 having slope 1 indicating that Equation 5.11 represents the data well.

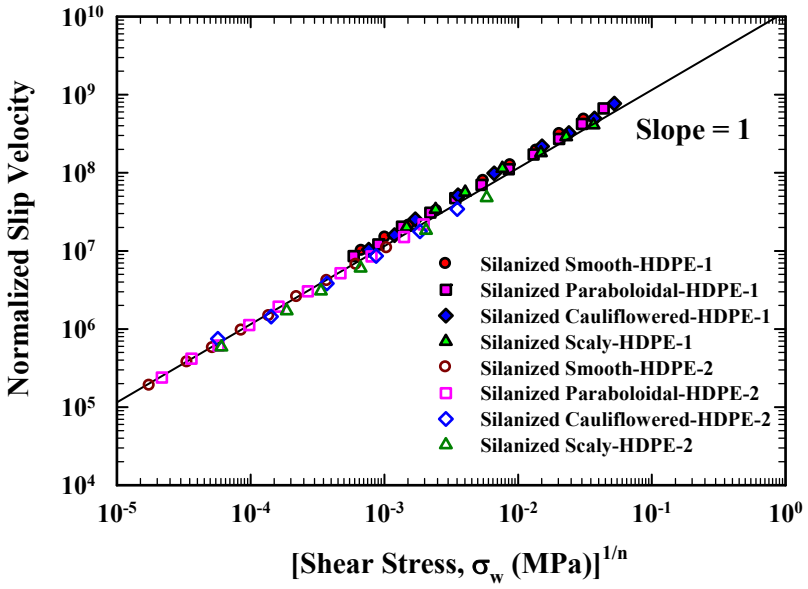

FIGURE 5.13: Normalized slip velocity versus shear stress with power of 1/n for HDPE-1 and HDPE-2 for different dies.

5.1.8 Morphology of extrudates

Samples were collected from smooth and patterned dies known as extrudates in order to study the surface morphological changes as a result of flow over irregularities of surface roughness. The different local deformation history in the flow over different micro/nano-patterns and the memory effects of polymer melts are expected to manifest themselves on morphological surface differences on the extrudates. The morphology of the HDPE-2 extrudates were studied with profilometry and are depicted in FIGURE 5.14. The surface of extrudate from smooth die (FIGURE 5.14(a)) is free of roughness (plain) as expected. However, patterned roughness is observed on the surfaces of HDPE extrudates obtained from the patterned dies (FIGUREs 5.14(b)-(d)). The free surface fraction, φ of the patterned dies seems to scale with the characteristic length (peak to valley distance) of the extrudate surface (refer TABLE 5.5). By increasing the degree of roughness of die surface patterns, the average roughness on the extrudate surface also increases. These results show that by increasing the pitch size and free surface fraction of the pattern, the polymer melt flows deeper into the cavities.

TABLE 5.5: Comparison of smooth and patterned dies and the corresponding extrudates of HDPE-2.

Type of Surface	Die Free Surface Fraction, φ	Peak to Valley of extrudate (μm)
Smooth	0	0.1
Paraboloidal	0.17	1.6
Cauliflowered	0.45	9.4
Scaly	0.53	8.5

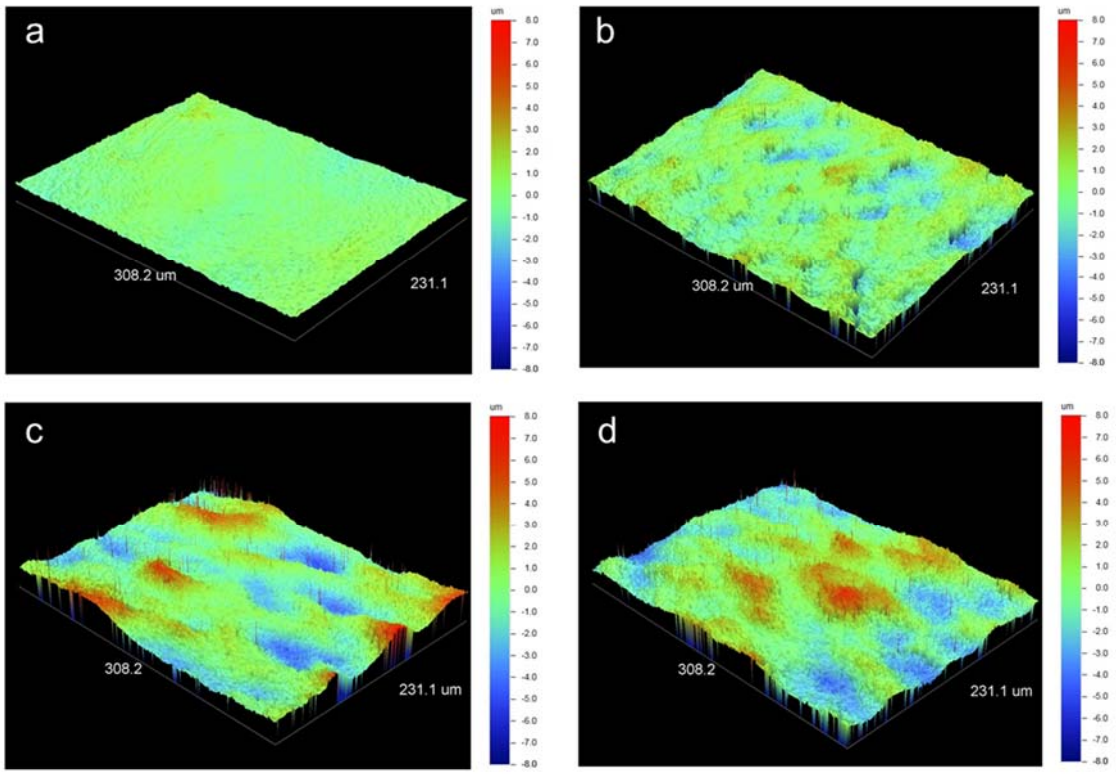

FIGURE 5.14: Profilometry images of HDPE-2 extrudates from **(a)** Silanized Smooth **(b)** Silanized Paraboloidal **(c)** Silanized Cauliflowered and **(d)** Silanized Scaly patterns.

5.2 Conclusions

In this chapter, the slip velocity of two HDPEs with different MW characteristics was studied in an attempt to elucidate the effects of surface roughness and energy on slip velocity of polymers. It was observed that although silanization changes the flow curve of polymers extruding from smooth die, it has negligible effect on the patterned dies. These observations confirm that for smooth die, the effective surface of polymer/wall interactions is larger than rough dies where polymer/wall interactions are only confined to the peaks of asperities. For rough dies, due to high pressure and large size of asperities (in comparison with average coil size) polymer melt penetrates the cavities of the substrate. Therefore, interactions between flowing chains and trapped chains within asperities replace chain/wall interactions resulting in decrease of slip velocity. Slip

velocities were calculated using rheology and 3-D FEM simulations to apply the necessary corrections to experimental data due to end effects. Our proposed slip model based on double reptation theory was modified to include the effects of surface energy and topology (roughness). It was found that slip velocity scales inversely with square of work of adhesion and it is an exponential function of the "free surface fraction" (degree of roughness) of the roughened dies.

Chapter 6: Slip Dynamic Slip of Polydisperse Linear Polymers using Partitioned Plate

In this chapter, the slip velocity of an industrial grade high molecular weight HDPE supplied by ExxonMobil Company (HDPE-3) is studied in steady and dynamic shear experiments using the stress/strain controlled rotational rheometer equipped with parallel partitioned plate geometry. Moreover, fluoroalkyl silane-based coating is used to understand the effect of surface energy on slip in steady and dynamic conditions. The multimode integral Kaye-Bernstein-Kearsley-Zapas (K-BKZ) constitutive model is applied to predict the transient shear response of the HDPE melt obtained from rotational rheometer. It is found that a dynamic slip model with a slip relaxation time is needed to adequately predict the experimental data at large shear deformations. Comparison of the results before and after coating, shows that the slip velocity is largely affected by surface energy. Decreasing surface energy by coating increases slip velocity and decreases the slip relaxation time.

6.1 Results and discussions

Small angle oscillatory shear (SAOS), step strain relaxation, and uniaxial extension experiments were used to fully characterize HDPE-3. Moreover, rotational rheometry with parallel partitioned plate geometry was used to study the slip velocity of this polymer in steady and unsteady flows. The K-BKZ constitutive model under no slip, static slip and dynamic slip conditions was used to predict the transient shear response of HDPE-3. It was found that including the dynamic slip with a slip relaxation time is necessary to explain the transient shear response of HDPE-3 at large and fast shear deformations. Furthermore, fluoroalkyl silane-based coating using dip coating method was used to study surface energy dependency of slip velocity. It was observed that the slip velocity is increased and the slip relaxation time is decreased by reducing surface energy due to coating.

6.1.1 Mathematical modelling

The K-BKZ constitutive model proposed by Papanastasiou *et al.* (1983) and modified by Luo and Tanner (1988) used in this study, is given by:

$$\tau = \frac{1}{1-\theta}\int_{-\infty}^{t} m(t-t')h(I_{C^{-1}}, I_C)[C_t^{-1}(t') + \theta C_t(t')]dt' \tag{6.1}$$

Where t is the current time, $m(t-t')$, is the memory function of linear viscoelasticity and $h(I_{C^{-1}}, I_C)$ is the damping function. I_C and $I_{C^{-1}}$ are the first invariants of the Cauchy–Green tensor C_t, and its inverse Finger strain tensor, C_t^{-1}, θ is a material constant given by $N_2/N_1 = \theta/(1-\theta)$, N_1 and N_2 are first and second normal stress differences, respectively. The memory function is defined as:

$$m(t-t') = \sum_{i=1}^{N} \frac{g_i}{\lambda_i} \exp\left(\frac{-(t-t')}{\lambda_i}\right) \tag{6.2}$$

where λ_i and g_i are the relaxation times and relaxation moduli, respectively, and N is the number of relaxation modes.

The damping function can be determined by performing sudden step strain experiments and recording the relaxation shear stress data at various levels of imposed strains. The strain dependent damping function has many forms in the literature. Papanastasiou *et al.* (1983) suggested the following equation for damping function, known as PSM (Papanastasiou, Scriven, Macosko) damping function:

$$h(I_{C^{-1}}, I_C) = \frac{\alpha_p}{(\alpha_p - 3) + \beta_p I_{C^{-1}} + (1-\beta_p) I_C} \tag{6.3}$$

where α_p and β_p are model constants to be determined from shear and elongational flow data, respectively. For the case of simple shear, $I_C = I_{C^{-1}} = 3 + \gamma^2$, and thus, the PSM damping function reduces to the following simple form:

$$h(\gamma) = \frac{\alpha_p}{\alpha_p + \gamma^2} \tag{6.4}$$

6.1.2 Rheological characterization

6.1.2.1 Small-amplitude oscillatory shear (SAOS)

FIGURE 6.1 presents the master curves of the linear viscoelastic moduli, *G'* and *G"* and complex viscosity, η^*, of HDPE-3 at the reference temperature of 190°C. Moreover, the six-mode Maxwell model was used to fit the viscoelastic moduli, and the fitted parameters, relaxation times, λ_i, and the relaxation moduli, g_i are listed in TABLE 6.1.

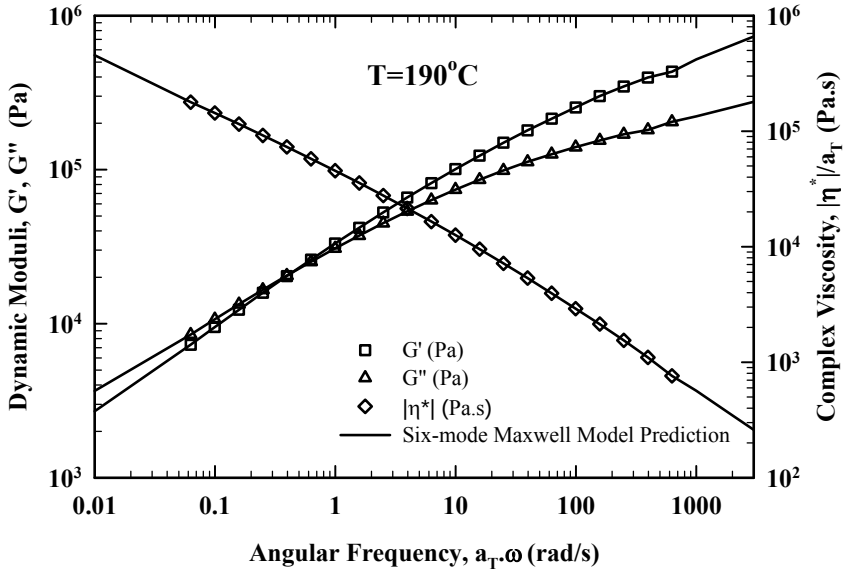

FIGURE 6.1: The master curves of storage (*G'*), loss moduli (*G"*), complex viscosity (η^*) and the corresponding fitting of the six-mode Maxwell model of HDPE-3 at the reference temperature of 190°C.

TABLE 6.1: Relaxation spectrum and K-BKZ model (with PSM damping function) parameters for HDPE-3 at the reference temperature of 190ºC.

Relaxation spectrum	
g_i (Pa)	λ_i (s)
409473.3	0.0008
187286.8	0.008
103796.4	0.058
47630.8	0.408
18669.6	2.96
8792.8	29.11
PSM parameters	
α_p	β_p
8.5	0.45

6.1.2.2 Step-strain stress relaxation

Stress relaxation tests at various step strains from 0.05 to 10 were performed at T=190 ºC using the parallel partitioned plate geometry mounted on MCR 702 with gap, h_p=0.75 mm. As previously mentioned, this feature allows accurate measurement of rheological data of the highly viscoelastic polymer melts at high shear rates and strains. FIGURE 6.2 shows the relaxation modulus data at different levels of step strains. The curves obtained at low values of step strains ($\gamma \leq 0.1$) are independent of strains and are considered to represent the linear relaxation modulus. These curves agree well with the relaxation modulus obtained from relaxation spectrum using SAOS experiments. Curves for other strains are below the linear relaxation modulus, indicating the "dampening" of the linear response. By shifting the data of non-linear regime to linear viscoelastic data, the damping function, $h(\gamma)$ is determined using the following equation:

$$h(\gamma) = \frac{G(\gamma, t)}{G(t)} \tag{6.5}$$

Where $G(\gamma, t)$ and $G(t)$ are the non-linear and linear relaxation modulus, respectively. The determined damping function is plotted versus strain, γ in FIGURE 6.3, along with the PSM fitting

(Equation 6.4) [Papanastasiou *et al*. (1983)]. As depicted in FIGURE 6.3, using $\alpha_p = 8.5$ results in a satisfactory fit of the experimental data. This parameter is listed in TABLE 6.1.

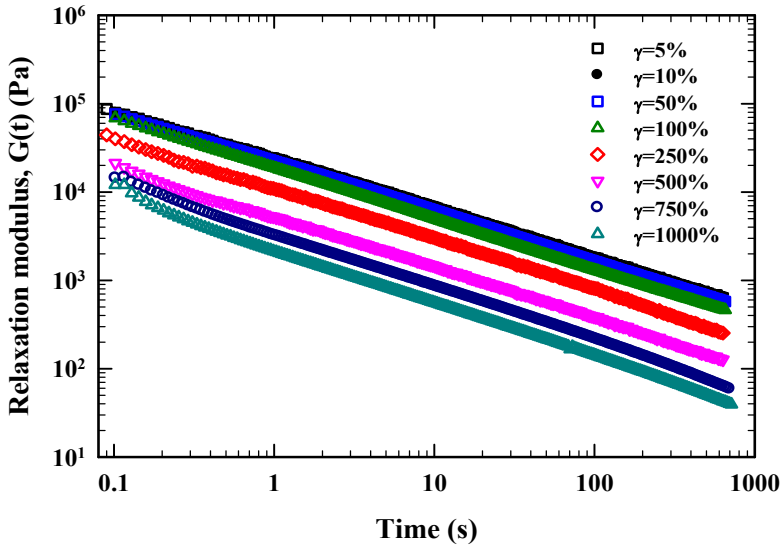

FIGURE 6.2: Step-strain relaxation data after imposition of different levels of step strains for HDPE-3 at 190°C.

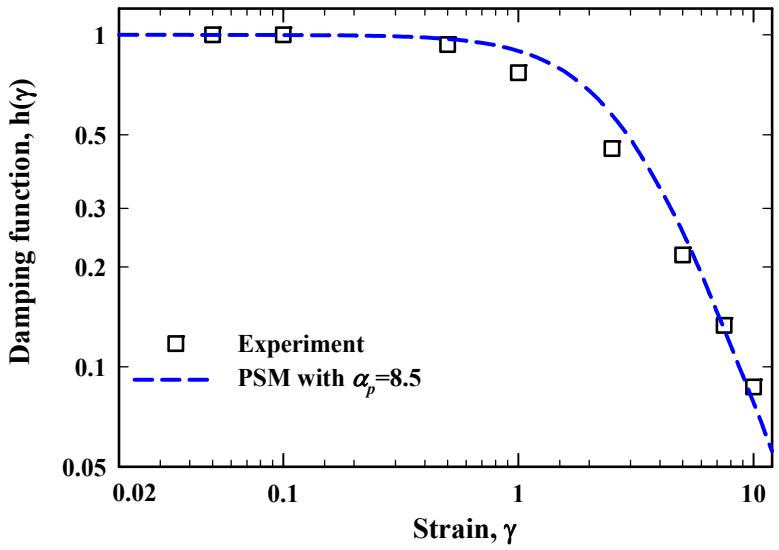

FIGURE 6.3: The damping function obtained from step stain relaxation experiments along with the fit of the PSM model (Equation 6.4) using $\alpha_p = 8.5$.

6.1.2.3 Uniaxial extension

Uniaxial extensional tests were conducted at T=190 ºC, at different Hencky strain rates ranging from 0.5 to 10 s^{-1} using the SER2 fixture. FIGURE 6.4 plots the uniaxial stress growth coefficient, η_E^+ versus time, along with the K-BKZ model (with PSM damping function) predictions. The optimum value of the "β_p" that fits the extensional data well is 0.45 (listed in TABLE 6.1).

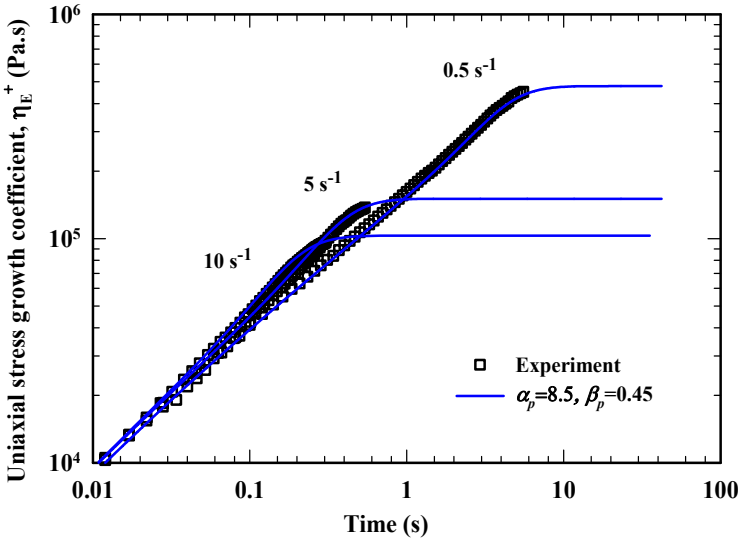

FIGURE 6.4: Experimental data (symbols) and the K-BKZ PSM model predictions (lines) of the uniaxial stress growth coefficient (η_E^+) at different Hencky strain rates at T=190 ºC.

6.1.3 Surface energy

To alter the surface energy, the lower plate of the partitioned parallel plate geometry have been coated with fluoroalkyl silane using solution based dip-coating method. By this method, fluoro groups have been deposited on the surface reducing the surface energy [Moradi *et al.* (2013), Moradi (2014)].

6.1.4 Static slip velocity

The slip velocity of the HDPE melt is studied using rotational rheometer equipped with the parallel partitioned plate geometry with different gap spacings between the parallel disks.

6.1.4.1 Slip velocity from rotational rheometer equipped with parallel partitioned plate

The newly developed partitioned plate has been used to study slip at higher shear rates. Start-up of steady shear experiments were performed for HDPE-3 at three different gaps, namely 0.5, 0.75, and 1 mm. This geometry allows measuring the non-linear shear flow behavior of highly viscoelastic polymer melts, which suffer from edge fracture in regular parallel plate geometries. Reliable data can be obtained with this system at high shear rates and strains by avoiding effects of edge fracture [Meissner *et al.* (1989), Snijkers and Vlassopoulos (2011), Konaganti *et al.* (2016)]. FIGURE 6.5 depicts the gap dependence of the shear stress growth coefficient response for all three gaps at the nominal shear rate of 20 s^{-1} (which is the average shear rate through the radius of the center plate, equal to $\frac{2\Omega R}{3h_p}$ where Ω is the angular velocity, R is the radius of the center plate, and h_p is the gap between the upper and lower plates). Both the steady-state shear stress value and the maximum value of the overshoot scale with the gap spacing h_p. The gap dependence is consistent with the assumption of slip and such data can be used to calculate the slip velocity.

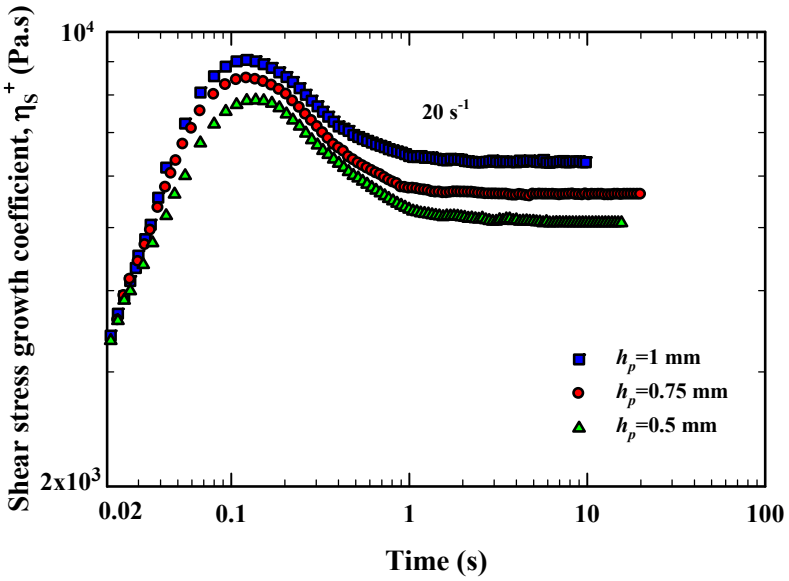

FIGURE 6.5: The shear stress growth coefficient, η_S^+ response of HDPE-3 at nominal shear rate of 20 s^{-1} using rotational rheometer equipped with a parallel partitioned plate at three different gaps.

In order to calculate the slip velocity from the start-up of shear data, the method described by Yoshimura and Prud'homme (1988) is used. FIGURE 6.6 shows the flow curves (shear stress at the edge of the center disk, σ_R versus the nominal shear rate at edge of the center disk, $\dot{\gamma}_{AR}$) of HDPE-3 at different gaps along with the LVE data. The nominal shear rate at the edge of the center plate away from the edge fracture is calculated from the following equation:

$$\dot{\gamma}_{AR} = \frac{\Omega R}{h_p} \tag{6.6}$$

Where Ω is the velocity, R is the radius of the rotating plate (center plate), and h_p is the gap between the upper and lower plates. The shear stress at the edge of the center plate, σ_R is determined by differentiating the torque, T with respect to $\dot{\gamma}_{AR}$ as follows:

$$\sigma_R = \frac{T}{2\pi R^3}\left[3 + \frac{d\ln T}{d\ln \dot{\gamma}_{AR}}\right] \tag{6.7}$$

It can be seen form FIGURE 6.6, that the stress response at large values of shear rate is gap dependent. Moreover, a considerable deviation from the LVE curve is observed at large shear deformations. These data can be used to calculate the slip velocity as a function of shear stress by using the Mooney analysis or deviation from LVE curve [Park *et al.* (2008), Hatzikiriakos (2012), Ansari *et al.* (2013a), Chatzigiannakis *et al.* (2017b)]. The Mooney analysis for parallel plates is defined by the following equation [Mooney (1931)]:

$$\dot{\gamma}_{AR} = \dot{\gamma}_R + \frac{2V_S}{h_p} \tag{6.8}$$

Where $\dot{\gamma}_R$ is the true shear rate at the edge. The slip data calculated from Mooney analysis [Mooney (1931)] and that from the deviation of flow curve at different gaps from LVE (Equation 6.9) are plotted together in FIGURE 6.7. Very good agreement between these two methods is found.

$$V_S = \frac{h_p}{2}(\dot{\gamma}_{AR} - \omega) \tag{6.9}$$

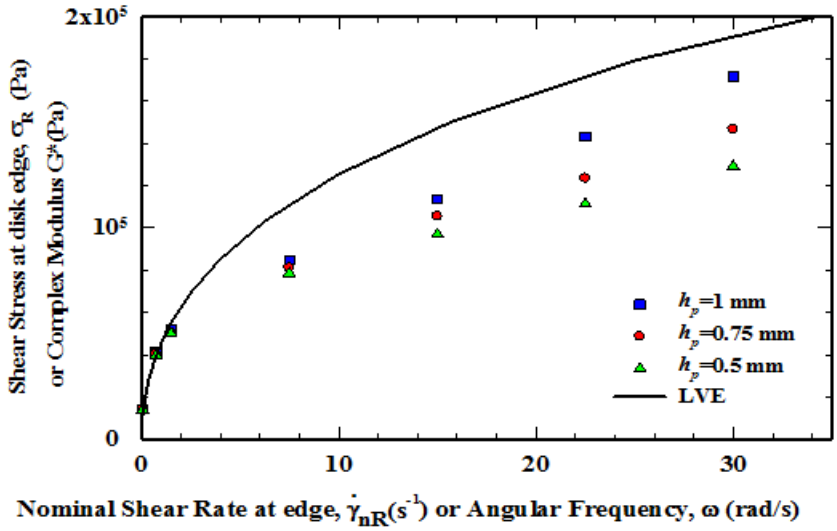

FIGURE 6.6: The flow curves of the studied polymer obtained from the parallel partitioned plate rheometer at different gaps along with the LVE data plotted as a flow curve.

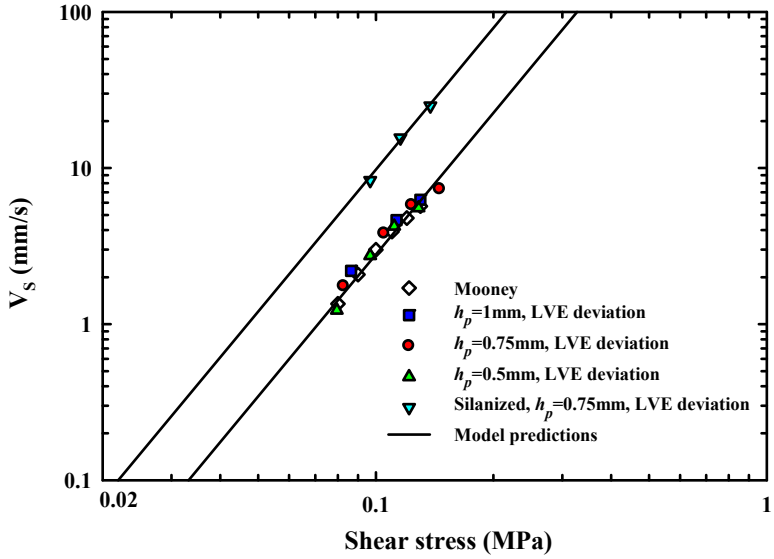

FIGURE 6.7: The slip velocity as a function of shear stress for HDPE-3 before and after silanization at T=190 °C. The solid lines represent the slip prediction based on double reptation theory (Equation 6.10).

Similarly, the deviation from the LVE curve was used to calculate slip velocity of HDPE-3 after coating the lower plate with fluoroalkylsilane by taking into account that only one plate is treated (using $V_S^l = h_p(\dot{\gamma}_{AR} - \omega) - V_S$, where V_S^l is the slip velocity on treated lower plate and V_S is the slip velocity on clean/ untreated upper plate which is known from previous experiment). The start-up of shear tests were performed for gap of 0.75 mm at different values of nominal shear rate. The slip data calculated from deviation of flow curve after silanization from LVE curve are added to FIGURE 6.7. As expected, silanization has increased the polymer slip velocity in agreement with data previously reported in literature [Wang and Drda (1997), Ebrahimi *et al.* (2016a)].

6.1.4.2 Slip modelling based on double reptation theory

As discussed in Chapter 3, elements from the theory of double reptation were used to relate the slip velocity of several HDPEs with their molecular weights and their distributions. Thus, for a given MWD of a HDPE melt, Equation 3.10 can be used to generate its slip velocity versus shear

stress relationship without performing any additional experiments. Moreover, the effects of surface roughness and energy on slip velocity were included in this model to produce a general relationship (Equation 5.11). Consolidating the effects of all parameters the constant *A'* can be recovered as defined in Equation 5.5. The values of *A'* and *n* for HDPE-3 are reported in TABLE 6.2. The calculated slip velocities of HDPE-3 on clean and silanized surfaces based on double reptation theory (Equation 5.11) are depicted in FIGURE 6.7 with solid lines. As can be seen from this figure, excellent agreement between experimental and calculated velocities is observed.

TABLE 6.2: Static and dynamic slip velocity coefficients for slippage of HDPE-3 on clean/ untreated and silanized substrates at ambient pressure.

Type of Surface	Static Slip		Dynamic Slip
	A' $(mms^{-1}MPa^{-n})$	n	λ_S (s)
Clean/ untreated	2915.7	0.33	0.224
Silanized	10205	0.33	0.107

6.1.5 Dynamic slip velocity

As discussed in Chapter 1, the static slip velocity models imply that the slip velocity adjusts instantaneously to the wall shear stress and they do not consider slip relaxation effects observed in transient flows. Therefore, dynamic models must be used in transient conditions to address these slip relaxation effects. [Pearson and Petrie (1965), Hatzikiriakos and Dealy (1991), Hatzikiriakos and Kalogerakis (1994), Hatzikiriakos (1994), Graham (1995), Lan *et al*. (2000), Kazatchkov and Hatzikiriakos (2010), Kaoullas and Georgiou (2015)]

By applying double reptation method and substituting Equation 5.11 for smooth surface (free surface fraction, φ=0) to Equation 1.18, following relation is obtained which includes shear stress dependence of slip velocity, molecular weight and its distribution, surface energy, as well as slip relaxation effects:

$$V_S + \lambda_S \frac{dV_S}{dt} = A\left(\frac{W_{adh}}{W_{adh,e}}\right)^2 \left\{\int_0^\infty \left[M^\beta w(M) \int_M^\infty w(M')dM'\right]dM\right\}\sigma_w^{1/n} \tag{6.10}$$

This model includes dynamic response and the steady shear properties. In order to check its applicability in predicting the transient response of polymer melts in start-up of shear experiments, the K-BKZ model (with PSM damping function) is coupled with Equation 6.10 and the predictions are compared with experimental data.

6.1.5.1 Start-up of steady shear (untreated surfaces)

FIGURE 6.8 shows the shear stress growth coefficient, η_S^+ , of HDPE-3 at different nominal shear rates of 0.05, 0.5 and 1 s^{-1} using the parallel partitioned plate geometry with gap, $h_p=0.75mm$ at temperature of 190◦C along with the K-BKZ PSM model predictions under no slip condition. Very good agreement between model prediction and experimental results are observed, as no significant slippage was detected at these small values of shear deformations using rotational rheometer. Simply slip is small enough that does not manifest itself in these macroscopic measurements. However, at the higher nominal shear rate of 5 s^{-1} steady and dymanic slip effects become evident (FIGURE 6.9 (a)). The K-BKZ PSM model predictions under no slip, static slip, and dynamic slip conditions using the optimum value of λ_S that best describes the experimental data are also shown in FIGURE 6.9 (a). At this higher shear rate, the slip becomes sizable from the macroscopic point of view and the K-BKZ PSM model under the assumption of no slip overpredicts the experimental results. Therefore, the steady state slip is considered by coupling the K-BKZ PSM model with the static slip model (Equation 5.11). As shown in FIGURE 6.9, the predictions are improved and the K-BKZ PSM model under static slip condition can predict the steady-state value accurately. However, it fails to capture the overshoot response of the polymer, and a dynamic slip velocity model is needed to predict the transient shear response and the overshoot. The model prediction using dynamic slip model with slip relaxation time, $\boldsymbol{\lambda_S}$=0.224s fits the experimental data very well. Therefore, a dynamic slip model (Equation 6.10) coupled with the K-BKZ model is necessary in predicting both the steady-state and transient behavior of HDPE-3. Similar results are reported for the nominal shear rates of 10 and 20 s^{-1} in Figure 6.9 (b), confirming the applicability of the K-BKZ model under dynamic slip condition in accurately predicting the experimental results at high shear rates using the same value of λ_S=0.224s.

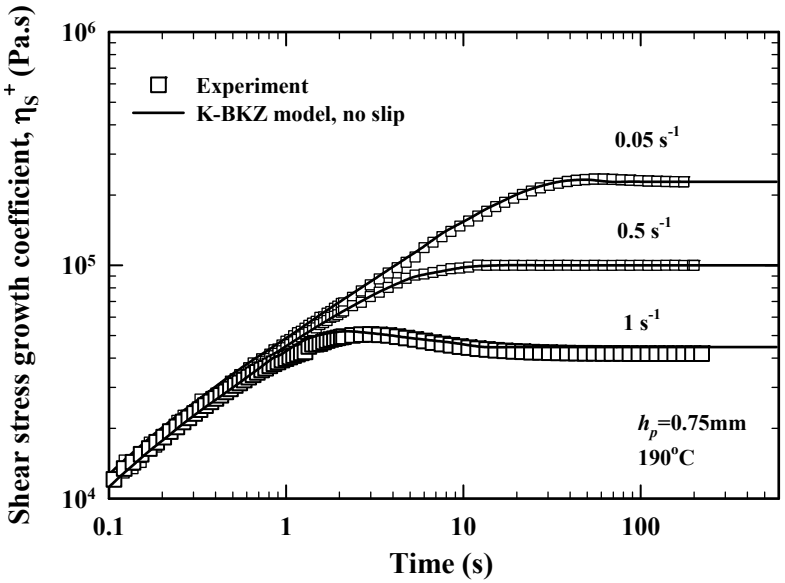

FIGURE 6.8: Start-up of steady shear of HDPE-3 at gap, h_p=*0.75mm*, temperature of 190◦C at various values of the nominal shear rates and comparisons with the K-BKZ PSM model predictions under no slip condition. Good agreement implies that the slip effects are negligible for these macroscopic measurements.

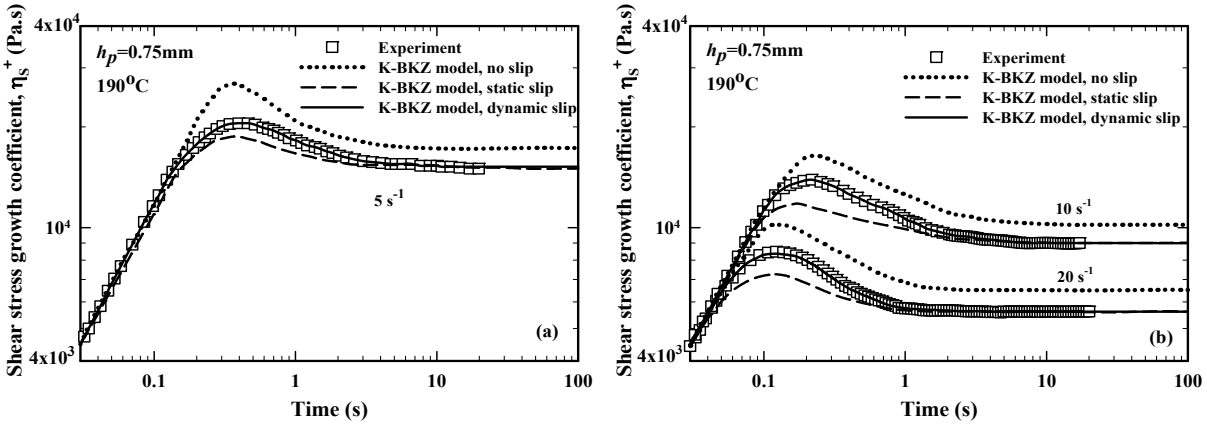

FIGURE 6.9: Start-up of steady shear of HDPE-3 at gap, h_p=*0.75mm*, temperature of 190◦C at the nominal shear rates of (a) 5s^{-1} and (b) 10 and 20 s^{-1} along with the K-BKZ PSM model predictions with no-slip, with static slip and with dynamic slip conditions.

6.1.5.2 Start-up of steady shear (silanized surfaces)

As mentioned, the lower plate of parallel partitioned plate geometry was coated with fluoroalkyl silane using a solution based dip-coating method in order to alter the surface energy and thus the slip behavior of the polymer. The hypothesis was to examine if the slip relaxation time was still the same. A different relaxation time would imply a different slip mechanism. The shear stress response of HDPE-3 at the nominal shear rate of 10 s^{-1} for clean/ untreated and silanized lower plate is demonstrated in FIGURE 6.10. It is clear that silanization has increased the slip velocity resulting in a decrease of steady state shear stress [Ebrahimi *et al.* (2016a)]. Moreover, the magnitude of overshoot and its location has been changed in the presence of coating. A different value of slip relaxation time, λ_S=0.107s has been calculated to fit the experimental data in the presence of coating implying a different slip mechanism. In the case of silanized substrate, silanization reduces the surface energy and thus the adhesion of polymer chains to the surface. Note that in the case of clean/ untreated surface, the number of entanglements of the chains in the bulk with the chains adsorbed next to the solid boundary plays a significant role i.e. slip is a result of disentanglement known as cohesive failure. In the case of silanization, these entanglements are significantly reduced and the mechanism of slip is mostly governed by direct desorption of the chains next to the silanized surface (adhesive failure) [Hatzikiriakos (2012)]. Therefore, in this case, weaker bonds are formed on the surface and the slip velocity is increased resulting in decrease in the steady-state value of shear stress. Moreover, polymer chains relax more readily and surface bonds are ruptured under lower strains resulting in the faster overshoot of shear stress [Park *et al.* (2017)]. The fitted stress relaxation time is reduced from λ_S=0.224s for clean/ untreated surface to λ_S=0.107s for silanized surface. These values are added to TABLE 6.2.

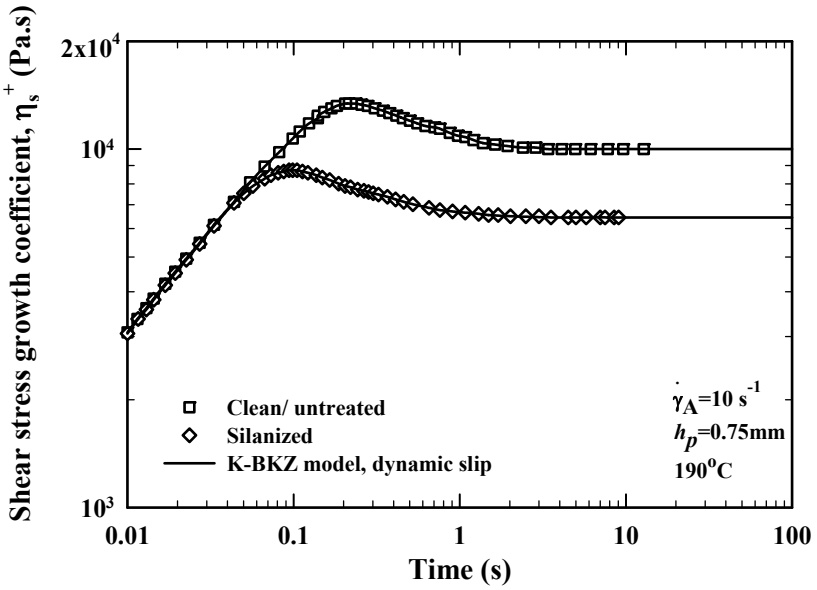

FIGURE 6.10: Start-up of steady shear of HDPE-3 at nominal shear rate of 10 s^{-1} using parallel partitioned plate rheometer with clean/ untreated and silanized lower plate and comparisons with the K-BKZ PSM model predictions under dynamic slip conditions.

6.2 Conclusions

In this chapter, the slip behavior of a HDPE melt was studied in steady and unsteady flows. Slip velocity was calculated using a rotational rheometer with a parallel partitioned plate geometry which allows accurate measurements in high shear deformations and rates of deformation by postponing edge fracture [Snijkers and Vlassopoulos (2011), Konaganti *et al.* (2016), Konaganti (2017)]. Moreover, silanization was applied in order to change the surface energy. The double reptation mixing rule was used to predict the slip velocity [Ebrahimi *et al.* (2015, 2016a, 2016b)], and very good agreement was observed between experimental and calculated results (refer FIGURE 6.7).

Start-up of steady shear experiments at various values of shear rates were performed and a constitutive equation, K-BKZ model with PSM damping function, under no slip, static slip, and dynamic slip conditions was used to predict the transient shear response of HDPE-3. Our results show that at higher shear rates ($\geq 5s^{-1}$), where slip becomes sizable from the macroscopic point

of view, although a static slip model can accurately predict the steady state shear values, it fails to predict the overshoot that occurs during the start-up. Therefore, a dynamic slip model is needed to preserve the dynamics of the flow and predict the overshoot correctly. By silanization of the substrate and reducing surface energy, slip velocity is increased and the slip relaxation time is reduced. The fitted stress relaxation time is changed from λ_S=0.224s for clean/ untreated surface to λ_S=0.107s for silanized surface indicating also that the slip mechanism in both cases is different i.e. disentaglement (cohesive failure) in the case of clean/ untreated surfaces versus direct desorption (adhesive failure) in the case of silanized surfaces.

Chapter 7: Conclusions and Recommendations

In this PhD thesis, the slip behavior of several groups of polymers including monodisperse and polydisperse polymers was studied to fully understand the effects of both polymer and surface characteristics under steady and dynamic conditions. This work has generated a comprehensive model to predict the slip velocity of polydisperse linear polymers based on polymer MW and MWD, as well as surface energy and morphology. This chapter summarizes the important results obtained from the experiments and modeling reported in the thesis. Recommendations for further work are also provided.

7.1 Conclusions

Key conclusions and contributions to the knowledge are described as following:

- The double reptation mixing rule was used to develop a general expression to calculate the dependence of the slip velocity on polymer MW and MWD. The applicability of the derived relationship was confirmed by accurately predicting the slip velocity of several polydisperse unimodal HDPEs (with different MW and MWD).
- The dependence of slip velocity on wall shear stress was investigated, and it was explained that the slip velocity is a power-law function of the wall shear stress to an exponent *m* which is equal to inverse of the local slope of the flow curve of the corresponding polymer, $n \equiv d\log(\sigma_w)/d\log(\dot{\gamma}_w)$.
- The dependence of slip velocity on molecular weight was explained based on theoretical models. For highly entangled flexible polymers such as PBD and HDPE, arm retraction is the dominant mechanism of relaxation resulting in scaling $V_s \propto M_w^{-2}$. However, for stiff polymers with high entanglement molecular weights such as PS, constraint release is the main relaxation mechanism leading to the relation $V_S \propto M_w^{-3}$.
- It was observed that the proposed model underestimates the slip velocity of bimodal HDPEs due to the segregation of shorter chains to the surface. Therefore, Van der Gucht (2002) method was used to calculate the MWD at the surface of these bimodal

HDPEs. These calculated surface-MWDs were further used to calculate the slip based on our proposed slip model and a significant improvement was found.

- Novel experiments were performed to fully understand the effects of surface energy and topology on the slip of polymer melts. Laser ablation was used to fabricate controlled roughness on the slit die surfaces. Moreover, solution based dip-coating method was applied to reduce the surface energy of the substrates.
- The proposed slip model based on double reptation theory was modified to include the effects of surface energy and topology (roughness). Work of adhesion and the "free surface fraction" (degree of roughness) of the substrates were incorporated in the model to take into account surface conditions.
- The newly available Parallel Partitioned Plate fixture from AntonPaar was used to procure non-linear rheological data of the studied HDPE melt for shear strains as high as 10 and shear rates as high as $20s^{-1}$ which was not possible using conventional fixtures. Using this fixture, the slip velocity of the HDPE melt was studied under steady and dynamic conditions.
- A constitutive equation, integral K-BKZ model with PSM damping function, under no slip, static slip, and dynamic slip conditions was used to predict the transient shear response of the HDPE melt. The experimental results have shown that at higher shear rates ($\geq 5s^{-1}$), where slip becomes sizable from the macroscopic point of view, a dynamic slip model is needed to preserve the dynamics of the flow and predict the overshoot correctly. Moreover, by silanization of the substrate and reducing surface energy, the slip velocity is increased and the slip relaxation time is reduced.

7.2 Recommendations for future work

There are many areas in the subject of polymer slip, which need to be addressed in the future. The following suggestions can be considered for future work:

- In order to completely understand the dependence of slip velocity on polymer characteristics, the present work should be extended to polymers with other than linear

architecture such as branched and star polymers. This would allow one to study the effects of polymer architecture on slip of polymer melts. Moreover, it would be of great interest to compare the slip relaxation time of linear and non-linear polymer melts under dynamic flows.

- It would be helpful to use flow-induced molecular weight fractionation methods to accurately calculate the concentration of shorter chains in the surface. Therefore, better predictions of experimental results would be obtained at high values of shear stress.
- It would be very useful to conduct experiments to precisely relate surface migration of shorter chains to the polymer polydispersity. These experimental data can be used subsequently to develop fractionation models.
- A systematic study on slip of polymer solutions on hydrophobic, and superhydrophobic and superoleophobic surfaces would be interesting to be performed.

Bibliography

Adjari, A., Brochard-Wyart, F., de Gennes, P. G., Leibler, L., Viovy, J. L., & Rubinstein, M. (1994). Slippage of an entangled polymer melt on a grafted surface. *Physica A: Statistical Mechanics and its Applications*, *204*(1-4), 17-39.

Allal, A., & Vergnes, B. (2007). Molecular design to eliminate sharkskin defect for linear polymers. *Journal of Non-Newtonian Fluid Mechanics*, *146*(1), 45-50.

Allal, A., & Vergnes, B. (2009). Molecular interpretation of the "stick–slip" defect of linear polymers. *Journal of Non-Newtonian Fluid Mechanics*, *164*(1), 1-8.

Anastasiadis, S. H., & Hatzikiriakos, S. G. (1998). The work of adhesion of polymer/wall interfaces and its association with the onset of wall slip. *Journal of Rheology*, *42*(4), 795-812.

Ansari, M., Hatzikiriakos, S. G., Sukhadia, A. M., & Rohlfing, D. C. (2011). Rheology of Ziegler–Natta and metallocene high-density polyethylenes: broad molecular weight distribution effects. *Rheologica acta*, *50*(1), 17-27.

Ansari, M., Inn, Y. W., Sukhadia, A. M., DesLauriers, P. J., & Hatzikiriakos, S. G. (2012a). Melt fracture of HDPEs: metallocene versus Ziegler–Natta and broad MWD effects. *Polymer*, *53*(19), 4195-4201.

Ansari, M., Zisis, T., Hatzikiriakos, S. G., & Mitsoulis, E. (2012b). Capillary flow of low-density polyethylene. *Polymer Engineering & Science*, 52(3), 649-662.

Ansari, M., Hatzikiriakos, S. G., Sukhadia, A. M., & Rohlfing, D. C. (2012c). Melt fracture of two broad molecular weight distribution high-density polyethylenes. *Polymer Engineering & Science*, *52*(4), 795-804.

Ansari, M. (2012d). *Rheology and processing of high-density polyethylenes (HDPEs): Effects of molecular characteristics* (Doctoral dissertation, University of British Columbia).

Ansari, M., Mitsoulis, E., & Hatzikiriakos, S. G. (2013a). Capillary extrusion and swell of a HDPE melt exhibiting slip. *Advances in Polymer Technology*, *32*(S1), E369-E385.

Ansari, M., Inn, Y. W., Sukhadia, A. M., DesLauriers, P. J., & Hatzikiriakos, S. G. (2013b). Wall slip of HDPEs: Molecular weight and molecular weight distribution effects. *Journal of Rheology*, *57*(3), 927-948.

Archer, L. A., "Wall slip: Measurement and modelling issues," in *Polymer processing instabilities control and understanding*, edited by S. G. Hatzikiriakos and K. B. Migler (Marcel Dekker, NY, 2005).

Archer, L. A., Chen, Y. L., & Larson, R. G. (1995). Delayed slip after step strains in highly entangled polystyrene solutions. *Journal of Rheology*, *39*(3), 519-525.

Awati, K. M., Park, Y., Weisser, E., & Mackay, M. E. (2000). Wall slip and shear stresses of polymer melts at high shear rates without pressure and viscous heating effects. *Journal of non-newtonian fluid mechanics*, *89*(1), 117-131.

Azese, M. N. (2015). In an attempt to generalize wall slip in fluid flows using a series expansion of the wall shear stress: Case of non-Newtonian [Phan-Thien-Tanner fluid]. *European Journal of Mechanics, B/Fluids*, *52*, 109–119.

Azese, M. N. (2016). On the generalization of velocity slip in fluid flows using a steady-state series expansion of the wall shear stress: Case of simple Newtonian fluids. *European Journal of Mechanics, B/Fluids*, *57*, 204–213.

Barone, J. R., & Wang, S. Q. (2000). Adhesive wall slip on organic surfaces. *Journal of non-newtonian fluid mechanics*, *91*(1), 31-36.

Barrat, J. L. (1999). Influence of wetting properties on hydrodynamic boundary conditions at a fluid/solid interface. *Faraday discussions*, *112*, 119-128.

Bartolo, D., Bouamrirene, F., Verneuil, É., Buguin, A., Silberzan, P., & Moulinet, S. (2006). Bouncing or sticky droplets: Impalement transitions on superhydrophobic micropatterned surfaces. *EPL (Europhysics Letters)*, *74*(2), 299.

Bergem, N. (1976, August). Visualization studies of polymer melt flow anomalies in extrusion. In *Proceedings of the VIIth International Congress on Rheology, Chalmers University of Technology, Gothenburg, Sweden* (pp. 50-54).

Birinci, E., & Kalyon, D. M. (2006). Development of extrudate distortions in poly (dimethyl siloxane) and its suspensions with rigid particles. *Journal of Rheology*, *50*(3), 313-326.

Black, W. B. (2000). *Wall slip and boundary effects in polymer shear flows* (Doctoral dissertation, University of Wisconsin-Madison).

Blyler, L. L., & Hart, A. C. (1970). Capillary flow instability of ethylene polymer melts. *Polymer Engineering & Science*, *10*(4), 193-203.

Bocquet, L., & Barrat, J. L. (1993). Hydrodynamic boundary conditions and correlation functions of confined fluids. *Physical review letters*, *70*(18), 2726.

Bocquet, L., & Barrat, J. L. (1994). Hydrodynamic boundary conditions, correlation functions, and Kubo relations for confined fluids. *Physical review E*, *49*(4), 3079.

Boukany, P. E., & Wang, S. (2010). Shear Banding or Not in Entangled DNA Solutions. *Macromolecules*, *43*, 6950–6952.

Brochard, F., & De Gennes, P. G. (1992). Shear-dependent slippage at a polymer/solid interface. *Langmuir*, *8*(12), 3033-3037.

Brochard-Wyart, F., De Gennes, P. G., Hervert, H., & Redon, C. (1994). Wetting and slippage of polymer melts on semi-ideal surfaces. *Langmuir*, 10(5), 1566-1572.

Brochard-Wyart, F., Gay, C., & De Gennes, P. G. (1996). Slippage of polymer melts on grafted surfaces. *Macromolecules*, *29*(1), 377-382.

Busse, W. F. (1964). Two decades of high-polymer physics: A survey and forecast. *Physics Today*, *17*(9), 32-41.

Cassie, A. B. D., & Baxter, S. (1944). Wettability of porous surfaces. *Transactions of the Faraday society*, *40*, 546-551.

Chatzigiannakis, E., Ebrahimi, M., & Hatzikiriakos, S. G. (2017a). On the molecular weight dependence of slip velocity of polymer melts. *Journal of Rheology*, *61*(4), 731-739.

Chatzigiannakis, E., Ebrahimi, M., Wagner, M. H., & Hatzikiriakos, S. G. (2017b). Wall slip of polyisobutylenes : effect of molecular characteristics. *Rheologica Acta*, *56*, 85–94.

Chovelon, J. M., Aarch, L. El, Charbonnier, M., & Romand, M. (1995). Silanization of Stainless Steel Surfaces : Influence of Application Parameters. *The Journal of Adhesion*, *50*(1), 43–58.

Cottin-Bizonne, C., Barrat, J. L., Bocquet, L., & Charlaix, E. (2003). Low-friction flows of liquid at nanopatterned interfaces. *Nature materials*, *2*(4), 237-240.

Cottin-Bizonne, C., Barentin, C., Charlaix, É., Bocquet, L., & Barrat, J. L. (2004). Dynamics of simple liquids at heterogeneous surfaces: molecular-dynamics simulations and hydrodynamic description. *The European Physical Journal E*, *15*(4), 427-438.

Dao, T. T., & Archer, L. A. (2002). Stick− slip dynamics of entangled polymer liquids. *Langmuir*, *18*(7), 2616-2624.

Dealy, J. M., & Wissbrun, K. F. (2012). *Melt rheology and its role in plastics processing: theory and applications*. Springer Science & Business Media.

Dealy, J. M., & Wang, J. (2013). *Melt rheology and its applications in the plastics industry*. Springer Science & Business Media.

Den Otter, J. L., Wales, J. L. S., & Schijf, J. (1967). The velocity profiles of molten polymers during laminar flow. *Rheologica Acta*, *6*(3), 205-209.

Des Cloizeaux, J. (1988). Double reptation vs. simple reptation in polymer melts. *EPL (Europhysics Letters)*, *5*(5), 437.

Des Cloizeaux, J. (1990). Relaxation and viscosity anomaly of melts made of long entangled polymrs. Time-dependent reptation. *Macromolecules*, *23*(21), 4678-4687.

Drda, P. P., & Wang, S. Q. (1995). Stick-slip transition at polymer melt/solid interfaces. *Physical review letters*, *75*(14), 2698.

Durliat, E., Hervet, H., & Leger, L. (1997). Influence of grafting density on wall slip of a polymer melt on a polymer brush. *EPL (Europhysics Letters)*, *38*(5), 383.

El Kissi, N., & Paiu, J. M. (1990). The different capillary flow regimes of entangled polydimethylsiloxane polymers: macroscopic slip at the wall, hysteresis and cork flow. *Journal of Non-Newtonian Fluid Mechanics*, *37*(1), 55-94.

El Kissi, N., Leger, L., Piau, J. M., & Mezghani, A. (1994). Effect of surface properties on polymer melt slip and extrusion defects. *Journal of non-newtonian fluid mechanics*, *52*(2), 249-261.

Ebrahimi, M., Ansari, M., & Hatzikiriakos, S. G. (2015). Wall slip of polydisperse linear polymers using double reptation. *Journal of Rheology*, *59*(3), 885–901.

Ebrahimi, M., Konaganti, V. K., Moradi, S., Doufas, A. K., & Hatzikiriakos, S. G. (2016a). Slip of polymer melts over micro/nano-patterned metallic surfaces. *Soft Matter*, *12*(48), 9759–9768.

Ebrahimi, M., Ansari, M., Inn, Y. W., & Hatzikiriakos, S. G. (2016b). Surface fractionation effects on slip of polydisperse polymer melts. *Physics of Fluids*, *28*(9), 93101.

Fetters, L. J., Lohse, D. J., Richter, D., Witten, T. A., & Zirkel, A. (1994). Connection between polymer molecular-weight, density, chain dimensions, and melt viscoelastic properties. *Macromolecules*, *27*(17), 4639-4647.

Forsberg, P., Nikolajeff, F., & Karlsson, M. (2011). Cassie–Wenzel and Wenzel–Cassie transitions on immersed superhydrophobic surfaces under hydrostatic pressure. *Soft Matter*, *7*(1), 104-109.

Funatsu, K., & Kajiwara, T. (1988). Stress measurement of viscoelastic fluids by flow birefringence technique and slip phenomena of polymer melts. *Encyclopedia of Fluid Mechanics*, *7*.

Galt, J., & Maxwell, B. (1964). Velocity profiles for polyethylene melts. *Modern Plastics*, *42*(4), 115-189.

Gao, L., & McCarthy, T. J. (2009). Wetting 101°. *Langmuir*, *25*(24), 14105-14115.

Goldstein, S. (Ed.). (1938). *Modern developments in fluid dynamics: an account of theory and experiment relating to boundary layers, turbulent motion and wakes* (Vol. 1). Clarendon Press.

Graham, M. D. (1995). Wall slip and the nonlinear dynamics of large amplitude oscillatory shear flows. *Journal of Rheology*, *39*(4), 697-712.

Granick, S., Zhu, Y., & Lee, H. (2003). Slippery questions about complex fluids flowing past solids. *Nature materials*, *2*(4), 221-227.

Hariharan, A., Kumar, S. K., & Russell, T. P. (1990). A lattice model for the surface segregation of polymer chains due to molecular weight effects. *Macromolecules*, *23*(15), 3584-3592.

Hatzikiriakos, S. G., & Dealy, J. M. (1991). Wall slip of molten high density polyethylene. I. Sliding plate rheometer studies. *Journal of rheology*, *35*(4), 497-523.

Hatzikiriakos, S. G., & Dealy, J. M. (1992a). Wall slip of molten high density polyethylenes. II. Capillary rheometer studies. *Journal of Rheology*, *36*(4), 703-741.

Hatzikiriakos, S. G., & Dealy, J. M. (1992b). Role of slip and fracture in the oscillating flow of HDPE in a capillary. *Journal of Rheology*, *36*(5), 845-884.

Hatzikiriakos, S. G., Stewart, C. W., & Dealy, J. M. (1993). Effect of surface coatings on wall slip of LLDPE. *International Polymer Processing*, *8*(1), 30-35.

Hatzikiriakos, S. G., & Dealy, J. M. (1993). Effects of interfacial conditions on wall slip and sharkskin melt fracture of HDPE. *International Polymer Processing*, *8*(1), 36-43.

Hatzikiriakos, S. G., & Kalogerakis, N. (1994). A dynamic slip velocity model for molten polymers based on a network kinetic theory. *Rheologica Acta*, *33*, 38–47.

Hatzikiriakos, S. G. (1995). A multimode interfacial constitutive equation for molten polymers. *Journal of Rheology*, *39*, 61–71.

Hatzikiriakos, S. G., Kazatchkov, I. B., & Vlassopoulos, D. (1997). Interfacial phenomena in the capillary extrusion of metallocene polyethylenes. *Journal of Rheology*, *41*(6), 1299-1316.

Hatzikiriakos, S. G. (2012). Wall slip of molten polymers. *Progress in Polymer Science*, *37*(4), 624-643.

Hatzikiriakos, S. G. (2015). Slip mechanisms in complex fluid flows. *Soft Matter*, *11*, 7851–7856.

Hay, G., Mackay, M. E., McGlashan, S. A., & Park, Y. (2000). Comparison of shear stress and wall slip measurement techniques on a linear low density polyethylene. *Journal of non-newtonian fluid mechanics*, *92*(2), 187-201.

Helfand, E. (1976). Theory of inhomogeneous polymers. Lattice model for solution interfaces. *Macromolecules*, *9*(2), 307-310.

Henson, D. J., & Mackay, M. E. (1995). Effect of gap on the viscosity of monodisperse polystyrene melts: slip effects. *Journal of Rheology*, *39*(2), 359-373.

Hill, D. A., Hasegawa, T., & Denn, M. M. (1990). On the apparent relation between adhesive failure and melt fracture. *Journal of Rheology*, *34*(6), 891-918.

Huang, D. M., Sendner, C., Horinek, D., Netz, R. R., & Bocquet, L. (2008). Water slippage versus contact angle: A quasiuniversal relationship. *Physical review letters*, *101*(22), 226101.

Inn, Y. W, Sukhadia A. M., and Deslauriers P. J., "Flow-induced fractionation of bimodal metallocene polyethylene in capillary extrusion," in Annual Technical Conference—ANTEC, Conference Proceedings (Society of Plastics Engineers, 2014), p. 1108.

Inn, Y. W. (2015, April). Melt fracture, wall slip, and flow-induced fractionation of bimodal polyethylenes. In M. Zatloukal (Ed.), *AIP Conference Proceedings* (Vol. 1662, No. 1, p. 030004). AIP Publishing.

Israelachvili, J. N. (2011). *Intermolecular and surface forces*. Academic press.

Jacob N.. Israelachvili. (1985). *Intermolecular and Surface Forces: With Applications to Colloidal and Biological Systems*. Academic Press.

Jam, J. E., Nekoomanesh, M., Ahmadi, M., & Arabi, H. (2012). From molecular weight distribution to linear viscoelastic properties and back again: application to some commercial high-density polyethylenes. *Iranian Polymer Journal*, *21*(6), 403-413.

Johnson, M. B., Wilkes, G. L., Sukhadia, A. M., & Rohlfing, D. C. (2000). Optical properties of blown and cast polyethylene films: surface versus bulk structural considerations. *Journal of applied polymer science*, *77*(13), 2845-2864.

Joseph, P., Cottin-Bizonne, C., Benoît, J. M., Ybert, C., Journet, C., Tabeling, P., & Bocquet, L. (2006). Slippage of water past superhydrophobic carbon nanotube forests in microchannels. *Physical review letters*, *97*(15), 156104.

Joshi, Y. M., Lele, A. K., & Mashelkar, R. A. (2000). Slipping fluids: a unified transient network model. *Journal of non-newtonian fluid mechanics*, *89*(3), 303-335.

Joshi, Y. M., Lele, A. K., & Mashelkar, R. A. (2001). Molecular model for wall slip: Role of convective constraint release. *Macromolecules*, *34*(10), 3412-3420.

Joshi, Y. M., & Lele, A. K. (2002). Dynamics of end-tethered chains at high surface coverage. *Journal of Rheology*, *46*(2), 427-453.

Kalika, D. S., & Denn, M. M. (1987). Wall Slip and Extrudate Distortion in Linear Low-Density Polyethylene. *Journal of Rheology*, *31*(8), 815-834.

Kalyon, D. M., & Gevgilili, H. (2003). Wall slip and extrudate distortion of three polymer melts. *Journal of Rheology*, *47*(3), 683–699.

Kanoh, Y., Shibata, T., Nishimura, T., Usui, H., & Saeki, T. (1997). Wall slip of molten polymers in various conduits-Influence of solid surface conditions. *Nihon Reoroji Gakkaishi*, *25*(1), 37-41.

Kaoullas, G., & Georgiou, G. C. (2015). Start-up and cessation Newtonian Poiseuille and Couette flows with dynamic wall slip. *Meccanica*, *50*(7), 1747–1760.

Kazatchkov, I. B., Hatzikiriakos, S. G., & Stewart, C. W. (1995). Extrudate distortion in the capillary/slit extrusion of a molten polypropylene. *Journal of plastic film and sheeting*, *11*(1), 38-57.

Kazatchkov, I. B., & Hatzikiriakos, S. G. (2010). Relaxation effects of slip in shear flow of linear molten polymers. *Rheologica acta*, *49*(3), 267-274.

Kietzig, A. M., Hatzikiriakos, S. G., & Englezos, P. (2009). Patterned superhydrophobic metallic surfaces. *Langmuir*, *25*(8), 4821-4827.

Konaganti, K., V., Ansari, M., Mitsoulis, E., & Hatzikiriakos, S. G. (2016). The effect of damping function on extrudate swell. *Journal of Non-Newtonian Fluid Mechanics*, *236*, 73–82.

Konaganti, V. K. (2017). *Extrudate swell of high density polyethylene in capillary and slit dies* (Doctoral dissertation, University of British Columbia).

Lan, S. K., Giacomin, A. J., & Ding, F. (2000). Dynamic slip and nonlinear viscoelasticity. *Polymer Engineering & Science*, *40*(2), 507-524.

Lau, H. C., & Schowalter, W. R. (1986). A model for adhesive failure of viscoelastic fluids during flow. Journal of Rheology, 30(1), 193-206.

Larson, R. G. (1992). Instabilities in viscoelastic flows. Rheologica Acta,31(3), 213-263.

Lee, B. L., & White, J. L. (1974). An experimental study of rheological properties of polymer melts in laminar shear flow and of interface deformation and its mechanisms in two-phase stratified flow. *Transactions of the Society of Rheology*, *18*(3), 467-492.

Lee, B. L., & White, J. L. (1975). Notes: Experimental Studies of Disperse Two-Phase Flow of Molten Polymers Through Dies. *Transactions of the Society of Rheology*, *19*(3), 481-492.

Lee, C., & Choi, C. H. (2008). Structured surfaces for a giant liquid slip. *Physical review letters*, *101*(6), 064501.

Léger, L., Hervet, H., Massey, G., & Durliat, E. (1997). Wall slip in polymer melts. *Journal of Physics: Condensed Matter*, *9*(37), 7719.

Léger, L., Raphaël, E., & Hervet, H. (1999). Surface-anchored polymer chains: Their role in adhesion and friction. In *Polymers in confined environments* (pp. 185-225). Springer Berlin Heidelberg.

Legrand, F., Piau, J. M., & Hervet, H. (1998). Wall slip of a polydimethylsiloxane extruded through a slit die with rough steel surfaces: Micrometric measurement at the wall with fluorescent-labeled chains. *Journal of Rheology*, *42*(6), 1389-1402.

Léonforte, F., Servantie, J., Pastorino, C., & Müller, M. (2011). Molecular transport and flow past hard and soft surfaces: computer simulation of model systems. *Journal of Physics: Condensed Matter*, *23*(18), 184105.

Lim, F. J., & Schowalter, W. R. (1989). Wall slip of narrow molecular weight distribution polybutadienes. *Journal of Rheology*, *33*(8), 1359-1382.

Liu, T. Y., Soong, D. S., & Williams, M. C. (1981). Time-dependent rheological properties and transient structural states of entangled polymeric liquids—A kinetic network model. *Polymer Engineering & Science*, *21*(11), 675-687.

Luo, X.-L., & Tanner, R. I. (1988). Finite element simulation of long and short circular die extrusion experiments using integral models. *International Journal for Numerical Methods in Engineering*, *25*(1), 9–22.

Lupton, J. M., & Regester, H. W. (1965). Melt flow of polyethylene at high rates. *Polymer Engineering & Science*, *5*(4), 235-245.

Mackay, M. E., & Henson, D. J. (1998). The effect of molecular mass and temperature on the slip of polystyrene melts at low stress levels. *Journal of Rheology*, *42*(6), 1505-1517.

Macosko, C. W. (1994). Rheology principles, measurements, and applications, VCH Publ. *Inc, New York*.

Meissner, J., Garbella, R. W., & Hostettler, J. (1989). *Measuring normal stress differences in polymer melt shear flow*. Journal of Rheology (1978-present), 33(6), 843-864.

Mhetar, V., & Archer, L. A. (1998a). Slip in entangled polymer solutions. *Macromolecules*, *31*(19), 6639-6649.

Mhetar, V., & Archer, L. A. (1998b). Slip in entangled polymer melts. 1. General features. *Macromolecules*, *31*(24), 8607-8616.

Mhetar, V., & Archer, L. A. (1998c). Slip in entangled polymer melts. 2. Effect of surface treatment. *Macromolecules*, *31*(24), 8617-8622.

Migler, K. B., Hervet, H., & Leger, L. (1993). Slip transition of a polymer melt under shear stress. *Physical review letters*, *70*(3), 287.

Migler, K. B., Massey, G., Hervet, I., & Leger, L. (1994). The slip transition at the polymer-solid interface. *Journal of Physics: Condensed Matter*, *6*(23A), A301.

Milner, S. T. (1996). Relating the shear-thinning curve to the molecular weight distribution in linear polymer melts. *Journal of Rheology*, *40*(2), 303-315.

Mitsoulis, E., Kazatchkov, I. B., & Hatzikiriakos, S. G. (2005). The effect of slip in the flow of a branched PP melt: experiments and simulations. *Rheologica acta*, *44*(4), 418-426.

Mooney, M. (1931). Explicit formulas for slip and fluidity. *Journal of Rheology (1929-1932)*, *2*(2), 210-222.

Moradi, S., Kamal, S., Englezos, P., & Hatzikiriakos, S. G. (2013). Femtosecond laser irradiation of metallic surfaces: effects of laser parameters on superhydrophobicity. *Nanotechnology*, *24*(41), 415302.

Moradi, S., Englezos, P., & Hatzikiriakos, S. G. (2014). Contact angle hysteresis of non-flattened-top micro/nanostructures. *Langmuir*, *30*(11), 3274-3284.

Moradi, S. (2014). *Super-hydrophobic nanopatterned interfaces: optimization and manufacturing* (Doctoral dissertation, University of British Columbia).

Moradi, S., Kamal, S., & Hatzikiriakos, S. G. (2015). Superhydrophobic laser-ablated stainless steel substrates exhibiting Cassie–Baxter stable state. *Surface Innovations*, *3*(3), 151-163.

Münstedt, H., Schmidt, M., & Wassner, E. (2000). Stick and slip phenomena during extrusion of polyethylene melts as investigated by laser-Doppler velocimetry. *Journal of Rheology*, *44*(2), 413-427.

Musil, J., & Zatloukal, M. (2011). Experimental investigation of flow induced molecular weight fractionation during extrusion of HDPE polymer melts. *Chemical engineering science*, *66*(20), 4814-4823.

Musil, J., & Zatloukal, M. (2012a). Experimental investigation of flow induced molecular weight fractionation phenomenon for two linear HDPE polymer melts having same Mn and M w but different M_z and M_{z+1} average molecular weights. *Chemical engineering science*, *81*, 146-156.

Musil, J., & Zatloukal, M. (2012b). Flow induced molecular weight fractionation during capillary flow of linear polymer melt. In *Recent Advances in Fluid Mechanics, Heat & Mass*

Transfer and Biology–Proceedings of the 9th WSEAS International Conference on Fluids, Boston, MA (pp. 162-167).

Myerholtz, R. W. (1967). Oscillating flow behavior of high-density polyethylene melts. *Journal of Applied Polymer Science*, *11*(5), 687-698.

Navier, C. L. M. H. (1823). Mémoire sur les lois du mouvement des fluides. *Mem. Acad. Sci. Inst. Fr*, *6*(1823), 389-416.

Ngai, K. L., & Plazek, D. J. (1985). Relation of internal rotational isomerism barriers to the flow activation energy of entangled polymer melts in the high-temperature Arrhenius region. *Journal of Polymer Science: Polymer Physics Edition*, *23*(10), 2159-2180.

Noroozi, N., Thomson, J. A., Noroozi, N., Schafer, L. L., & Hatzikiriakos, S. G. (2012). Viscoelastic behaviour and flow instabilities of biodegradable poly (ε-caprolactone) polyesters. *Rheologica acta*, *51*(2), 179-192.

Othman, N., Jazrawi, B., Mehrkhodavandi, P., & Hatzikiriakos, S. G. (2012). Wall slip and melt fracture of poly (lactides). *Rheologica acta*, *51*(4), 357-369.

Papanastasiou, A. C., Scriven, L. E., & Macosko, C. W. (1983). An Integral Constitutive Equation for Mixed Flows : Viscoelastic Characterization. *Journal of Rheology*, *27*(4), 387–410.

Park, H. E., Lim, S. T., Smillo, F., Dealy, J. M., & Robertson, C. G. (2008). Wall slip and spurt flow of polybutadiene. *Journal of Rheology*, *52*(5), 1201-1239.

Park, J. D., Ahn, K. H., & Wagner, N. J. (2017). Structure-rheology relationship for a homogeneous colloidal gel under shear startup. *Journal of Rheology*, *61*(1), 117-137.

Pearson, J. R. A., & Petrie, C. J. S. (1965). On the melt-flow instability of extruded polymers.

Quéré, D. (2002). Rough ideas on wetting. *Physica A: Statistical Mechanics and its Applications*, *313*(1), 32-46.

Ramamurthy, A. V. (1986). Wall slip in viscous fluids and influence of materials of construction. *Journal of Rheology*, *30*(2), 337-357.

Reiter, G., Demirel, A. L., & Granick, S. (1994). From static to kinetic friction in confined liquid films. Science-AAAS-Weekly Paper Edition-including Guide to Scientific Information, 263(5154), 1741-1743.

Reyssat, M., Pépin, A., Marty, F., Chen, Y., & Quéré, D. (2006). Bouncing transitions on microtextured materials. *EPL (Europhysics Letters)*, *74*(2), 306.

Robert, L., Demay, Y., & Vergnes, B. (2004). Stick-slip flow of high density polyethylene in a transparent slit die investigated by laser Doppler velocimetry. *Rheologica Acta*, *43*(1), 89-98.

Rorrer, N. A., & Dorgan, J. R. (2014). Molecular-scale simulation of cross-flow migration in polymer melts. *Physical Review E*, *90*(5), 052603.

Rosenbaum, E. E., Hatzikiriakos, S. G., & Stewart, C. W. (1995). Flow implications in the processing of tetrafluoroethylene/hexafluoropropylene copolymers. *International Polymer Processing*, *10*(3), 204-212.

Rothstein, J. P. (2010). Slip on superhydrophobic surfaces. *Annual Review of Fluid Mechanics*, *42*, 89-109.

Sabzevari, S. M. (2015). *Wall Slip of Polydisperse Linear Polymer Melts* (Doctoral dissertation, Concordia University).

Sagiv, J. (1980). Organized monolayers by adsorption. 1. Formation and structure of oleophobic mixed monolayers on solid surfaces. *Journal of the American Chemical Society*, *102*(1), 92–98.

Sanchez-Reyes, J., & Archer, L. A. (2003). Interfacial slip violations in polymer solutions: Role of microscale surface roughness. *Langmuir*, *19*(8), 3304-3312.

Scheutjens, J. M. H. M., & Fleer, G. J. (1979). Statistical theory of the adsorption of interacting chain molecules. 1. Partition function, segment density distribution, and adsorption isotherms. *J. phys. Chem*, *83*(12), 1619-1635.

Scheutjens, J. M. H. M., & Fleer, G. J. (1980). Statistical theory of the adsorption of interacting chain molecules. 2. Train, loop, and tail size distribution. *The Journal of Physical Chemistry*, *84*(2), 178-190.

Schnell, E. (1956). Slippage of water over nonwettable surfaces. *Journal of Applied Physics*, *27*(10), 1149-1152.

Schreiber, H. P., & Storey, S. H. (1965). Molecular fractionation in capillary flow of polymer fluids. *Journal of Polymer Science Part C: Polymer Letters*, *3*(9), 723-727.

Schreiber, H. P., Storey, S. H., & Bagley, E. B. (1966). Molecular fractionation in the flow of polymeric fluids. *Transactions of the Society of Rheology*, *10*(1), 275-297.

Sendner, C., Horinek, D., Bocquet, L., & Netz, R. R. (2009). Interfacial water at hydrophobic and hydrophilic surfaces: Slip, viscosity, and diffusion. *Langmuir*, *25*(18), 10768-10781.

Sentmanat, M., Muliawan, E. B., & Hatzikiriakos, S. G. (2004). Fingerprinting the processing behavior of polyethylenes from transient extensional flow and peel experiments in the melt state. *Rheologica Acta*, *44*(1), 1-15.

Servantie, J., & Müller, M. (2008). Statics and dynamics of a cylindrical droplet under an external body force. *The Journal of chemical physics*, *128*(1), 014709.

Shelby, M. D., & Caflisch, G. B. (2004). Shear field induced diffusion and molecular weight fractionation during polymer processing. *Polymer engineering and science*, *44*(7), 1283.

Snijkers, F., & Vlassopoulos, D. (2011). Cone-partitioned-plate geometry for the ARES rheometer with temperature control. *Journal of Rheology*, *55*(6), 1167-1186.

Stewart, C. W. (1993). Wall slip in the extrusion of linear polyolefins. *Journal of Rheology*, *37*(3), 499-513.

Struglinski, M. J., & Graessley, W. W. (1985). Effects of polydispersity on the linear viscoelastic properties of entangled polymers. 1. Experimental observations for binary mixtures of linear polybutadiene. *Macromolecules*, *18*(12), 2630-2643.

Tchesnokov, M. A., Molenaar, J., Slot, J. J. M., & Stepanyan, R. (2005). A molecular model for cohesive slip at polymer melt/solid interfaces. *The Journal of chemical physics*, *122*(21), 214711.

Theodorou, D. N. (1988). Lattice models for bulk polymers at interfaces. *Macromolecules*, *21*(5), 1391-1400.

Tretyakov, N., & Müller, M. (2013). Correlation between surface topography and slippage: a Molecular Dynamics study. *Soft Matter*, *9*(13), 3613-3623.

Tsenoglou, C. (1991). Molecular weight polydispersity effects on the viscoelasticity of entangled linear polymers. *Macromolecules*, *24*(8), 1762-1767.

Tuminello, W. H. (1986). Molecular weight and molecular weight distribution from dynamic measurements of polymer melts. *Polymer Engineering & Science*, *26*(19), 1339-1347.

Van der Gucht, J., Besseling, N. A. M., & Fleer, G. J. (2002). Surface segregation in polydisperse polymer melts. *Macromolecules*, *35*(17), 6732-6738.

Vega, J. F., Rastogi, S., Peters, G. W. M., & Meijer, H. E. H. (2004). Rheology and reptation of linear polymers. Ultrahigh molecular weight chain dynamics in the melt. *Journal of Rheology*, *48*(3), 663-678.

Vinogradov, G. V., & Ivanova, L. I. (1967). Viscous properties of polymer melts and elastomers exemplified by ethylene-propylene copolymer. *Rheologica Acta*, *6*(3), 209-222.

Vinogradov, G. V., Yanovskii, Y. G., Borisenkova, E. K., Yarlykov, B. V., & Berezhnaya, G. V. (1972). Viscoelastic properties and flow of narrow distribution polybutadienes and polyisoprenes. *Journal of Polymer Science Part A-2: Polymer Physics*, *10*(6), 1061-1084.

Wagner, M. H. (1976). Analysis of time-dependent non-linear stress-growth data for shear and elongational flow of a low-density branched polyethylene melt. *Rheologica Acta*, *15*(2), 136-142.

Wang, S. Q., & Drda, P. A. (1996a). Superfluid-Like Stick− Slip Transition in Capillary Flow of Linear Polyethylene Melts. 1. General Features. *Macromolecules*, *29*(7), 2627-2632.

Wang, S. Q., & Drda, P. A. (1996b). Stick− Slip Transition in Capillary Flow of Polyethylene. 2. Molecular Weight Dependence and Low-Temperature Anomaly. *Macromolecules*, *29*(11), 4115-4119.

Wang, S. Q., & Drda, P. A. (1997). Stick-slip transition in capillary flow of linear polyethylene: 3. Surface conditions. *Rheologica acta*, *36*(2), 128-134.

Wenzel, R. N. (1936). Resistance of solid surfaces to wetting by water. *Industrial & Engineering Chemistry*, *28*(8), 988-994.

Woo Inn, Y. (2013). Melt fracture and wall slip of metallocene-catalyzed bimodal polyethylenes in capillary flow. *Journal of Rheology*, *57*(2), 393-406.

Worth, R. A., Parnaby, J., & Helmy, H. A. A. (1977). Wall slip and its implications in the design of single screw melt-fed extruders. *Polymer Engineering & Science*, *17*(4), 257-265.

Yoshimura, A., & Prud'homme, R. K. (1988). Wall slip corrections for Couette and parallel disk viscometers. Journal of Rheology, 32(1), 53-67.

Zhu, Y., & Granick, S. (2002). Apparent slip of Newtonian fluids past adsorbed polymer layers. *Macromolecules*, *35*(12), 4658-4663.